GROUTED TRANSVERSE FULL-DEPTH PRECAST BRIDGE DECK JOINT INTEGRITY

by

Erika Dawn Weber

A dissertation submitted to the faculty of
The University of Utah
in partial fulfillment of the requirements for the degree of

Doctor of Philosophy

Department of Civil and Environmental Engineering

The University of Utah

May 2014

The University of Utah Graduate School

STATEMENT OF DISSERTATION APPROVAL

The dissertation of Erika Dawn Weber has been approved by the following supervisory committee members:

Chris P. Pantelides	, Chair	February 7, 2014 Date Approved
Lawrence D. Reaveley	, Member	February 7, 2014 Date Approved
Janice Chambers	, Member	February 7, 2014 Date Approved
Luis Ibarra	, Member	February 7, 2014 Date Approved
Daniel Adams	, Member	February 7, 2014 Date Approved
Pedro Romero	, Member	February 11, 2014 Date Approved

and by **Michael Barber**, Chair of the Department of

Civil and Environmental Engineering

David B. Kieda, Dean of The Graduate School

ABSTRACT

Many states are implementing Accelerated Bridge Construction (ABC) methods to reduce traffic delays due to bridge construction. One such method is the use of precast concrete full-depth panels to construct bridge decks. The grouted transverse joint between precast concrete deck panels is the most vulnerable element of the bridge deck system. To extend the longevity of bridge decks it is imperative to improve the integrity of the grouted transverse joint. The focus of this research is to compare different methods to protect, strengthen, and analyze the capacity of the grouted transverse joint. This is done through four separate papers focusing on: the protection of the joint using different overlay systems; the capacity and behavior of the transverse joint using Fiber Reinforced-Polymers (FRP) composite rods at different posttensioning levels; finite element modeling of the transverse joint under concentrated truck tire loads; and an analytical approach, comparing the applied concentrated truck tire load with the capacity of the joint. Minimal research has been done on the capacity of the joint under concentrated loads, which are the majority of the loads applied to bridge decks. No previous research has been provided using Carbon FRP rods for posttensioning of the transverse bridge deck joint.

Several observations, conclusions and recommendations were found with this research. It was found that overlay systems reduce the chloride intrusion for the transverse joint between full depth precast bridge deck panels. Posttensioning across the

transverse joint provided increased joint shear transfer capacity and will impede deck cracking, and therefore lead to longer useful life of the bridge deck. The use of carbon FRP rods for posttensioning is beneficial in improving the integrity of the joint. Prior to the initial joint cracking the deck behaved monolithically which leads to the simpler design methods for the design and distribution methods of concentrated loads acting on the deck. The proposed effective distribution width of 36 in. was acceptable in the design of the transverse joint precast bridge decks under concentrated loads.

TABLE OF CONTENTS

LIST OF TABLES

ACKNOWLEDGEMENTS

I would like to thank my mentors, Dr. Chris Pantelides and Dr. Larry Reaveley, for their constant support and efforts into both my degree and research. Additionally I wish to thank the other members of my committee: Dr. Janice Chambers, Dr. Luis Ibarra, Dr. Romero and Dr. Dan Adams.

I am grateful for the Civil and Environmental Engineering Department, Hansen Eagle Precast, the various overlay suppliers, and SIKA for their contribution to this research. This research would not have been possible without the help of many students and friends, including Lexy Smith, Ruifen Liu, Yiran Cui, and Wenjing Xu. I would like to give a special thanks to Korin Holden, who has been a great support throughout the program.

I wish to thank "Uncle" Mark Bryant, who not only helped with the lab but taught and helped me with my degree in ways that could not be taught in a classroom. I would not have been able to finish this research without his knowledge and assistance.

CHAPTER 1

INTRODUCTION

Many states are implementing Accelerated Bridge Construction (ABC) methods to reduce traffic delays and improve safety at bridge construction sites. One of these methods is the use of precast concrete full-depth panels for bridge deck construction. The panels are built and cured off-site and then brought on-site and placed on new or existing bridge girders. The benefits of the ABC method include the reduction of time affecting traffic and road closures for bridge construction and increased safety at the construction site.

Utah DOT is implementing a proposed design life for new bridges of 75 years. The life of a bridge is dependent upon the life of its weakest component, which is the bridge deck (Tadros et al., 1998). For precast concrete full-depth panels the grouted transverse joint between panels is the most vulnerable element of the bridge deck system. Bridge deck panel performance is dependent on and manifested in the behavior of the joint (Issa et al., 1995b). In order to improve the longevity of precast concrete bridge decks, it is imperative to improve the integrity and durability of the joint. Three methods to help improve the integrity and durability of the joint are protecting the joint, strengthening the joint, and analyzing the joint under major loading.

Overlays protect the bridge deck from chloride intrusion. The majority of

research on overlays is for cast-in-place decks; however, overlays are often used on precast bridge decks. One method of improving the integrity of the joint is to protect the system from chloride intrusion through the use of overlays at the joint. Studies have found moisture leakage at bridge transverse joints, under overlay systems, for non-posttensionded transverse joints (Culmo, 2010, Linford and Reaveley 2004). For this purpose Utah DOT has required all new bridges utilizing precast deck panels be posttensioned. Research of the chloride penetration and the bond strength of overlay systems at the transverse joint under cyclic loading at minimal posttensioning levels is beneficial to protecting the transverse joint.

The majority of the loads on the transverse joint are due to concentrated loads from truck tires; however, the majority of research for grouted transverse joints is on their capacity under uniform loading. To improve the integrity of the joint it is imperative to understand the effects of the grouted transverse bridge deck joint under concentrated truck tire loads. A study including laboratory tests, computer modeling and mathematical predictions, of the failure modes of the transverse joint under concentrated truck tire load with no and low posttensioning levels is useful to understand panel deck joint performance.

Posttensioning in bridge decks is performed by posttensioning steel tendons which are also susceptible to chloride attack. It is beneficial to improve the integrity of the transverse joint through the use of posttensioning across the joint with carbon fiber rods which do not corrode.

1.1 References

Culmo, M. (2010). *Performance of Accelerated Bridge Construction Projects in Utah as of June 2010*, Lessons Learned Report, Utah Department of Transportation, Salt Lake City, UT.

Hanna, K. E., Morcous, G., & Tadros, M. K. (December 2010). *Second Generation Precast Deck Panel (NUDECK) System*. University of Nebraska, Lincoln. Lincoln, Nebraska: Nebraska Department of Roads.

Issa, M. A., Idriss, A.-T., Kaspar, I. I., & Khayyat, S. Y. (1995, January-February). Full Depth Precast and Precast, Prestressed Concrete Bridge Deck Panels. *PCI Journal*, 40, 59-80.

Issa, M. A., Ribeiro do Valle, C. L., Islam, S., Abdalla, H. A., & Issa, M. A. (2003, July-August). Performance of Transverse Joint Grout Materials in Full-Depth Precast Concrete Bridge Deck Systems. *PCI Journal*, 48, 2-13.

Issa, M. A., Yousif, A. A., Issa, M. A., Kaspar, I. I., & Khayyat, S. Y. (1995, May-June). Field Performance of Full-Depth Precast Concrete Panels in Bridge Deck Reconstruction. *PCI Journal*, 40, 82-108.

Issa, M. A., Yousif, A. A., Issa, M. A., Kaspar, I. I., & Khayyat, S. Y. (1998, January-February). Analysis of Full Depth Precast Concrete Bridge Deck Panels. *PCI Journal*, 43, 74-85.

Linford, M. S., & Reaveley, L. D. (2004). A Study of the I-15 *Reconstruction Project to Investigate Variables Affecting Bridge Deck Cracking*. Salt Lake City, UT.

CHAPTER 2

LITERATURE REVIEW

Many studies have been performed on full-depth precast concrete bridge deck panel systems. Issa et al. (1995a) performed a field investigation of several bridges using full-depth precast concrete bridge decks in several states. It was reported that these systems had an overall excellent performance record. In certain cases the decks did not perform well; this was due to lack of longitudinal posttensioning across the joint, poor construction procedures and materials, panel-to-panel configuration, and the type of connection between the deck and connecting bridge system. Each of these issues needs to be addressed in order to improve integrity of the joint and thus the life of the entire bridge system.

For a bridge deck joint and system to be considered acceptable it must meet several requirements. These include: a) limited impact to surrounding traffic flow, b) sufficient seismic capacity, c) no cracks due to repeated service load, d) no water leakage from water on the deck, and e) ability to transfer live load (Hieber, 2005; NCHRP 584, 2004; Tadros, 1998). To improve the integrity and life of the joint and meet the above criteria, research has been performed on the use of bridge deck overlays, specific joint configuration, material used in the joint, and amount of longitudinal posttensioning across the joint.

The use of overlays addresses issues associated with construction procedures and materials to prevent or postpone the intrusion of chlorides from deicing salts that lead to corrosion of steel inside the concrete deck. Overlays create a protective barrier and a smooth riding surface (NCHRP 333, 2004; Markowski, 2005). The majority of research on bridge deck overlays has been performed on cast-in-place concrete bridge decks.

In 1999, the Illinois DOT evaluated two thin-lift polymer bridge deck overlays on two adjacent bridges (Pfeirer et al., 1999). Half-cell potential tests were performed prior to overlay placement and pull-off tests were performed on test patches prior to full use of the overlay systems. Performance evaluation of these systems concluded that polymer overlay systems had the potential to provide an impermeable and durable surface with high skid resistance for 15 or more years provided the system was applied correctly. In addition, the study concluded that to ensure acceptable overlay performance contractors should be trained in application procedures.

In 2003, the New Hampshire DOT performed field research on two thin overlay bridge deck systems (Real et al., 2004). The two overlay systems were applied on the precast concrete full-depth bridge decks which had replaced the original decks. One overlay system was inspected 25 months after placement and the second 34 months after placement. One system showed some cracks and snow plow damage at the expansion joints, but it had not suffered significant deterioration. The New Hampshire DOT report recommended maintenance of a flush finish of the overlay at the joint to prevent snow plow damage. A second system had significant bond loss between the overlay and the deck, with large areas of overlay missing and the remaining overlay showing problems due to wear.

Many research studies have been performed on the specific joint configuration of full-depth precast bridge deck panel systems. There are three types of grouted joint configurations for the transverse joint between deck panels, with a variation of dimensions for each configuration. These include 1) male to female joints, 2) female to female joints, and 3) butt end joints.

Research studies have shown that the preferable joint in regard to ease of construction is concave to concave joints, commonly referred to as female to female joints. Sullivan et al. (2008) compared epoxied male to female joints with female to female joints for cyclic and ultimate load and found that the latter joint performed well for constructability and water leakage. Performance of a transverse joint configuration was shown to be a constructability issue and not a strength or fatigue issue for a simply supported span configuration.

Issa et al. (2003) observed that a female to female joint configuration may be used with a joint width between panels of 1/4 in. at the bottom of the joint. When there are irregularities between the joints, water leakage occurs. It was also noted that male to female and butt joints were prone to leakage.

The use of longitudinal posttensioning has two commonly documented significant effects on the transverse joint between precast concrete panels in a bridge deck. (Issa 1995, Porter 2009). First, it keeps the joint in compression, helping to prevent water leakage that occurs at the grouted joint. Second, by increasing the posttensioning pressure across the joint, the capacity of the joint increases and cracking at the joint is postponed. This allows higher live load levels to transfer across the joint. The minimum AASHTO posttensioning stress is 250 psi (1724 kPa). The minimum posttensioning stress across

the joint after losses used by Utah DOT is 300 psi.

Laboratory tests and finite element modeling simulations on the amount of posttensioning required to keep the joint in compression were performed by Issa et al. (1998). Based on HS20-44 truck loading it was recommended that a minimum posttensioning stress of 200 psi (1379 kPa) should be used for simply supported conditions and positive moment sections at the midspan of continuous bridge decks. It was also recommended that a posttensioning stress of 450 psi (3103 kPa) be used at the interior support of continuous decks where negative moment occurs.

The capacity of the joint prior to initial cracking for posttensioned and non-posttensioned joints has been evaluated by several researchers. Kim et al. (2003) proposed the use of principal stress equations and tensile strength of the grout to predict the cracking strength of grouted joints. Static shear tests were performed on three grouted joint specimens. The ratio between the calculated load at initial cracking and the tested value was found to range between 0.96 and 1.01.

Roberts (2011) used standard American Concrete Institute (ACI 318) shear capacity equations of concrete to compare the strength of posttensioned female to female joints for six jointed specimen tests. These included the simplified concrete shear strength equation, the shear strength when axial load is applied, and the shear capacity of posttensioned members. The panels were posttensioned in the short direction, perpendicular to the grouted pocket. The shear strength of the posttensioned joint exceeded the calculated capacity for all three equations.

Several researchers have used the finite element method to model the transverse joint between precast concrete bridge deck panels. Research at Utah State University was

performed on several joint configurations in both the laboratory and with finite element models (Julander, 2009; Porter, 2009; James, 2012; Wells, 2012). These included shear and flexural tests on posttensioned female to female transverse joints, female to female joints strengthened through posttensioning provided by curved bolts across the joint, and female to female transverse joints strengthened by welded studs and welded rebar. It was found that the posttensioned panels had higher ultimate and initial cracking capacity. The error regarding the cracking force predicted by the finite element method and the experimental results ranged between 2% and 32%. The error regarding the ultimate capacity predicted by the finite element method and the experimental results ranged between 4% and 8%. The initial cracking strength and ultimate strength for the posttensioned joint was dependent upon the bond strength between the concrete and grout.

Research has been performed on the behavior of cast-in-place concrete bridge decks under concentrated loads as well as the capacity of the transverse joint between precast bridge deck panels. Minimal research has been done on the relationship and effects of concentrated loads on the capacity of the transverse joint between precast bridge deck panels.

Petrou et al. (1996) performed laboratory testing of concrete decks under concentrated load. It was found that the primary failure mode for "beam" deck strips was ductile flexural failure due to yielding of the steel reinforcement and that the primary failure mode for decks that had brittle failure was punching shear.

Tao (2009) provided a method for determining the required transverse reinforcement for a concrete bridge deck under a concentrated load. It was observed that

slabs with small width to length ratios behaved in one-way action while slabs with larger width to length ratios had two-way bending. Tao's proposed method states that the maximum moment due to uneven distribution is proportional to the average moment over the length of the panel.

The capacity of the joint prior to initial cracking for posttensioned and non-posttensioned joints has been analyzed by several researchers. Kim et al. (2003) proposed the use of principal stress equations and the tensile strength of the grout to predict the cracking strength of grouted joints. Static shear tests were performed on three grouted joint specimens by Kim et. al. (2003). The ratio between the calculated load at initial cracking and the tested value was found to range between 0.96 and 1.01.

Roberts (2011) compared the tested strength of posttensioned female to female joints with standard shear capacity equations of concrete, as found in section 11.2 of the ACI 318 (ACI 318-11). Grouted panels that were 10 ft x 4 ft were tested for shear capacity across the joint. The panels were posttensioned in the short direction, perpendicular to the grouted pocket. He found that the shear strength of the posttensioned joint exceeded the calculated capacity for all three equations.

Shear friction was utilized by Saenz et al. (2004) as part of a strut and tie model for concrete wrapped with fiber-reinforced composites. Push off tests were performed and the capacity for externally strengthened specimens with fiber-reinforced composite laminates was compared to a strut and tie model. It was found that the strut and tie model gave conservative results and was successful in representing the behavior of the concrete

.

2.1 References

ACI(2010). (n.d.). Report on High Strength Concrete. *Report ACI 363R-10*. Farmington Hills, MI.

Badie, S. S., & Tadros, M. K. (2007). *NCHRP Report 584 Full-Depth Precast Concrete Bridge Deck Panel Systems. Washington D.C.*: Transportation Research Board of the National Academies.

Badwan, I. Z., & Liang, R. Y. (2007). Performance Evaluation of Precast Posttensioned Concrete Multibeam Deck. *Journal of Performance of Constructed Facilities*.

Benteley. (2013). RAM CONCEPT V8i Release 5.0.2.

Hanna, K. E., Morcous, G., & Tadros, M. K. (December 2010). *Second Generation Precast Deck Panel (NUDECK) System*. University of Nebraska, Lincoln. Lincoln, Nebraska: Nebraska Department of Roads.

American Concrete Institute.(2011). *ACI 318-11 Building Code Requirements for Structural Concrete*. Farmington Hills, MI.

Issa, M. A., Idriss, A.-T., Kaspar, I. I., & Khayyat, S. Y. (1995, January-February). Full Depth Precast and Precast, Prestressed Concrete Bridge Deck Panels. *PCI Journal*, 40, 59-80.

Issa, M. A., Ribeiro do Valle, C. L., Islam, S., Abdalla, H. A., & Issa, M. A. (2003, July-August). Performance of Transverse Joint Grout Materials in Full-Depth Precast Concrete Bridge Deck Systems. *PCI Journal*, 48, 2-13.

Issa, M. A., Yousif, A. A., Issa, M. A., Kaspar, I. I., & Khayyat, S. Y. (1995, May-June). Field Performance of Full-Depth Precast Concrete Panels in Bridge Deck Reconstruction. *PCI Journal*, 40, 82-108.

Issa, M. A., Yousif, A. A., Issa, M. A., Kaspar, I. I., & Khayyat, S. Y. (1998, January-February). Analysis of Full Depth Precast Concrete Bridge Deck Panels. *PCI Journal*, 43, 74-85.

James, P. H. (2012). Finite Element Modeling of Full Depth Precast Concrete Bridge Deck Connections in Bending and Shear. *Master'sThesis*, Utah State University, 2012.

Julander, J. (2009). Finite Element Modeling of Full Depth Concrete Transverse Bridge Deck Connections. *Master's Thesis*, Utah State University, 2009.

Markowski, S. M. (2005). Experimental and Analytical Study of Full-Depth Precast/Prestressed Concrete Deck Panels for Highway Bridges. *Master's Thesis*,

University of Wisconsin-Madison, 2005.

National Cooperative Highway Research Program. (2004). *NCHRP Synthesis 333 Concrete Bridge Deck Performance, A Synthesis of Highway Practice*. Washington D.C.: Transportation Research Board of the National Academies.

Petrou, M. F., Perdikaris, P. C., & Duan, M. (1996). Static Behavior of Noncomposite Concrete Bridge Decks Under Concentrated Loads. *Journal of Bridge Engineering*, 143-154.

Pfeifer, B., & Kowlaski, G. (1999). *Evaluation of Thin Lift Polymer Bridge Deck Overlays on I-57 Bridges at Clifton, IL.* Construction Report, IL-PRP-132, Springfield, IL: Illinois Department of Transportation.

Porter, S. D. (2009). Laboratory Testing of Precast Bridge Deck Panel Transverse Connections for Use in Accelerated Bridge Construction. *Master'sThesis*, Utah State University, 2009.

Real, W. (2004). *Experimental Feature 2004-2 and 2005-2 Poly-Carb Flexogrid Bridge Deck Overlay System and Stirling Lloyd Save Track HW*. Concord, New Hampshire: New Hampshire Department of Transportation.

Shim, C.-S., Choi, K.-Y., & Chang, S.-P. (2001). Design of Transverse Joints in Composite Bridges with Precast Decks. *KSCE Journal of Civil Engineering*, 17-27.

Sullivan, S., & Roberts-Wollmann, C. (2008). Experimental and Analytical Investigation of Full Depth Precast Deck Panels on Prestressed I-Girders. Contract Report VTRC 09-CR4 Charlottesville, VA: Virginia Transportation Research Council.

Tao, Z. (2009). Biaxial Bending Analysis of the Slabs Under Concentrated Loads. *2009 International Conference on Engineering Computation*, (pp. 213-216).

Wells, Z. B. (2012). Peformance of Post-Tensioned Curved-Strand Connections in Transverse Joints of Precast Brigde Decks. *Master's Thesis*, Utah State University, 2012.

CHAPTER 3

RESEARCH OBJECTIVES

The purpose of this research is to improve the integrity of the grouted transverse bridge deck joint. Protecting the joint, strengthening the joint, and analyzing the joint under major loading conditions are beneficial in improving the integrity of the joint.

Overlays protect the bridge deck from chloride intrusion. The majority of research on overlays is for cast-in-place decks; however, overlays are often used on precast bridge decks. One method of improving the integrity of the joint is to protect the system from chloride intrusion through the use of overlays at the joint.

One common method of strengthening the transverse joint is through the use of posttensioning across the joint. Posttensioning in bridge decks is performed by posttensioning steel tendons which are also susceptible to chloride attack. It is beneficial to improve the integrity of the transverse joint through the use of posttensioning across the joint with carbon fiber rods.

The majority of the loads on the transverse joint are due to concentrated loads from truck tires; however, the majority of research for grouted transverse joints is on their capacity under uniform loading. To improve the integrity of the joint it is imperative to analyze the grouted transverse bridge deck joint under concentrated truck tire loads.

This research focuses on four main objectives to improve the integrity of the joint,

which include:

1) Determine the effectiveness of overlay systems to protect the transverse bridge deck joint from chloride intrusions.
2) Determine the benefits of posttensioning using carbon fiber reinforced rods across the grouted transverse joint on the capacity of the joint under concentrated truck tire loading.
3) Determine the effectiveness of finite element modeling in predicting the capacity and behavior of the grouted transverse bridge deck joint under concentrated truck tire loads.
4) Determine an acceptable method to find the capacity of grouted transverse bridge deck joints for concentrated truck tire loads.

To accomplish these objectives, this research presents experimental and analytical methods for composite grouted joints in four papers. These papers are presented in Chapters 4 through 7. Chapter 4 addresses the use of overlays to protect the joint from chloride attack on composite grouted specimens. Chapter 5 focuses on the strengthening of the transverse joint through the use of posttensioning with carbon fiber reinforced rods. Chapter 6 focuses on finite element modeling of the joint and is a comparison to laboratory tested specimens in Chapter 5. Chapter 7 uses the finite element model provided in Chapter 6 to compare analytical methods including a strut and tie model to determine the capacity of the joint under concentrated loads. Lastly, Chapter 8 provides a summary of the findings from this research and Chapter 9 provides recommendations for future research.

CHAPTER 4

EXPERIMENTAL EVALUATION OF BRIDGE DECK OVERLAYS FOR PRECAST CONCRETE PANELS USED IN ACCELERATED BRIDGE CONSTRUCTION

4.1 Abstract

As part of Accelerated Bridge Construction (ABC) methods, bridge decks are constructed using precast concrete elements ranging from half-depth or full-depth precast concrete panels to self-propelled modular transport of entire superstructures. The present research focuses on potential cracking that may develop in ABC bridge decks due to lifting, transportation, and placement of the deck system. The ability of three different types of bridge deck overlays to provide a durable and resilient roadway surface is investigated. The three types of overlays were thin bonded polymer, polyester polymer concrete, and methyl methacrylate. The experiments included pull-off and chloride tests. Two configurations were tested: (1) application of the overlay before movement of the bridge deck panels, and (2) application of the overlay after movement of the bridge. Criteria used to evaluate the three types of overlay systems included: (a) bond strength between the overlay and precast concrete bridge deck, and (b) amount of chloride penetration.

4.2 Introduction

Steel reinforcement in concrete bridge decks is prone to corrosion caused by chloride ions from deicing materials. Various overlays are used to delay or postpone this corrosion. The Utah Department of Transportation (Utah DOT) is implementing Accelerated Bridge Construction (ABC) methods. This construction process includes half-depth precast concrete deck panels, full-depth precast concrete deck panels, Self-Propelled Modular Transport (SPMT) precast concrete deck and superstructure bridges, and slide-in bridges. ABC concrete bridge decks undergo additional deflection due to installation-induced stresses prior to deflections from traffic and other loads. There are concerns regarding the potential of cracking of concrete decks in ABC bridges. The purpose of this research is to compare the performance of three types of overlay systems for precast concrete panels used in bridge decks. These included a total of five overlay systems: three thin bonded polymer overlays, one polyester polymer concrete overlay, and one methyl methacrylate based overlay system. In addition, the research is concerned with the sequence of applying the overlay to the concrete bridge deck, specifically applying the overlay before or after the placement of the precast concrete panels on the girders.

The two areas of concern for leakage in ABC concrete bridge decks are joints, specifically between precast concrete bridge deck panels, and locations where cracking may already have occurred in the precast concrete panels due to lifting and placement-induced stresses. Research has been carried out regarding the performance of precast concrete bridge decks including several overlay systems. The present research focuses on initial cracking due to lifting and placement of the precast concrete panels and its

effect on the performance of the overlay system.

4.3 Previous Research

Many studies have been performed on full-depth precast concrete bridge deck panel systems. Issa et al. (1995a) performed a field investigation of several bridges using full-depth precast concrete bridge decks in several states. It was reported that these systems had an overall excellent performance record. In certain cases the decks did not perform well; this was due to lack of longitudinal posttensioning across the joint, poor construction procedures and materials, panel-to-panel configuration, and the type of connection between the deck and the connecting bridge system. Each of these issues needs to be addressed in order to improve integrity of the joint and the life of the entire bridge system.

For a bridge deck joint and system to be considered acceptable it must meet several requirements. These include: a) limited impact to surrounding traffic flow, b) sufficient seismic capacity, c) no cracks due to repeated service load, d) no water leakage from water on the deck, and e) ability to transfer live load (Hieber, 2005; NCHRP 584, 2004; Tadros, 1998). To improve the integrity and life of the joint and meet the above criteria, research has been performed on the use of bridge deck overlays, specific joint configuration, material used in the joint, and amount of longitudinal posttensioning across the joint.

The use of overlays addresses issues associated with construction procedures and materials to prevent or postpone the intrusion of chlorides from deicing salts that lead to corrosion of steel inside the concrete deck. Overlays create a protective barrier and a

smooth riding surface (NCHRP 333, 2004; Markows, 2005). The majority of research on bridge deck overlays has been performed on cast-in-place concrete bridge decks.

Overlay systems are required to have a long term stable bond, sufficient wear resistance, sufficient freeze-thaw resistance, and protection of the reinforcement from chloride intrusion to attain a sufficient service life (Paulsson et al., 1998).

Bridge decks are particularly susceptible to reduced life span due to the use of deicing salts. The chlorides of deicing salts leads to corrosion of the deck rebar. This corrosion leads to loss of steel cross sectional area, loss of bond between the steel and concrete and concrete cracking due to expansion of the corroded steel . There are many different methods implemented around the country to prevent or postpone the corrosion of deck reinforcing bars (Badaei, et. al., 1988). These include the use of stainless steel reinforcement, epoxy-coated reinforcement, larger reinforcing bar cover, low-slump, dense concrete overlay, latex modified concrete overlay, interlayer membrane with asphalt overlay, thin polymer overlay and concrete sealers.

Badaie et. al. (1988) provided a study of the performance of bridge deck protective strategies at the time. The performance of the protective strategy was defined as a function of the bar corrosion effectiveness, the degree of concrete cracking in the decks and the durability of the bridge decks and their protective components. From their study it was found that latex-modified concrete overlays had less scaling than low-slump, dense concrete overlays. Debonding was attributed to inadequate texturing of the substrate and methods of applying bonding agents that result in no bond or insufficient bond when construction is complete. The “effective service period” for 1.5 in. thick latex-modified concrete overlay and 2 in. (50.8 mm) thick low-slump, dense concrete

overlay was found to be around 50 years when the application of deicing salts did not exceed 12 tons per lane-mile. When using only an increased bar cover it was found that when salt applications reach 30-40 tons per lane-mile per year, the effective service period may be 10 to 15 years. It was found that epoxy-coating the top steel, combined with limits a water/cement ratio of 0.45 and a top mat concrete cover of 2 1/2 in. (63.5 mm) cover should provide 50-years of corrosion-free life even in severe chloride environments.

Liang et al. (2010) evaluated different topical protection systems for bridge decks and the associated life-cycle cost. Core samples were taken from five existing bridge decks and tested for chloride levels. All the bridge decks tested had no corrosion and had chloride concentration levels much lower than the critical level . It was concluded that the difference in the effectiveness of the different topical protection systems was not significant and that the inspection results could not be directly used to evaluate the effectiveness of the topical protection methods for later stages of corrosion. It was also found from further study that decks with a waterproofing membrane had a longer service life than bare decks.

One method of postponing the chloride intrusion to the reinforcing steel is the use of hydrophobic treatment of the concrete to further reduce its permeability. De Vries (1997) provided laboratory research on the chloride intrusion of concrete with hydrophobic treatment. The specimens underwent a year of cyclic chloride testing with 24 hour periods of ponding with a 10% NaCl solution (by mass) and 6 days of dry exposure at 20^{o} C and 50% RH. It was found that hydrophobic treatment of concrete strongly reduces the penetration of chloride under deicing salt/drying cycles.

In 1999, the Illinois DOT evaluated two thin-lift polymer bridge deck overlays on two adjacent bridges (Pfeirer et al., 1999). Half-cell potential tests were performed prior to overlay placement and pull-off tests were performed on test patches prior to full use of the overlay systems. Performance evaluation of these systems concluded that polymer overlay systems had the potential to provide an impermeable and durable surface with high skid resistance for 15 or more years provided the system was applied correctly. In addition, the study recommended that contractors should be trained in application procedures to ensure acceptable overlay performance.

In 2003, the New Hampshire DOT performed field research on two thin overlay bridge deck systems (Real et al., 2004). The two overlay systems were applied on the precast concrete full-depth bridge decks which had replaced the original decks. One overlay system was inspected 25 months after placement; the second, 34 months after placement. One system showed some cracks and snowplow damage at the expansion joints but had not suffered significant deterioration. A second system had significant bond loss between the overlay and the deck, with large areas of overlay missing.

4.4 Experimental Investigation

The focus of the present research is to evaluate the ability of different overlay systems to improve the integrity of the joints precast concrete bridge deck panels under initial static deflection and cyclic loading. Three different overlay system types were tested, with five overall variations: a thin polymer overlay (three variations), a methyl methacrylate based overlay system, and a polyester polymer concrete overlay system, as shown in Figure 4.1. During cyclic loading, the precast concrete bridge deck panels were

posttensioned. Posttensioning was provided by carbon fiber posttensioning rods, as explained in section 4.4.2.1. Two different criteria are used to compare the five overlay systems: 1) bond strength between the overlay system and the precast concrete bridge deck panels, and 2) amount of chloride penetration through the overlay into the precast concrete bridge deck panels. These comparisons were made through field and laboratory tests.

4.4.1 Field Tests

Three bridge decks constructed with precast concrete panels using different overlays were examined. The overlay systems were all installed approximately 1 year before the field tests were carried out. Four locations were selected for performing bond tests on each bridge deck. Bond tests were performed adjacent to a transverse precast concrete panel joint at each bridge site per ASTM D4541 (2009). The location of the pull-off tests was near midspan of the bridge between the exterior and first interior girders at approximately the center of the slow lane. All three bridges used steel posttensioned precast concrete panels to construct the bridge decks and carried two traffic lanes in one direction. Two bridges consisted of precast concrete deck panels on prestressed concrete girders, and the third bridge consisted of precast concrete deck panels on steel girders. The overlay systems for the bridges were a methyl methacrylate overlay and two thin polymer overlays. The methyl methacrylate overlay was applied to one of the two bridges consisting of precast concrete deck panels on prestressed concrete girders.

4.4.2 Laboratory Tests

Three different laboratory testing procedures were designed for this research. Type I simulates the effects of the application of the overlay *after* lifting and placement of the precast concrete deck panel on the bridge. Type II simulates the effects of the application of the overlay *prior* to lifting and placement of the precast concrete deck panel onto the bridge. Both Type I and II procedures evaluate the bond strength of the overlay to the precast concrete deck panel and the penetration of chlorides through the overlay. Test Type I evaluates the performance of overlays placed after grouting the composite specimens while Test Type II evaluates the performance of overlays placed prior to placement of the deck panels onto the bridge. Type III is a chemical test which evaluates the penetration of chlorides through the overlay after a ponding procedure is applied to the precast concrete deck panel.

Five overlay systems were used in this research: TP1, TP2 and TP3 were thin polymer overlay systems from three different manufacturers; MM1 was a methyl methacrylate based overlay system; and PC1 was a polyester polymer concrete overlay system. Each overlay underwent Type I, II, and III testing protocols. Table 4.1 provides the test matrix for the laboratory tests.

4.4.2.1 Concrete Panel Specimens

Concrete specimens were cast for this research on two dates that were 1 week apart at Hansen Eagle Precast. The 28 day concrete compressive strength of the panels was 11,000 psi (76 MPa). A total of ten composite panels were constructed. The 3 ft (0.91 m) wide composite panels consist of two 1 ft -6 in. (0.46 m) wide single panels, as

shown in Figure 4.2, grouted together, as shown in Figure 4.3, per Type I and Type II testing protocols. Five specimens underwent each testing protocol. In addition, five 1 ft-6 in. x 1 ft-6 in. x 6 in. (0.46 m x 0.46m x 0.15 m) plain concrete specimens were built for the Type III tests.

The single and composite panels were reinforced with #6 grade 60 steel bars. The panels were posttensioned before the cyclic tests with 3/8 in. (10 mm), carbon fiber rods. The layout of the panels and the grouted joint pocket of the panels are shown in Figures 4.4 through 4.6. Figures 4.4 and 4.5 describe the single and composite panel dimensions. Figure 4.6 provides the joint geometry and dimensions. The top surface of the specimens was sand blasted to remove the top layer of cement paste.

The composite panels were posttensioned with 3/8 in. (9.5.25 in.) carbon fiber rods as shown in Figure 4.7, before cyclic loading was applied. Rod anchoring was achieved using a Fiber Reinforced Polymer (FRP) anchor developed by Burningham et. al. (2014). Posttensioning was applied through tightening a four-bolt plated anchoring system to create tensile strains along the rods. Posttensioning levels were determined through recorded strain gauge readings on the carbon fiber rods. The induced strain from posttensioning on the rods was between 2,500 to 3,000 microstrain, which correlates to a rod stress of approximately 25% of the design tensile capacity of the rod. This corresponds to a force of approximately 6.2 kip (27.6 kN) for each of the two rods and a stress of approximately 14.8 psi (102 kPa) in the panel, which is less than the panel stress currently specified in practice. This posttensioning was present during cyclic loading, and was removed prior to the ponding protocol. A low level of posttensioning was used to achieve conservative loading conditions compared to typical posttensioning

used in construction.

4.4.2.2 Type I: Application of Overlay System After Lifting and Placement of Precast Concrete Panel on the Bridge

During Type I tests, two single 1 ft–6 in. (0.46 m) by 8 ft (2.44 m) concrete deck panels were turned upside-down and deflected to induce initial cracking on the top face of the panel. This simulates initial cracking during lifting and placement. The two panels were then turned back over and joined through a grouted joint to construct a composite 3 ft (0.91 m) by 8 ft (2.44 m) panel. The dimensions of single and composite specimens are shown in Figures 4.4 and 4.5. The deck overlay system was then applied per manufacturer's specifications on the top face of the composite specimen where initial cracking was previously imposed. Initial bond tests were performed on the composite specimen. The specimens underwent a five 8.5 hour cyclic displacement controlled loadings on one side of the grouted connection simulating the gravity load transfer through the grout in the field. After each day of cyclic loading, two pull-off tests were performed adjacent to the grouted joint. During cyclic loading the specimens were posttensioned with two 3/8 in (9.5 mm) diameter posttensioning carbon fiber reinforced polymer (CFRP) rods to a force of approximately 15 kip (66.72 kN), with the configuration shown in Figure 4.8. The two CFRP rods connecting the two single panels were 4 ft (1.21 m) apart. The anchor system for the two CFRP rods is described by Burningham et al. (2014). Currently, Utah DOT requires posttensioning in the longitudinal (traffic) direction for all bridge decks constructed with precast concrete panels; this is currently implemented with low relaxation steel strands.

The posttensioning force was removed after completion of the cyclic test to simulate the worst case conditions for the ponding test. A ponding test was performed subsequently on an 11 in. x 11 in. (279 mm x 279 mm) section over the grouted pocket for 90 days. An acrylic wall was installed around each section and a 3% sodium chloride solution by weight was placed on the designated section to an average depth of 1/2 in. (13 mm). A lid was placed over the ponding section and the depth of 1/2 in. (13 mm) was maintained, as shown in Figure 4.9. At the completion of the ponding period the solution was removed and the overlay was ground down to the top of the concrete. Concrete samples below the ponded section were taken and checked for chloride content per ASTM C1218-99 (1999).

4.4.2.3 Type II: Application of Overlay System Prior to Lifting and Placement of Precast Concrete Deck Panel on the Bridge

During Type II tests, the deck overlay was applied initially on the top of each of two 1 ft-6 in. (0.46 m) by 8 ft (2.44 m) single concrete deck panels, as shown in Figure 4.6, to simulate the application of the overlay system prior to the precast concrete panel being placed on the bridge. Subsequently, each single panel was turned upside-down and subjected to the same initial deflection as Type I specimens to induce initial cracking. The two precast concrete panel segments were turned over and joined through a grouted joint to construct a composite 3 ft (0.91 m) wide panel. A second application of the overlay system was then implemented at the splice over the grouted pocket and the composite precast concrete panel grouted specimen underwent the same cyclic, ponding, and chemical tests as Type I specimens.

4.4.2.4 Type III: Small Sample Chemical Test

In Type III tests, 1 ft-6 in. x 1 ft-6 in. x 6 in. (0.46 m x 0.46 m x 0.15 m) specimens were subjected to a chemical test. An 11 in. x 11 in. (0.28 m x 0.28 m) section of each specimen was used for the ponding test. An acrylic wall was installed around each section and a 3% sodium chloride solution by weight was placed on the designated section to an average depth of 1/2 in. (13 mm) for 90 days. At the completion of the ponding period, the solution was removed and the overlay was ground down to the top of the concrete. Concrete samples below the ponded section were taken and checked for chloride content per ASTM C1218 – 99 (1999). The bond strength and percent of chloride penetration into the panel were used to compare the ability of the five overlay systems to increase the integrity of the jointed system.

4.4.2.5 Test Setup and Instrumentation

A load frame with a hydraulic actuator were used to apply a displacement-controlled load for precracking and cyclic loading of Type I and Type II specimens, as shown in Figure 4.4. An electronic data acquisition system recorded strains during the application of the loading protocol.

The single panel specimens underwent a cyclic displacement-controlled loading protocol to create precracking on the overlay surface, prior to grouting as shown in Table 4.2. The specimens were loaded at midspan under a simple span condition. Figure 4.10 shows the precracking loading protocol that was used for Type I and II specimens.

The composite precast concrete specimens were loaded in a simple span condition for Type I and II cyclic loading. A displacement-controlled cyclic loading was applied at

the midspan of one of the 1 ft -6 in (0.46 m) wide halves, as shown in Figure 4.8. Figure 4.11 shows a sample of the first day cyclic loading protocol.

A total of eight strain gauges were applied to the reinforcing steel of the composite specimens. Four gauges were applied to each single 1 ft - 6 in. (0.46 m) wide specimen. The strain gauges were located at the center of the top and bottom reinforcing longitudinal bars adjacent to the grouted pocket and on the adjacent transverse bars, as shown in Figure 4.12. Additional strain gauges were attached to the carbon fiber posttensioning rods to measure the initial strain in the rods.

All bond tests were performed using a digital dynamometer per ASTM D7234 (2005). Test results were evaluated based on the pull-off pressure and on the layer that had failed in each test. This included whether the concrete failed, the bond between the overlay and the concrete failed, or the overlay failed.

All chloride tests were performed per ASTM C1218-99 (1999). Four samples were taken per hole at a depth increment of 0.125 in. (3 mm) for a total depth of 0.5 in. (12 mm). A titration test was performed on each sample to determine the percent of chloride in the sample per unit weight. The percent chloride for each sample is determined from the following equation (ASTM C1218-99).

$$Cl, \% = \frac{(3.545)[(V_1 - V_2)N - 0.10]}{W} \quad (1)$$

where V_1 is the volume (mL) of Silver Nitrate ($AgNO_3$) at the equivalent point of the sample; V_2 is the volume of silver nitrate of the blank solution (just water); and N is the normality of the silver nitrate solution used in titration which correlates the volume of

silver nitrate to Sodium Chloride (NaCl) content. The normality of the solution implies that no chlorides are present.

4.5 Evaluation of Results

4.5.1 Cyclic Tests

The applied displacements produced a small tensile strain in the reinforcing steel on the top longitudinal mat. Figure 4.13 shows the longitudinal strains at the bottom longitudinal steel for each composite specimen for the fifth day of cyclic testing for both Type I and Type II procedures. The average strain was approximately one half the yield strain of the steel reinforcement. Hairline cracks on the underside of the specimens were detected after cyclic loading. These cracks were spaced approximately 8 in. (203 mm) apart and extend the entire width of the specimen.

4.5.2 Pull-off Test Values

Pull-off tests were performed and the failure mode was recorded. Three different failure modes occurred during the pull-off tests: 1) epoxy failure, 2) overlay failure, and 3) concrete failure. Epoxy failure corresponds to failure of the glue used for the pull-off test and is not used as a comparison between bond strengths. Overlay failure corresponds to failure within the overlay or failure of the bond between the overlay and concrete. Concrete failure corresponds to the tensile capacity of the concrete and is considered preferable because the overlay has a higher bond strength than concrete tensile capacity. Failure in the concrete is the only acceptable failure mode for overlay systems used by Utah DOT for bridges. A comparison between the average valid (nonepoxy) pull-off

values can be found in Table 4.3 for the various overlay types for both Type I and II tests and the three bridge sites tests.

The pull-off tests from laboratory specimens performed better on average than those carried out at existing bridges. This could be caused by the difference between field and laboratory preparation and loading conditions and the compressive strength of the concrete deck panels. Type I tensile capacity was higher than Type II tensile capacity. The percent of concrete failures was also higher than that of Type II pull-off tests. Typical pull-off test results are shown in Figure 4.14.

A field problem observed by Utah DOT is that application of the overlay may be carried out before a complete removal of the concrete curing compound, which is typically done through shot blasting. Upon observation of the bridge MM1 pull-off tests, the bridge deck was tined prior to placement of the overlay.

4.5.3 Chloride Test Values

Chloride tests were performed after 90 days of ponding. Specimens with overlays had no measurable chloride content inside the concrete under the overlay. Ponding results showed an average chloride content of 2.96 lbs/yd^3 (1.76 Kg/m^3) for the first 1/8 in. (3 mm) below the concrete surface for concrete specimens with no overlay application. An average chloride content of 2.51 lbs/yd^3 (1.49 Kg/m^3) was found at a depth between 1/8 in. (3 mm) to 1/4 in. (6 mm) for the same specimens.

4.6 Conclusions and Recommendations

Two methods of application of different overlay systems applied to precast concrete panels were investigated: (a) application of the overlay applied after placement of the precast bridge deck panels and (b) application of the overlay prior to placement of the precast concrete bridge deck panels. Two properties were tested and compared to determine the performance of different overlay systems. Pull-off tests were used to compare the mechanical characteristics of the overlay system, specifically the bond between the overlay and the concrete bridge deck panel. Ponding tests were also carried out to compare the ability of the overlay system to resist chloride intrusion from deicing salts. The following conclusions can be made based on this research:

1) The majority of failures in the pull off tests for thin polymer overlays occurred in the concrete, which is the desired failure plane. This proves that the tensile strength of the thin polymer overlay and bond strength between the thin polymer and the concrete deck were stronger than the tensile strength of the concrete.
2) The majority of failures in the pull off tests for the methyl methacrylate based overlay and polyester polymer concrete overlay systems occurred in the overlay itself and the bond between the overlay with the average laboratory bond tensile strength between 330 and 572 psi, which is larger than the required Utah DOT minimum. This proves that while the bond failure mechanism was not in the desired failure plane, the minimum bond tensile strength can still be achieved.
3) Pull-off test results performed on specimens constructed in the laboratory had a higher frequency of failure in the concrete with bond tensile strengths from 200 to 400 psi larger than those recorded in the field.

4) The average pull strength of thin polymer overlay systems was 41% larger than the methacrylate based overlay. The polyester polymer concrete overlay system pull strength was 39% larger than the methacrylate system.
5) Results for all overlay systems showed no measurable chlorides. However, base specimens with no overlays had an average chloride content of 2.96 lbs/yd^3 (1.76 kg/m^3) for the first 1/8 in. (3 mm) below the concrete surface and 2.51 lbs/yd^3 (1.49 kg/m^3) for a depth between 1/8 in. (3 mm) to 1/4 in. (6 mm). This indicates that all overlay systems were sufficient to prevent chloride intrusion under the 90 day testing procedures.

It is recommended that overlay systems be applied per manufacturer's specifications. Bridge deck panels should be properly cleaned and prepared prior to installation of the overlay system to ensure an adequate bond between the overlay system and concrete. There was no significant difference between the performance of the overlay systems tested when applied prior to placement of the precast concrete deck panels and those applied after the placement of the precast concrete deck panels. Both methods are acceptable approaches for the placement of the overlay.

4.7 References

American Society for Testing and Materials, ASTM C1218-99 (2008). Standard Test Method for Water-Soluble Chloride in Mortar and Concrete. ASTM International, West Conshohocken, PA.

American Society for Testing and Materials, ASTM D4541-09 (2009). Standard Test Method for Pull-Off Strength of Coatings Using Portable Adhesion Testers. ASTM International, West Conshohocken, PA.

Babei, K. and Hawkins, N. M. (1998). Evaluation of Bridge-Deck Protective Strategies. *Concrete International*, 10, No. 12, 56-66.

Burningham, C.A., Pantelides, C.P., and Reaveley, L.D. (2014). New Unibody Clamp - Anchors for Post-tensioning Carbon Fiber Reinforced Polymer Rods. *PCI Journal,* 59(1), 103-113.

de Vries, Ing J. (1997). Hydrophobic Treatment of Concrete. *Construction and Building Materials*, 11, No. 4, 259-265.

Hieber, D. G., Wacker, J. M., Eberhard, M. O., and Stanton, J. F. (2005). *State-of-the-Art Report on Precast Concrete Systems for Rapid Constuction Bridges.* Washington State Transportation Commission, Seattle, WA.

Issa, M. A., Yousif, A. A., Issa, M. A., Kaspar, I. I., and Khayyat, S. Y. (1995). Field Performance of Full-Depth Precast Concrete Panels in Bridge Deck Reconstruction. *PCI Journal* , 40, No. 3, 82-108.

Liang, Y., Zhang, W. and Xi, Y. (2010). *Strategic Evaluation of Different Topical Protection Systems for Bridge Decks and the Associated Life-Cycle Cost Analysis.* Colorado Department of Transportation, Denver, CO.

Markowski, S. M. (2005). *Experimental and Analytical Study of Full-Depth Precast/Prestressed Concrete Deck Panels for Highway Bridges.* University of Wisconsin-Madison, Madison, WI.

National Cooperative Highway Research Program. (2004). *NCHRP Synthesis 333 Concrete Bridge Deck Performance, A Synthesis of Highwah Practice.* Transportation Research Board of the National Academies, Washington, D.C.

Pfeifer, B., and Kowlaski, G. (1999). *Evaluation of Thin Lift Polymer Bridge Deck Overlays on I-57 Bridges at Clifton, IL.* Springfield, IL: Illinois Department of Transportation.

Paulsson, J., and Silfwerbrand, J., (1998). *Durability of Repaired Bridge Deck Overlays*, Concrete International, 20, No. 2, February 1998, pp. 76-82

Real, W. (2004). *Experimental Feature 2004-2 and 2005-2 Poly-Carb Flexogrid Bridge Deck Overlay System and Stirling Lloyd Save Track HW.* New Hampshire Department of Transportation, Concord, NH.

Yamane, T., Tadros, M. K., Badie, S. S., and Baishya, M. C. (1998). Full Depth Precast, Prestressed Bridge Deck System. *PCI Journal*, 43, No. 3, 104-120.

Table 4.1: Overlay Test Matrix

Test Type	Specimen Size	Test type	Overlay Type	Specimen Name
I	3'-1"x 8'-0" Composite Specimen	Bond and Chloride Intrusion	Thin Polymer	TP1-TI
				TP2-TI
				TP3-TI
			Methyl Methacrylate	MM1-TI
			Polyester Polymer Concrete	PC1-TI
II	3'-1"x 8'-0" Composite Specimen	Bond and Chloride Intrusion	Thin Polymer	TP1-TII
				TP2-TII
				TP3-TII
			Methyl Methacrylate	MM1-TII
			Polyester Polymer Concrete	PC1-TII
III	1'-6"x1'-6"	Chloride Intrusion	Thin Polymer	TP1-TIII
				TP2-TIII
				TP3-TIII
			Methyl Methacrylate	MM1-TIII
			Polyester Polymer Concrete	PC1-TIII
			No Overlay	Base

Table 4.2: Five Day Cyclic Testing Protocol Schedule

Day	Maximum Displacement (in.)	Number of Cycles
1	0.1	7650
2	0.2	3825
3	0.2	3825
4	0.2	3825
5	0.3	2550

1 in. = 25.4 mm

Table 4.3: Average Valid (Nonepoxy) Pull-off Stress Test Results

	TP1		TP2		TP3		MM1		PC1	
	Average Valid Pull-Off Stress (psi)	Pecent Concrete Failure of Valid Tests (%)	Average Valid Pull-Off Stress (psi)	Pecent Concrete Failure of Valid Tests (%)	Average Valid Pull-Off Stress (psi)	Pecent Concrete Failure of Valid Tests (%)	Average Valid Pull-Off Stress (psi)	Pecent Concrete Failure of Valid Tests (%)	Average Valid Pull-Off Stress (psi)	Pecent Concrete Failure of Valid Tests (%)
Bridge	329	0	-	-	308	0	2	0	-	-
Type I	580	100	621	100	673	83	477	20	572	0
Type II	517	100	444	67	530	75	330	0	521	33

1 psi = 6.895 KPa

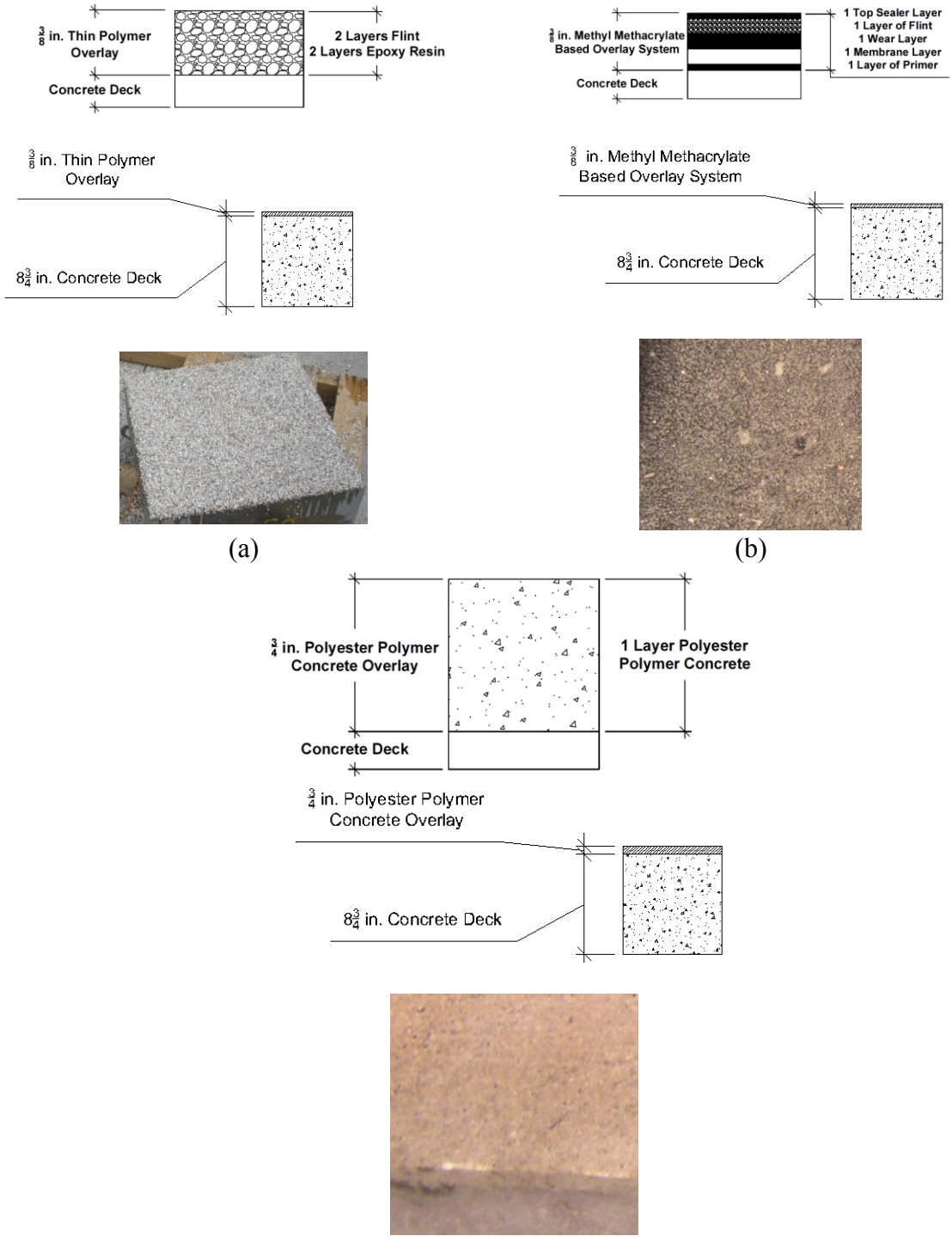

Figure 4.1: Overlay System: (a) Thin Polymer; (b) Methyl Methacrylate (c) Polyester Polymer Concrete: (1 in. = 25.4 mm)

Figure 4.2: Single Panel for Type II Specimen Prior to Grouting;

(1 ft = 0.305 m, 1 in. = 25.4 mm)

Figure 4.3: Type I Specimen Prior to Grouting and Placement of Overlay

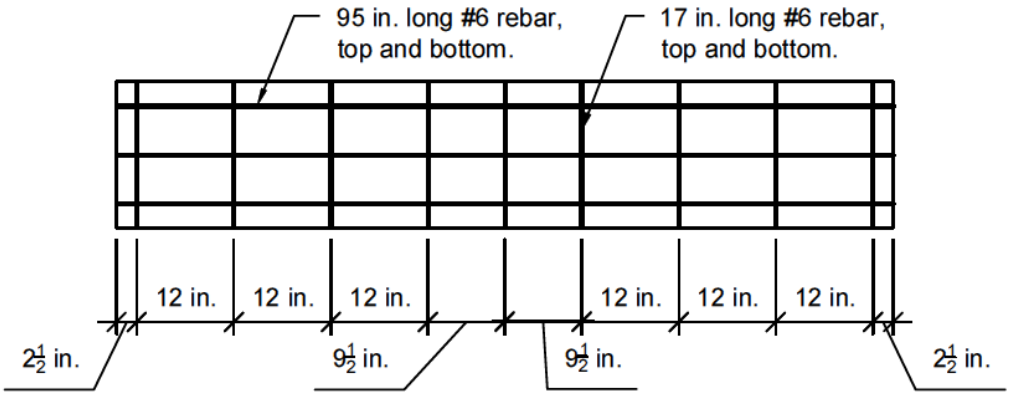

(a)

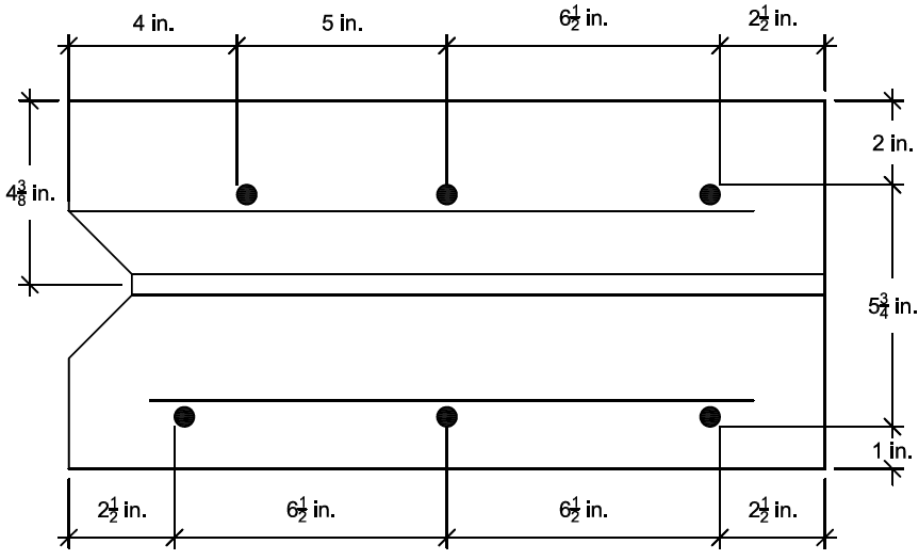

(b)

Figure 4.4: Single Panel Dimensions and Rebar Spacing: (a) Horizontal, (b) Longitudinal;

(1 in. = 25.4 mm; #6 = 19 mm)

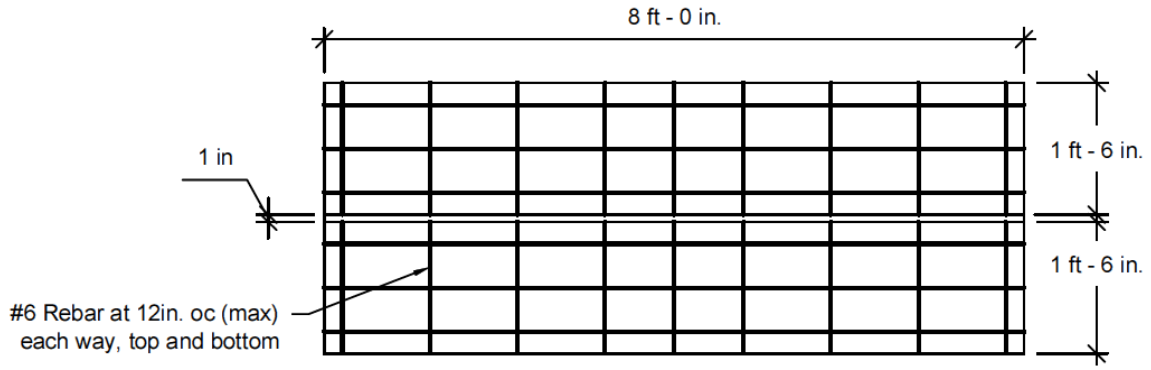

Figure 4.5: Composite Panel Dimensions (1 ft = 0.305 m; #6 = 19 mm)

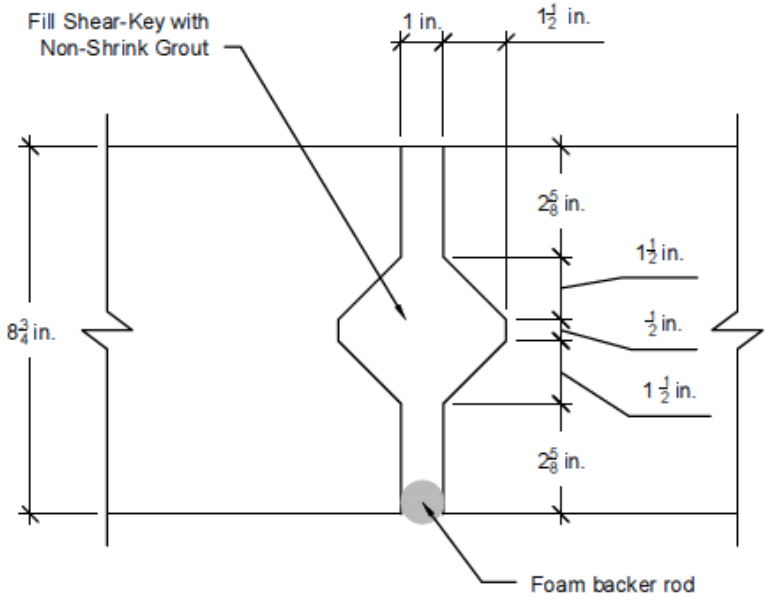

Figure 4.6: Grouted Pocket Dimension; (1 in. = 25.4 mm)

Figure 4.7: Elevation of Posttensioned 3 ft Composite Specimen Under Cyclic Loading;

(1 ft = 0.305 m)

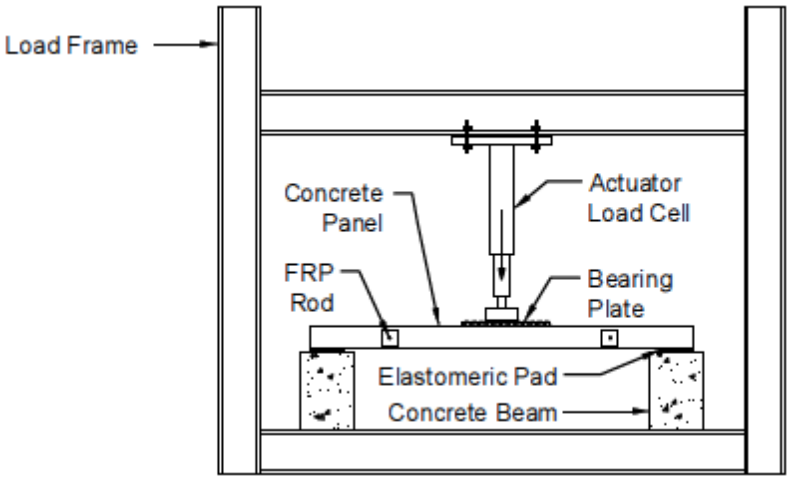

(a)

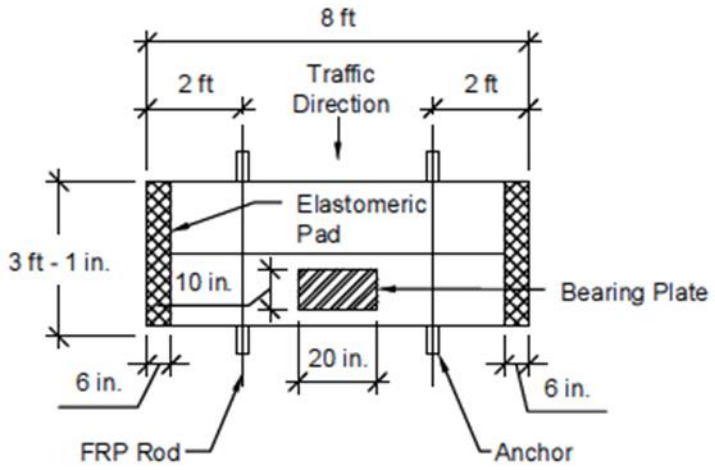

(b)

Figure 4.8: Testing Set Up for Type I and Type II Specimens; a) Elevation View of Testing Set Up, b) Plan View of Testing Set Up

(1 ft = 0.305 m; 1 in. = 25.4 mm)

Figure 4.9: Ponding Test Over Grouted Pocket After Cyclic Loading

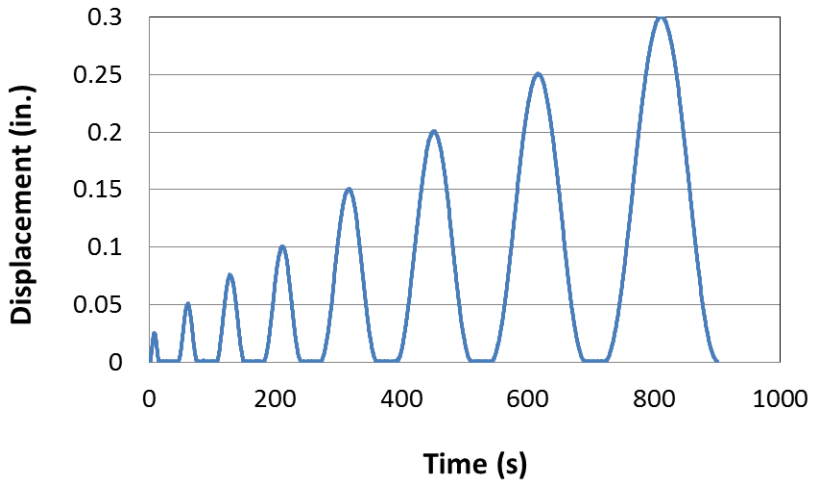

Figure 4.10: Precracking Loading Protocol for Type I and Type II Specimens;

(1 in. = 25.4 mm)

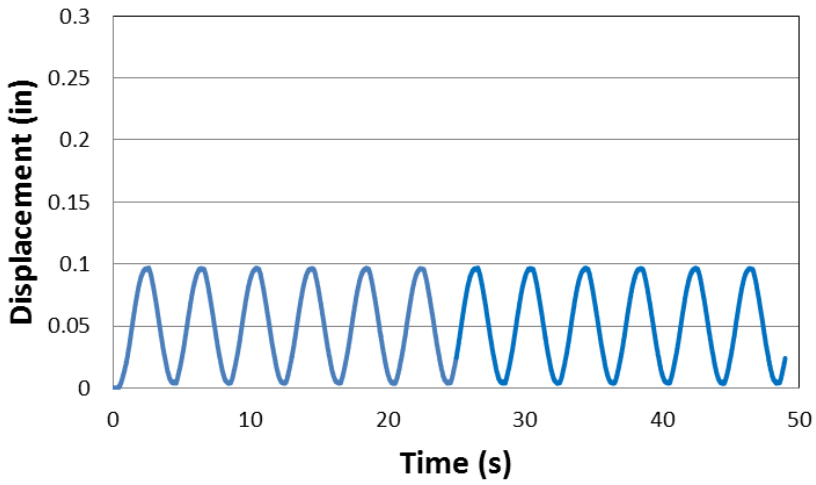

Figure 4.11: Sample of Day 1-Cyclic Protocol; (1 in. = 25.4 mm)

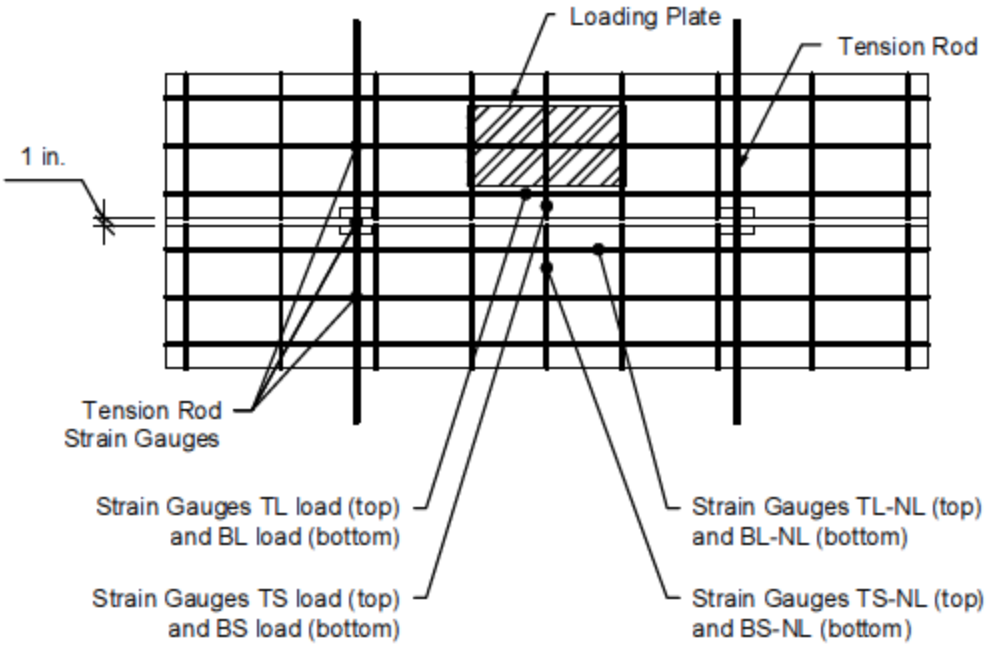

Figure 4.12: Strain Gauge Locations for Type I and II Specimens

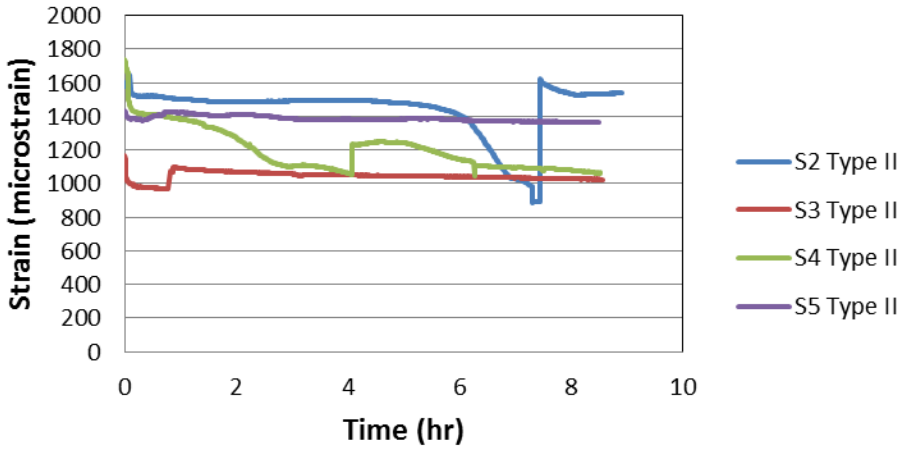

Figure 4.13: Maxiumum Strains During Testing for Day 5 Cyclic Loading

(a)

(b)

(c)

(d)

Figure 4.14: Concrete and Overlay Failure of Laboratory Specimens: (a) Type II TP1 Concrete Failure, (b) Type II TP2 Overlay Failure, (c) Type II MM1 Overlay Failure, (d) Type II PC1 Overlay Failure

CHAPTER 5

POSTTENSIONING OF PRECAST CONCRETE PANELS AT TRANSVERSE GROUTED DECK JOINTS WITH CFRP RODS

5.1 Abstract

Many states are implementing accelerated bridge construction (ABC) methods to reduce traffic delays due to bridge construction and increase safety at the construction site. One such method is the use of precast concrete full-depth panels to construct bridge decks. The grouted transverse joint between precast concrete deck panels is one of the most vulnerable elements of the bridge deck system. To extend the longevity of bridge decks it is imperative to improve the integrity of the grouted transverse joint. The focus of this paper is to compare the effect of different posttensioning levels on the initial performance, load capacity, and overall behavior of precast concrete panels at a grouted transverse deck joint. Nine composite specimens with grouted transverse joints were tested monotonically to failure. The tests consisted of three composite specimens without posttensioning, three composite specimens with 35 psi (241 kPa) posttensioning pressure, and three composite specimens with posttensioning pressure of 48.4 psi (334 kPa). Posttensioning was provided by fiber reinforced polymer (FRP) composite rods, because of their corrosion-resistant properties. In addition, two single concrete panels

were tested. It was found that the use of posttensioning increased both the initial and ultimate capacity of the composite specimens and changed the failure mode at the initial cracking load.

5.2 Introduction

Many states are implementing accelerated bridge construction (ABC) methods to reduce traffic delays and improve safety at bridge construction sites. One of these methods is the use of precast concrete full-depth panels for bridge deck construction. The panels are built and cured off-site and then placed on new or existing bridge girders. The benefits of the ABC method include reduction of time affecting traffic and road closures for bridge construction, and increased safety at the construction site.

Utah DOT is implementing a proposed design life for new bridges of 75 years. The life of a bridge depends on the life of its weakest component. The bridge deck is the weakest component of many bridges (Tadros et al., 1998). The grouted transverse joint between panels is the most vulnerable element for precast concrete full-depth panel bridge deck systems. Bridge deck panel performance depends on the behavior of the joint (Issa et al., 1995b). In order to improve the longevity of precast concrete bridge decks it is imperative to improve the integrity of the joint. The focus of this paper is to compare the effect of different posttensioning levels on the initial performance, load capacity, and behavior of precast concrete panels at a transverse deck joint. Posttensioning was achieved using carbon fiber reinforced polymer (CFRP) rods. CFRP rods have a major advantage for this application in that they are corrosion resistant.

5.3 Literature Review

The use of longitudinal posttensioning has two significant effects on the transverse joint between precast concrete panels in a bridge deck. First, it keeps the joint in compression, helping to prevent water leakage that occurs at the grouted joint. Second, by increasing the posttensioning pressure across the joint, the capacity of the joint increases. This allows higher live loads to transfer across the joint. The minimum AASHTO posttensioning stress is 250 psi (1724 kPa). The minimum posttensioning stress across the joint after losses used by the Utah DOT is 300 psi (Roberts, 2011).

Research has been performed on the amount of posttensioning required for the transverse joint. This research ranged from simple span to continuous span bridge decks and laboratory tests and finite element models. The majority of tests considered AASHTO HS-20 loading.

Laboratory tests and finite element modeling simulations on the amount of posttensioning required to keep the joint in compression were performed by Issa et al. (1998). Based on HS20-44 truck loading it was recommended that a minimum posttensioning stress of 200 psi (1379 kPa) should be used for simply supported conditions and positive moment sections at the midspan of continuous bridge decks. It was also recommended that a posttensioning stress of 450 psi (3103 kPa) be used at the interior support of continuous decks where negative moment occurs.

The capacity of the joint prior to initial cracking for posttensioned and non-posttensioned joints has been evaluated by several researchers. Kim et al. (2003) proposed the use of principal stress equations and tensile strength of the grout to predict the cracking strength of grouted joints. Static shear tests were performed on three

grouted joint specimens. The ratio between the calculated load at initial cracking and the tested value was found to range between 0.96 and 1.01.

Roberts (2011) compared the strength of posttensioned concave to concave joints, commonly referred to as female to female joints, from six tests with standard ACI shear capacity equations. These included the simplified concrete shear strength equation, the shear strength when axial load is applied, and the shear capacity of posttensioned members. The panels were posttensioned in the short direction, perpendicular to the grouted pocket. The shear strength of the posttensioned joint exceeded the calculated capacity for all three equations.

Swenty (2009) performed experimental and finite element analysis for posttensioning of the negative moment region of transverse bridge deck joints and the bond between the grouted joint material and the concrete deck. It was found that the joints posttensioned to 340 psi performed best and neither cracked nor leaked water. It was also found that blockouts with a roughened surface or those used an epoxy or grout equivalent to a particular grout used in testing performed well. It was recommended that the maximum design tension value should be limited to $1.5\sqrt{f'c}$, where f'c is the lowest of the grout and concrete compressive strength measured in psi located at the joint.

Bowers (2007) performed finite element modeling to determine the appropriate posttensioning level to keep the transverse joint in compression after creep and shrinkage losses. It was recommended that single span decks on steel girders and one, two, and three span precast decks on precast concrete girders use a posttensioning stress of 200 psi, while precast decks with two and three spans on steel girders required more posttensioning.

5.4 Experimental Research

Posttensioning of the transverse joint between precast concrete deck panels was provided by fiber reinforced polymer (FRP) composite rods. The authors are not aware of any other research using FRP posttensioned rods to posttension the transverse joint between precast concrete deck panels. The effect of different posttensioning levels on the initial cracking, ultimate capacity, and behavior of a grouted new female to female transverse joint for precast concrete panels is investigated. Nine grouted precast concrete composite specimens were tested monotonically to failure. Two monolithic precast concrete panels were also tested. The capacity and behavior of the joint was measured using strains in the bar and the CFRP rods, the applied force, and displacements.

5.4.1 Laboratory Tests

Nine grouted precast concrete composite specimens were tested monotonically to failure. The tests consisted of three composite specimens without any posttensioning (0A, 0B, and 0C), three composite specimens with the posttensioning force at 50% of the design tensile capacity of the posttensioning rods, or 35 psi (241 KPa) joint stress (35A, 35B, and 35C), and three composite specimens with the posttensioning force at 70% of the design tensile capacity of the posttensioning rods, or 48 psi (334 KPa) joint stress (48A, 48B, and 48C). In addition, two single precast concrete panels (SA and SB) were tested to failure. Table 5.1 summarizes the test matrix for this research. Single panels were 1 ft – 6 in. (0.46 m) wide, 8 ft (2.44 m) long and 8.75 in. (0.22 m) thick. Composite specimens are two single panels grouted together to construct a composite 3 ft (0.91 m) wide panel. Three-eighth inch diameter carbon FRP rods were used to stress the six

posttensioned composite specimens.

5.4.2 Precast Concrete Specimens

Precast concrete panels, as previously described in Chapter 4, were cast for this research at Hansen Eagle Precast, a PCI certified precast concrete plant. The 28 day concrete compressive strength of the panels was 11,000 psi (76 MPa). The average concrete compressive strength at the time of testing was 15,500 psi (107 MPa), which classifies these panels as high strength concrete. Panel dimensions and construction details are shown in Figures 4.4, 4.5 and 5.1. Figure 4.5 describes the composite panel dimensions. Figure 5.1 provides joint dimensions for the tested joint and the typical Utah DOT transverse joint. Figure 4.4 provides the reinforcement dimensions for the single panels used in the composite specimens. The panels were reinforced with nine #6 grade 60 steel bars at the top and bottom of the panel spaced at 12 in. (305 mm) on center. The composite specimens were grouted with a new female to female joint, as shown in Figure 5.1(a). This detail increases the concrete thickness above and below the joint compared to the typical female to female joint used by the Utah DOT shown in Figure 5.1(b). Six of the composite specimens were posttensioned before testing with 3/8 in. (9.524 mm) Carbon FRP rods, having a modulus of elasticity of 22,500 ksi (155,000 MPa) and a maximum design tensile strength of 27.5 kip (122.3 kN). Tensile tests by Burningham et al. (2014) for the CFRP rods used in the present research showed that the CFRP rods failed at a load range of 29.6 to 41.5 kips, corresponding to a true anchor efficiency of 108% to 151% based on the CFRP design strength. The tensile modulus of elasticity of the CFRP rods was measured as 22,500 ksi, which matches the manufacturer's design

recommendation. The grout had an average compressive strength of 4,500 psi (31 MPa), with a maximum recorded strength of 5,000 psi (34 MPa). Prior to posttensioning all panels had been precracked due to previous cyclic testing, which induced minor hairline cracks to simulate in-situ conditions.

5.4.3 Test Setup

A load frame with a 500 kip (2224 kN) hydraulic actuator was used to apply a monotonic displacement-controlled load under simple span conditions for all specimens. The concrete panels were supported on elastomeric pads as shown in Figure 4.8. An electronic data acquisition system was used to record strains in the rebar and CFRP posttensioning rods, and deflections during loading protocols. Loading was applied over a 10 in. by 20 in. (254 mm by 508 mm) area at the center of the single precast concrete panel, as specified in AASHTO (2012). The load on the composite specimens was applied at the center of one of the halves as shown in Figure 4.8. The posttensioned panels were stressed with 3/8 in. (9.525 mm) carbon fiber rods before loading. Figure 5.2 shows typical loading conditions for composite posttensioned specimens. In this figure, the anchors for the two posttensioned CFRP rods can be clearly seen. These were developed in earlier research by Burningham et al. (2014).

5.4.4 Instrumentation

Linear variable differential transformers (LVDTs) were placed on the underside of the specimen to measure vertical displacements along the centerline of each half, as shown in Figure 5.2. Several strain gauges were applied to the reinforcing steel of each

composite specimen. The strain gauges were located at the center of the top and bottom reinforcing longitudinal bars adjacent to the grouted pocket and on the adjacent transverse bars as shown in Figure 4.12. Additional strain gauges were attached to the CFRP posttensioning rods to measure the strain in the rods during loading. Three gauges were placed on each rod, two at the quarter points and one at midspan.

5.5 Experimental Evaluation

Figure 5.3 shows a comparison of the behavior of the joint of the composite specimens at different stages of loading. Figure 5.4 shows a comparison of the ultimate failure for the single and composite specimens. The non-posttensioned composite specimens had three major cracks: an initial crack at the bond interface, additional cracking at the joint, due to bending stresses between the panels, and a diagonal tension crack of the single loaded panel side of the specimen at failure. Several of the specimens had flexural failure; these are shown in Figures 5.3(a), 5.3(d) and 5.4(b). The posttensioned panels had two major cracks: an initial shear crack at the joint due to monolithic behavior of the panels, as shown in Figures 5.3(b) and 5.3(c), and a diagonal tension crack of the single loaded panel side of the specimen at failure, as shown in Figures 5.4(c) and 5.4(d). The state of the joint at the ultimate capacity is shown in Figures 5.3(e), 5.3(f), and 5.3(g). These are a continuation of the initial cracking load but not the cause of the ultimate failure. The use of posttensioning changed the failure mechanism at the initial cracking load. This indicates that the posttensioning stress was sufficient to overcome bond failure and that the joint bond capacity depends on the posttensioning stress. The ultimate failure of the specimens was similar for all tests and

occurred on the loaded panel, indicating that after the initial cracking load the panels no longer acted as a single specimen but essentially as separate panels.

During testing, several posttensioning rods failed. Figure 5.5 shows the failure of a single posttensioning rod. The rods failed at or near the anchoring system. This occurred after the initial cracking load and was caused by rotation at the end faces due to transverse bending of the specimen.

Figure 5.6 shows the force vs. displacement curves for each of the specimens. All the composite specimens had an initial cracking load and an ultimate load capacity. The initial cracking load refers to the load at the first significant crack in the joint, which caused an initial drop in capacity. After the ultimate load capacity the specimens experienced either a flexural or a shear failure of the loaded single panel. Table 5.2 summarizes the initial and ultimate load capacity of the specimens.

Single panels had an ultimate load capacity of 51 kip (227 kN). After the ultimate load capacity the specimens experienced either a flexural or a shear failure.

The non-posttensioned composite specimens had an initial drop in capacity at a displacement of 0.3 in. (7.6 mm) to 0.44 in. (11.2 mm) corresponding to an initial cracking load of 37.7 kip (168 kN) to 54.5 kip (242 kN). At this time the specimen developed an initial significant crack as shown in Figure 5.4(a). The ultimate capacity ranged from 60.5 kip (269 kN) to 64.3 kip (286 kN).

The 35 psi posttensioned composite specimens experienced initial cracking at 0.6 in. (15 mm) to 0.7 in. (18 mm) corresponding to an initial cracking load of 69.8 kip (311 kN) to 73 kip (325 kN). At this time the specimens developed an initial significant crack as shown in Figure 5.4(b). The ultimate capacity ranged from 79.3 kip (353 kN) to 89.3

kip (397 kN).

The 48 psi posttensioned composite specimens had an initial drop in capacity at 0.9 in. (23 mm) corresponding to an initial cracking load of 78.4 kip (349 kN). At this stage the specimen developed an initial significant crack as shown in Figure 5.4(c). The ultimate capacity was 80 kip (356 kN). All composite panels had similar force vs. displacement slope prior to the initial cracking load.

The composite specimens had the failure at the ultimate capacity occurring on the single loaded panel and had a larger ultimate load capacity than that of the single panels tested by 13 to 39 kip (58 to 173 kN). The ultimate load capacity of the composite specimens was larger than the initial cracking load. For the non-posttensioned composite specimens this ranged from an 11 to 70% increase of capacity from the initial cracking load. This ranged from an 11 to 24% increase for the 35A, 35B and 35C posttensioned panels and a 0 to 18% increase for the 48A, 48B and 48C posttensioned panels. This indicates that after the initial significant crack there was additional load transfer across the joint. The ultimate capacity of the joint was due to the shear and flexural capacity of the single loaded panel and not the capacity of the joint.

Figures 5.7 through-5.10 show typical strain vs. displacement graphs for the composite specimens. Figure 5.7 is the measured strain at the center of the top longitudinal steel reinforcement on the loaded side adjacent to the joint. The strain in the top steel reinforcing bars prior to the initial cracking load was similar for the different specimens. This strain is tensile indicating that the neutral axis is above the top steel reinforcement. Figure 5.8 is the measured strain at the center of the bottom longitudinal reinforcement on the loaded side adjacent to the joint. The strain in the bottom steel

reinforcing bars prior to the initial cracking load was similar for the different specimens. The strain of 2,000 microstrains were found in the bottom longitudinal bars prior to the initial cracking load of the posttensioned panels, indicating that the bottom reinforcement yielded prior to joint failure. Figure 5.9 is the measured strain at the center of the top longitudinal reinforcement on the nonloaded side adjacent to the joint. All the recorded strains were less than 400 microstrains prior to the initial cracking load, indicating minimal steel strain. These strains were tensile in nature, indicating the neutral axis was located above the top reinforcement. The tensile strains on the top reinforcement correspond to the neural axis located above the top reinforcing steel and adding additional tensile loads in the grout along the transvers joint.

The top rebar for the single panels yielded at a displacement of 1.28 in. (33 mm). The top rebar for the composite specimens, were in tension, however, it did not yield. The bottom reinforcement on the loaded side yielded at a displacement of 0.33 in. (8 mm) to 0.45 in. (11 mm) for the composite specimens. Figure 5.10 shows the average strain in the CFRP posttensioning rods for the 35 psi (241 kPa) and 48 psi (331 kPa) posttensioned specimens. Several of the rods failed at or below the ultimate tensile strain due to bending induced by vertical and rotational deformations between the panel end faces, which included vertical shear forces near the joint. Prior to the initial cracking load at the joint the strain in the CFRP posttensioning rods was constant. An increase in CFRP rod strain occurred after the initial cracking of the joint, indicating that plane sections no longer remained plane and a different deflection behavior of the panels across the joint occurred after the joint failed. Prior to the initial significant crack the panel behaved monolithically. However, after the initial significant crack of the transverse

joint the composite specimens behaved like two separate panels jointed together at a plastic hinge along the transverse joint.

Figures 5.11 through 5.15 are the measured strains on the reinforcing steel for the composite specimens. Bottom longitudinal nonloaded (BL NL) corresponds to the strain on the bottom longitudinal steel reinforcement adjacent to the joint on the nonloaded panel. Bottom longitudinal loaded (BL Load) corresponds to the strain on the bottom longitudinal steel reinforcement adjacent to the joint on the nonloaded panel. Top longitudinal nonloaded (TL NL) corresponds to the strain on the top longitudinal steel reinforcement adjacent to the joint on the nonloaded panel. Top longitudinal loaded (TL Load) corresponds to the strain on the Top longitudinal steel reinforcement adjacent to the joint on the nonloaded panel. Left tendon (L Tendon) and right tendon (R Tendon) correspond to the CFRP rods on the left and right side of the specimen. Tendon A and Tendon B refer to the strain gauge located at the quarter and center point.

Figure 5.11 is the recorded bottom longitudinal reinforcement strain for Specimen 0C. Prior to the initial joint cracking load the top reinforcement strains were similar for the loaded and nonloaded panels. After the initial cracking load the top reinforcement for the nonloaded panel had a drop of measured strain. This indicates a change of deflection behavior across the joint after the initial cracking load. Figure 5.12 shows the recorded strains for top and bottom longitudinal steel bars for Specimen 35A. Figure 5.13 shows the recorded strains for CFRP posttensioning rods for Specimen 35A. Figure 5.14 shows the recorded strains for top and bottom longitudinal steel bars on the loaded panel for Specimen 48C. Figure 5.15 shows the recorded strains for CFRP posttensioning rods for Specimen 48C. Prior to the initial cracking load the bottom steel reinforcement for all the

composite specimens had similar strain and displacement relationship regardless of posttensioning level. The strain in the posttensioning rods increased after the initial crack. These observations indicate that the specimens behaved as a uniform panel prior to the initial loading crack.

The use of posttensioning increased the initial cracking load by 58% to 65% and the ultimate capacity by 28% to 34% of the joint with no posttensioning. The increase of average posttensioning stress between 35 psi (241 kPa) to 48 psi (331 kPa) corresponding to 50% and 70% of the CFRP rod design ultimate capacity for the two rods, did not affect the ultimate capacity but had a slight increase of the initial cracking load. This is due to the fact that the panels and grout behave as a weak link system. The weakest portion of the non-posttensioned panels was the bonded interface between the grout and the concrete. The use of posttensioning was sufficient to overcome the bond failure, leaving the weakest component of the joint as the tensile capacity of the grout and concrete, which acts as a monolithic member. An increase of posttensioning stress from 35 psi (241 kPa) to 48 psi (331 kPa) is not sufficient to have a large effect on the increase in the tensile capacity of grout and concrete.

Figures 5.16 and 5.17 compare the center displacement on the loaded and nonloaded side of the composite specimens. Figure 5.16 provides a comparison of the center deflection for the loaded and nonloaded side on the 35 psi (241 kPa) specimens. The displacement behavior prior to the initial significant cracking of the joint was similar for the loaded and the nonloaded side. Figure 5.17 provides a comparison of the center displacement of the loaded vs. the nonloaded side of the panels during testing. The relationship between the displacements of the loaded and the nonloaded side was linear

prior to the initial significant joint crack, where a decrease in the vertical displacement on the unloaded side occurred. This initial relationship indicates that minimal to no vertical uplift occurred at the boundaries on the unloaded side prior to the initial significant crack, which is consistent with the actual boundary conditions found in bridge construction. After the initial significant crack, vertical uplift occurred at the boundaries on the unloaded side of the tested specimens. This differs from the actual boundary conditions found in bridge construction which restrains uplift of the panel at the connection to the bridge girder.

5.5.1 Comparison with AASHTO HL-93 Tire Loading

The AASHTO HL-93 truck tire load, of 16 kips (71 kN), was adjusted to determine the required capacity of the joint under the loading conditions provided. The load combination factor, γ_p, of 1.75 was applied for Strength I limit state load combinations. An importance factor, η_I, of 1.05 was applied for worst case conditions. A ductility factor, η_D, of 1.05 was applied due to the brittle nature of the failure modes. The redundancy factor, η_R, of 1.0 was applied. The factor φ of 0.9 was applied due to the shear failure of the grout and concrete at the joint. The required capacity of the joint under the testing conditions was 34.3 kips (153 kN). All specimens tested had an initial cracking capacity larger than the required AASHTO capacity for the HL-93 truck tire.

The average initial cracking load of the non-posttensioned panels was 32% larger than the factored AASHTO design HL-93 truck tire load, of 34.3 kips. This ranged from 109% to 128% for the average 35 psi and 48 psi posttensioned. The tested single panels had a capacity 50% larger than HL-93 truck tire load. The tested panels have a capacity

higher than the ASHTO required capacity for the given loading conditions, indicating an acceptable joint configuration for the HL-93 truck tire concentrated loading.

To account for the equivalent dynamic or impact truck tire load due to uneven deck surfaces for the design static capacity, the HL-93 truck tire load of 34.3 kips (153 kN) is multiplied by a dynamic load factor of 1.75 for the transverse joint. This provides an equivalent impact truck tire load of 60 kips (267 kN).

To account for the equivalent design fatigue load of the truck tire for 100 million cycles for the design static capacity, the fatigue truck tire load is multiplied by 7 (Bae et al., 2011). This provides an equivalent design fatigue load of 97 kips (431 kN).

As shown in Table 5.3, the non-posttensioned specimens had an average capacity that was 24% and 53% less than the equivalent impact and fatigue truck tire loads. The use of posttensioning was sufficient to overcome the required equivalent impact load by 19 to 30%. The minimal level of posttensioning was not sufficient to overcome the equivalent fatigue load.

5.6 Conclusions and Recommendations

Laboratory tests were carried out on nine precast concrete composite specimens to determine the effects of posttensioning on the grouted transverse joint. Several conclusions can be drawn from this study.

1) When the grout strength of the grouted transverse joint between precast bridge deck panels is lower than the panel concrete strength, the initial significant crack occurs in the grout or bond region and dictates the initial cracking load and ultimate load capacity of the system.

2) The use of posttensioning increased the initial cracking load by 58% to 65% and the ultimate capacity by 28% to 34% of the joint with no posttensioning.
3) There are different modes of initial joint failure, these include bond failure between the grout and the concrete, and tensile failure of the grout. The initial mode of failure for the non-posttensioned panels was the bond failure between the grout and concrete deck. The use of posttensioning was sufficient to overcome bond failure between the grout and the concrete, but not sufficient to overcome shear or tensile failure of the grout. An increase of the posttensioning stress from 35 psi (241 kPa) to 48 psi (331 kPa) was not sufficient to have a large effect on the increase the shear capacity of grout and concrete.
4) Composite specimens behave as monolithic members prior to the initial joint cracking load. The initial joint cracking load occurred prior to bottom reinforcement yielding for all composite specimens. These two observations indicate that the design capacity of the deck system may be determined through monolithic deck assumptions; however, the initial cracking load capacity of the joint may govern the design capacity of the concrete deck system.
5) The composite panels behave monolithically under typical design truck loads. All specimens tested had an initial cracking capacity larger than the required AASHTO capacity for the HL-93 truck tire. The initial cracking load of the non-posttensioned panels was 10% to 59% larger than the required factored AASHTO design HL-93 truck tire load capacity, of 34.3 kips. This ranged from 103% to 113% for the 35A, 35B, and 35C posttensioned panels and 98% to 129% for the 48A, 48B, and 48C posttensioned panels.

6) There is additional load transfer across the joint after the initial significant crack. The ultimate load for the composite specimens was 2 to 70% larger than the initial significant crack and was 17 to 73% larger than the initial cracking load of the composite specimens. The failure at the ultimate load capacity for the composite specimens occurred on the single loaded panel and had a larger ultimate load than that of the single panels tested.
7) The use of CFRP rods was beneficial in the posttensioning across the transverse joint of precast bridge deck panels.

Additional research should be done for higher posttensioning stress values than those used in this research.

5.7 References

American Association of State Highway and Transportaion Officials (AASHTO). (2012). AASHTO LRFD Bridge Design Specifications. *AASHTO*. Washington D.C.

Bae, H., Oliva, M. G., & Bank, L. C. (2011, September-October). Reinforcement Free Decks using Modified Strut and Tie Model. *ACI Structural Journal*, 108 (5), 562-571

Bowers, S. E. (2007). Recommendations for Longitudinal Post-Tensioning in Full-Depth Precast Concrete Bridge Deck Panels. *Master's Thesis*. Blacksburg, Virginia: Virginia Polytechnic Institute and State University.

Burningham, C. A., Pantelides, C. P., & Reaveley, L. D. (2014). New Unibody Clamp-Anchors for Post-tensioning Carbon Fiber Reinfocred Polymer Rods. *PCI Journal*, 59 (1), 103-113.

Hanna, K. E., Morcous, G., & Tadros, M. K. (December 2010). *Second Genration Precast Deck Panel (NUDECK) System*. University of Nebraska, Lincoln. Lincoln, Nebraska: Nebraska Department of Roads.

Issa, M. A., Idriss, A.-T., Kaspar, I. I., & Khayyat, S. Y. (1995, January-February). Full Depth Precast and Precast, Prestressed Concrete Bridge Deck Panels. *PCI Journal*, 40, 59-80.

Issa, M. A., Ribeiro do Valle, C. L., Islam, S., Abdalla, H. A., & Issa, M. A. (2003, July-August). Performance of Transverse Joint Grout Materials in Full-Depth Precast Concrete Bridge Deck Systems. *PCI Journal*, 48, 2-13.

Issa, M. A., Yousif, A. A., Issa, M. A., Kaspar, I. I., & Khayyat, S. Y. (1995, May-June). Field Performance of Full-Depth Precast Concrete Panels in Bridge Deck Reconstruction. *PCI Journal*, 40, 82-108.

Issa, M. A., Yousif, A. A., Issa, M. A., Kaspar, I. I., & Khayyat, S. Y. (1998, January-February). Analysis of Full Depth Precast Concrete Bridge Deck Panels. PCI Journal, 43, 74-85.

James, P. H. (2012). Finite Element Modeling of Full Depth Precast Concrete Bridge Deck Connections in Bending and Shear. *Master's Thesis*, Utah State University.2012

Julander, J. (2009). Finite Element Modeling of Full Depth Concrete Transverse Bridge Deck Connections. *Master's Thesis*, Utah State University, 2009

Kim, Y.-C., Shin, S., & Park, J.-J. i. (2003). Shear and Fatigue Strength of Grout-Type Transverse Joints. *Canadian Journal of Civil Engineering*, 607-614.

Porter, S. D. (2009). Laboratory Testing of Precast Bridge Deck Panel Transverse Connections for Use in Accelerated Bridge Construction. *Master's Thesis*, Utah State University. 2009

Roberts, K. S. (2011). Performance of Transverse Post-Tensioned Joints Subjected to Negative Bending and Shear Stresses of Full Scale, Full Depth, Precast Concrete Bridge Deck Systems. *Master's Thesis*, Utah State University. 2011

Swenty, M. K. (2009). The Investigatin of Transverse Joints and Grouts on Full Depth Concrete Bridge Deck Panels. *PhD Dissertation*. Blacksburg, Virginia: Virginia Polytechnic Institute and State University. 2009

Wells, Z. B. (2012). Peformance of Post-Tensioned Curved-Strand Connections in Transverse Joints of Precast Brigde Decks. *Master's Thesis*, Utah State University. 2012

Table 5.1: Posttensioning Test Matrix

Specimen Name	Specimen Size	Posttensioning Force (kips)
SA	1'-6"x 8'-0" Single Specimen	0
SB	1'-6"x 8'-0" Single Specimen	0
0A	3'-1"x 8'-0" Composite Specimen	0
0B	3'-1"x 8'-0" Composite Specimen	0
0C	3'-1"x 8'-0" Composite Specimen	0
35A	3'-1"x 8'-0" Composite Specimen	26
35B	3'-1"x 8'-0" Composite Specimen	26
35C	3'-1"x 8'-0" Composite Specimen	26
48A	3'-1"x 8'-0" Composite Specimen	36
48B	3'-1"x 8'-0" Composite Specimen	36
48C	3'-1"x 8'-0" Composite Specimen	36

Table 5.2: Tested Joint Capacity

Tested Specimen Name	Tested Values					
	Load at Initial Significant Crack (kips)	Displacement at Intial Crack (in.)	Load after Initial Significant Crack (kips)	Difference in Load (kips)	Ultimate Load (kips)	Total Post Tensioning Force (kips)
SA	NA	NA	NA	NA	51.0	NA
SB	NA	NA	NA	NA	52.0	NA
0A	54.5	0.5	44.1	10.4	60.5	0
0B	43.7	0.3	40.4	3.3	61.1	0
0C	37.7	0.3	32.8	4.9	64.3	0
35A	69.8	0.7	63.0	6.8	79.3	27.2
35B	72.0	0.6	63.3	8.7	89.3	28
35C	73.0	0.7	66.4	6.6	81.4	29.1
48A	78.1	0.9	70.3	7.8	78.1	37.7
48B	68.0	0.6	63.6	4.4	80.1	37.7
48C	78.4	0.9	77.3	1.1	80.0	38

Table 5.3: Average Tested and Required AASHTO Values

Average Joint Post Tensioning Stress (psi)	Average Tested Load at Initial Significant Crack (kips)	Factored AASHTO HL-93 Truck Tire Load (kips)	Percent Difference (%)	Factored DYNAMIC AASHTO HL-93 Truck Tire Load (kips)	Percent Difference (%)	Factored AASHTO Fatigue Truck Tire Load (kips)	Percent Difference (%)
0	45.3	34.3	32	60.0	-24	97.0	-53
35	71.6	34.3	109	60.0	19	97.0	-26
48	78.3	34.3	128	60.0	30	97.0	-19

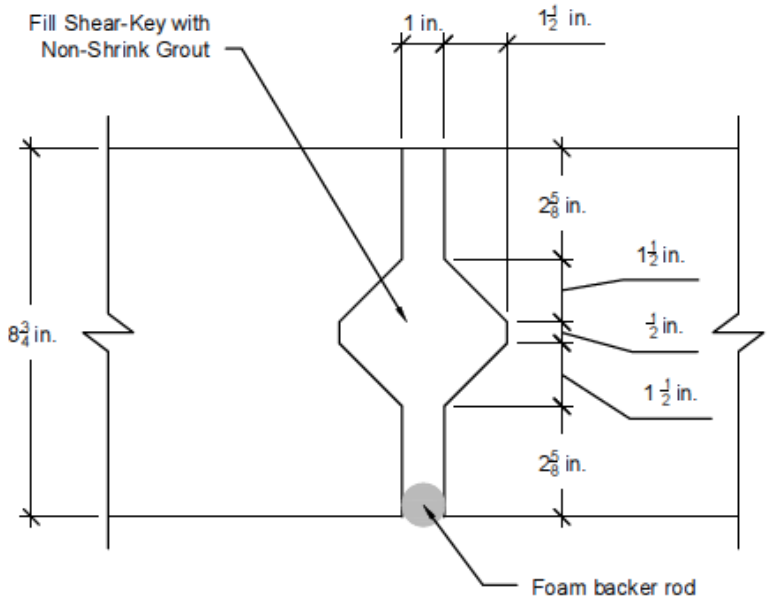

(a)

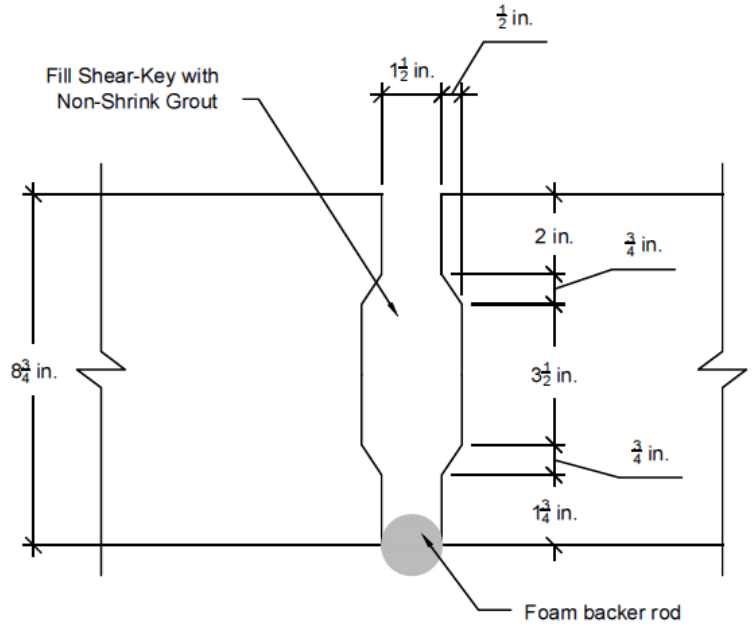

(b)

Figure 5.1: Grouted Joint Dimension: (a) New joint Used in Testing (b) Typical Utah DOT Joint (1 in. = 25.4 mm)

Figure 5.2: Posttensioned 3 ft Composite Specimen Under Cyclic Loading; (1 ft = 0.305 m)

(a)

(b)

(c)

(d)

(e)

(f)

(g)

Figure 5.3: Cracking Behavior of the Joint of the Composite Specimens: (a) Initial Crack of Non-Posttensioned Specimen, (b) Initial Crack of 35 psi Posttensioned Specimen, (c) Initial Crack of 48 psi Posttensioned Specimen, (d) Second Crack of Non-Posttensioned Specimen, (e) Joint Cracks after Ultimate Load for Non-Posttensioned Specimen, (f) Joint Cracks after Ultimate Load of 35 psi Posttensioned Specimen, (g) Joint Cracks after Ultimate Load of 48 psi Posttensioned Specimen

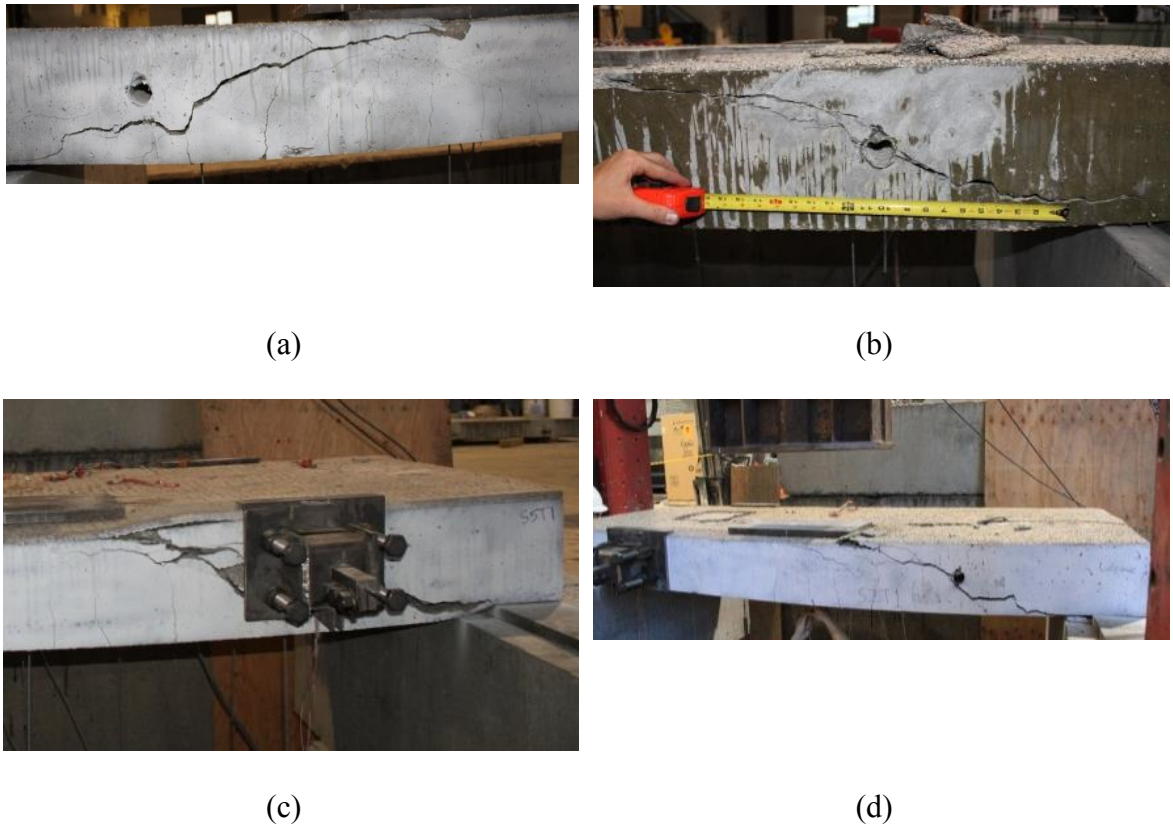

(a) (b)

(c) (d)

Figure 5.4: Ultimate Failure of Tested Specimens: (a) Final Crack of Single Panel, (b) Final Crack of Non-Posttensioned Composite Specimen at Ultimate Load, (c) Final Crack of 35 psi Posttensioned Composite Specimen, (d) Final Crack of 48 psi Posttensioned Composite Specimen at Ultimate Load

Figure 5.5: Failure of CFRP Posttensioning Rod

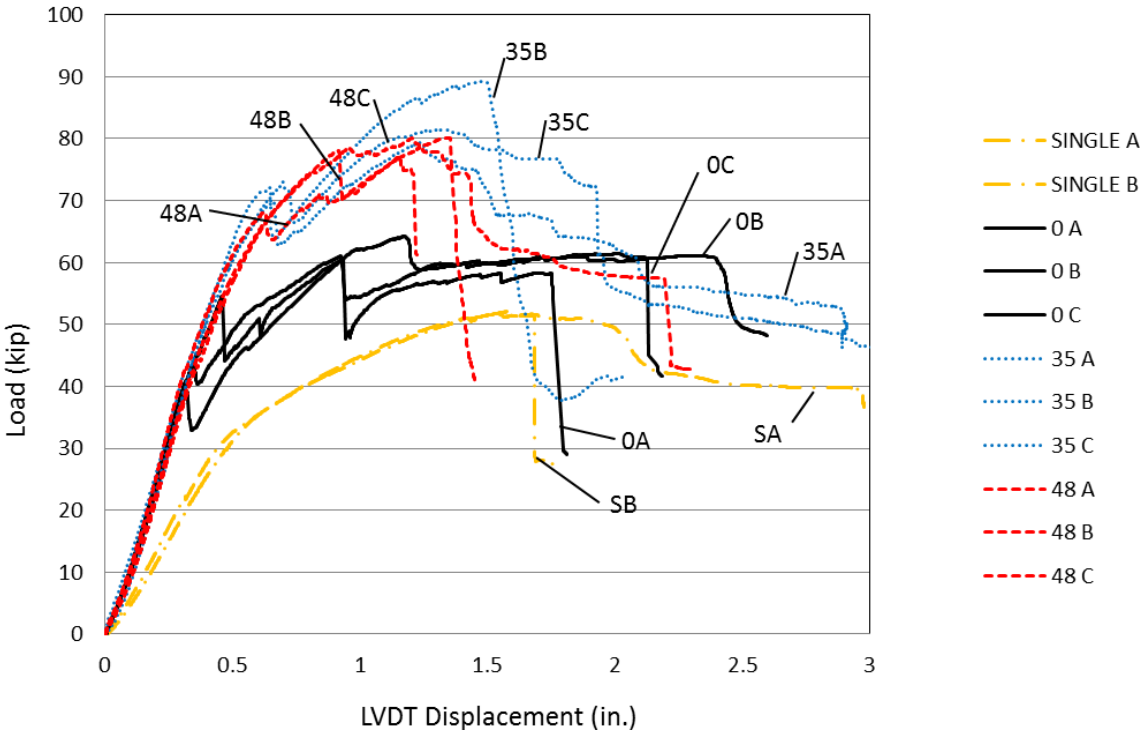

Figure 5.6: Tested Force vs. Displacement Graphs (1 in. = 25.4 mm, 1 kip = 4.44 kN)

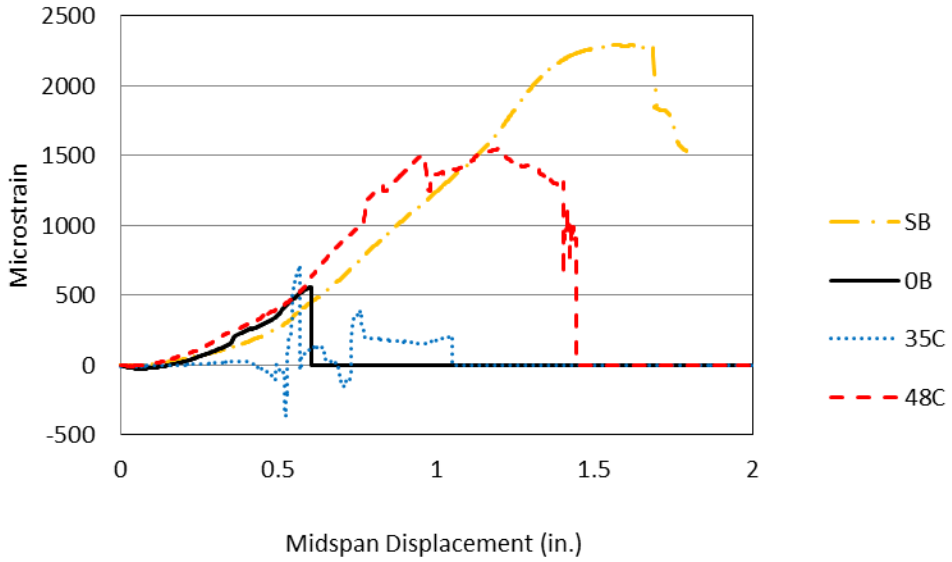

Figure 5.7: Strain vs. Displacement for Top Longitudinal Rebar on Loaded Side

(1 in. =25.4 mm)

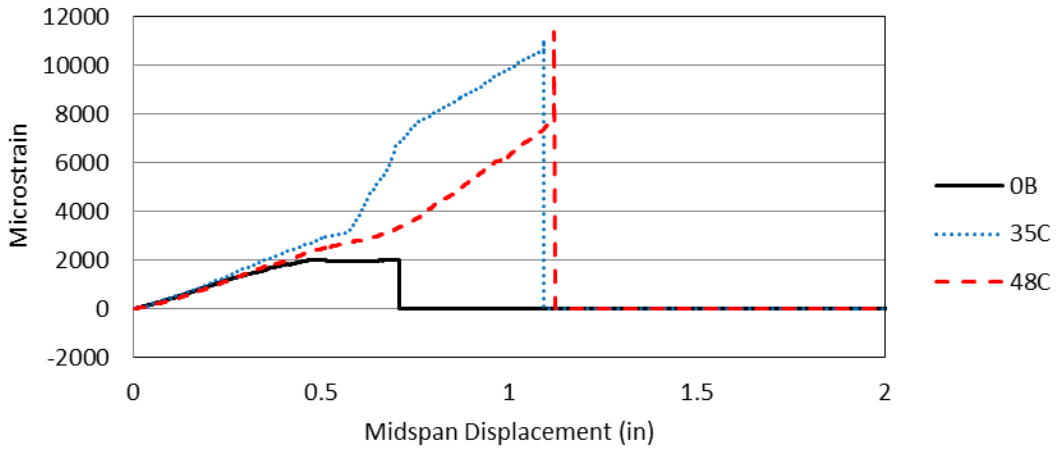

Figure 5.8: Strain vs. Displacement for Bottom Longitudinal Rebar on Loaded Side

(1 in. = 25.4 mm)

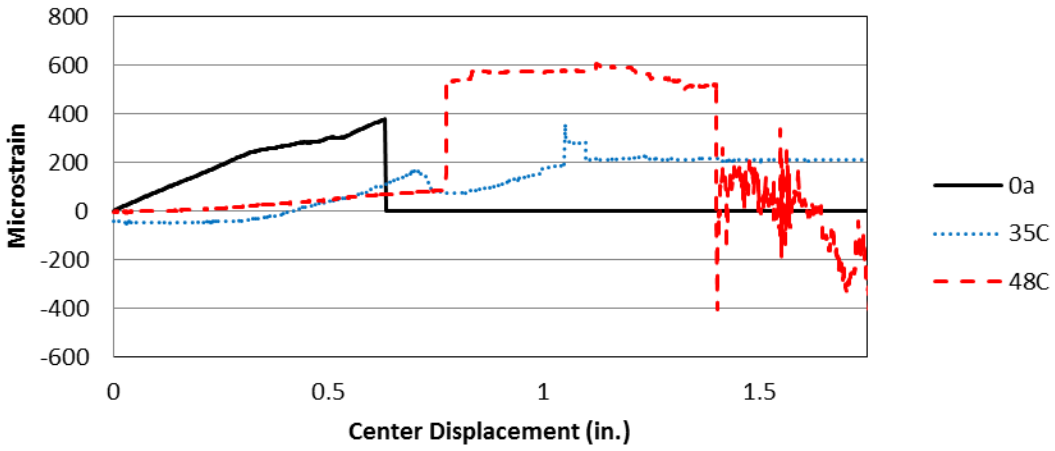

Figure 5.9: Strain vs. Displacement for Top Longitudinal Rebar on Nonloaded Side

(1 in. = 25.4 mm)

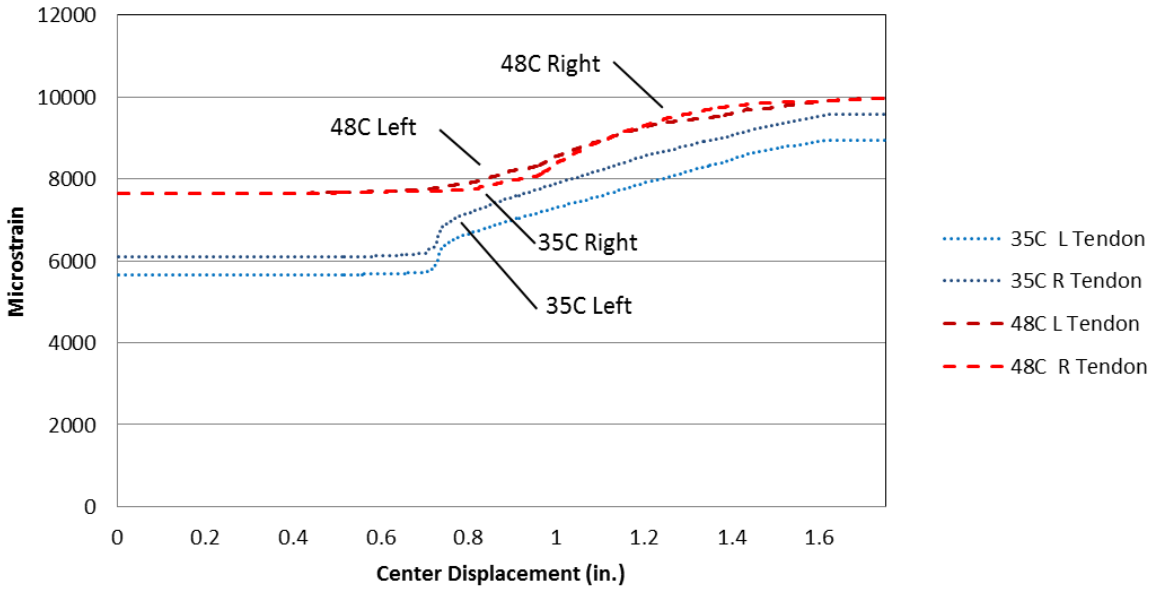

Figure 5.10: Strain vs. Panel Displacement for Posttensioning CFRP Rod

(1 in. =25.4 mm)

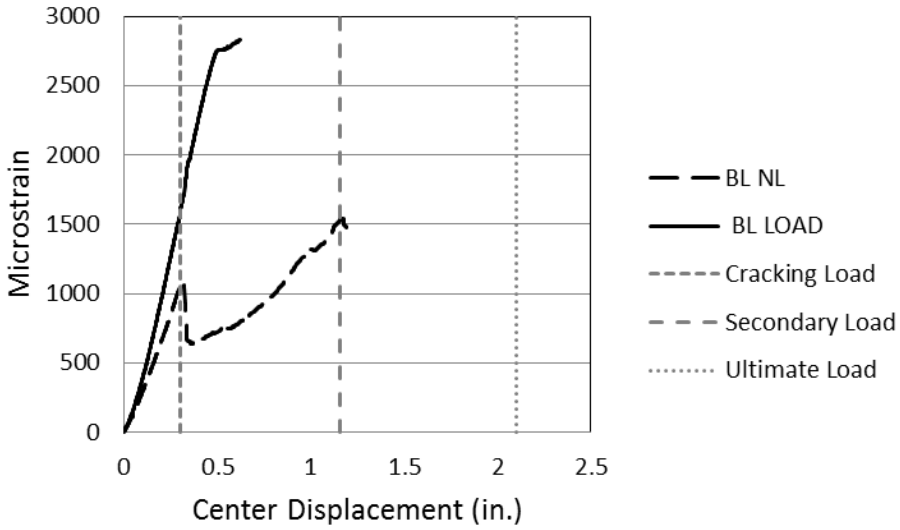

Figure 5.11: Bottom Longitudinal Rebar Strain vs. Panel Displacement for Non-Posttensioned Composite Specimen 0C

(1 in. = 25.4 mm)

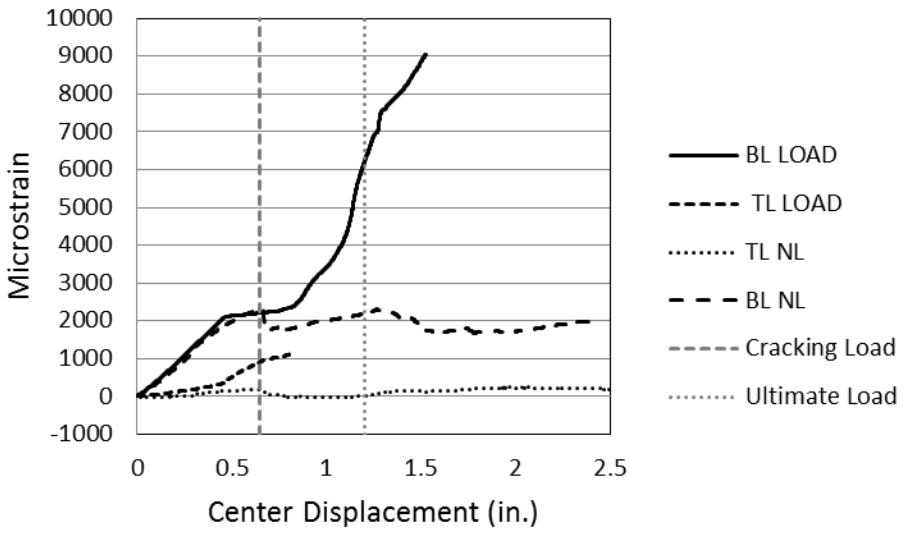

Figure 5.12: Longitudinal Steel Reinforcement Strain vs. Panel Displacement for 35 psi Posttensioned Composite Specimen 35A

(1 in. =25.4 mm)

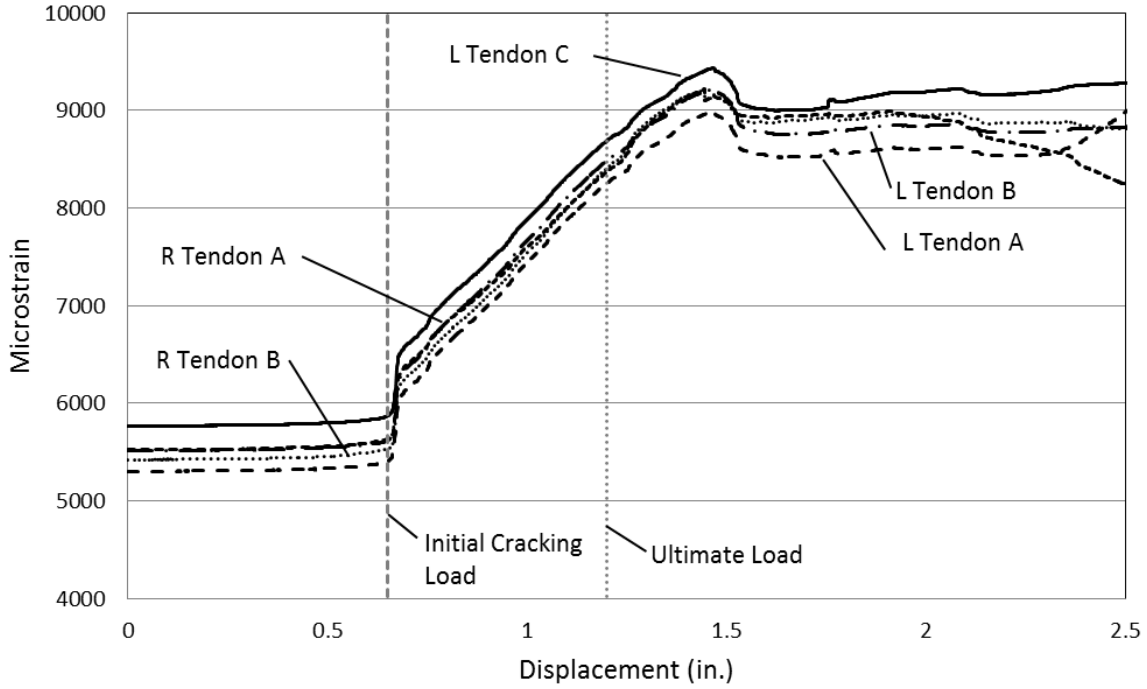

Figure 5.13: CFRP Tendon Strain vs. Panel Displacement for 35 psi Posttensioned Composite Specimen 35A

(1 in. = 25.4 mm)

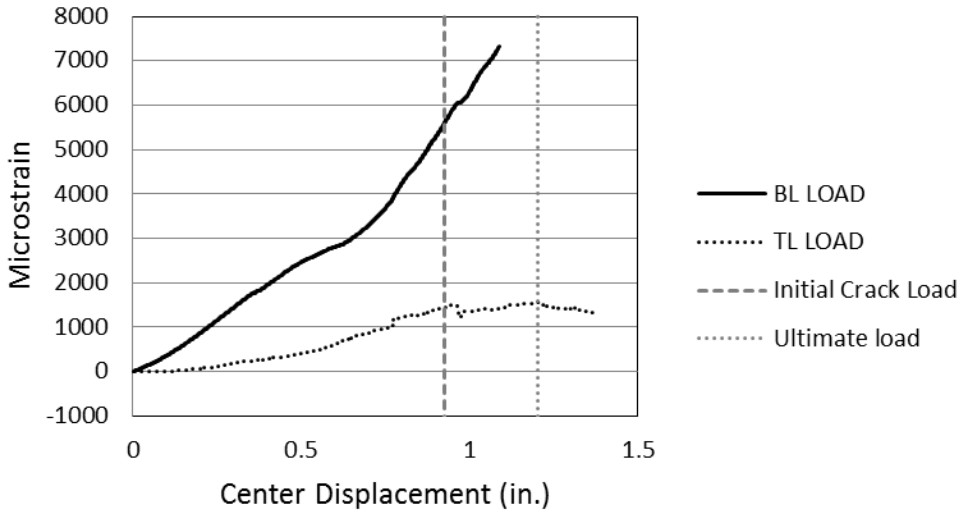

Figure 5.14: Longitudinal Steel Reinforcement Strain vs. Panel Displacement for 48 psi Posttensioned Composite Specimen 48C (1 in. = 25.4 mm)

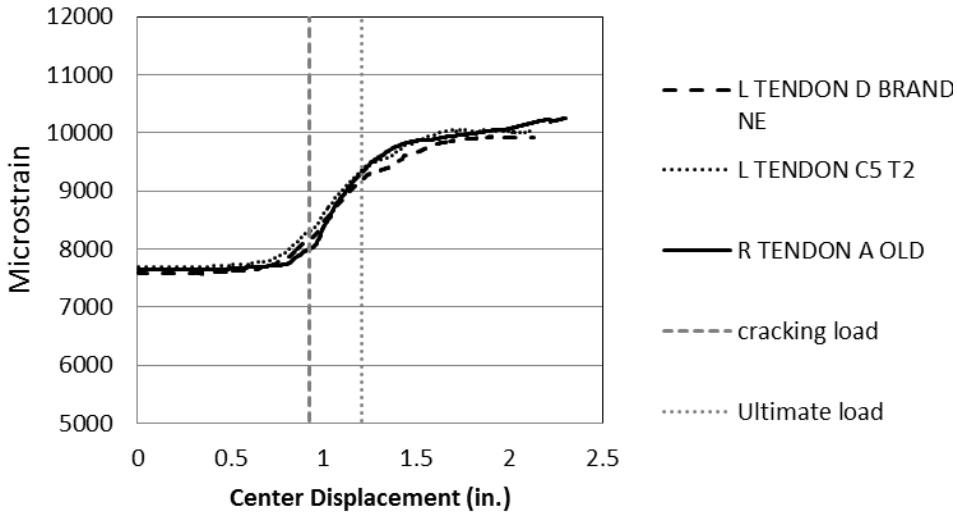

Figure 5.15: CFRP Tendon Strain vs. Panel Displacement for 48 psi Posttensioned Composite Specimen 48C (1 in. = 25.4 mm)

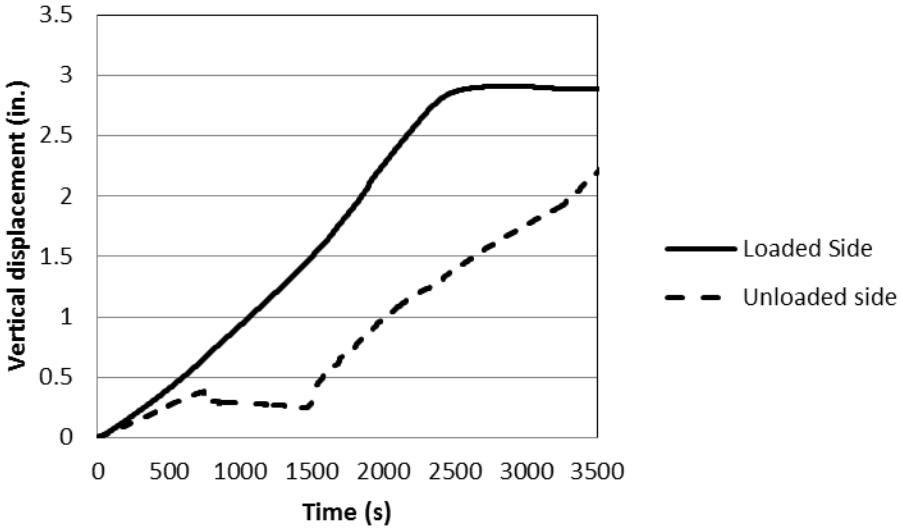

Figure 5.16: Panel Displacement vs. Testing Time for 35 psi Posttensioned Composite Specimen 35A (1 in. =25.4 mm)

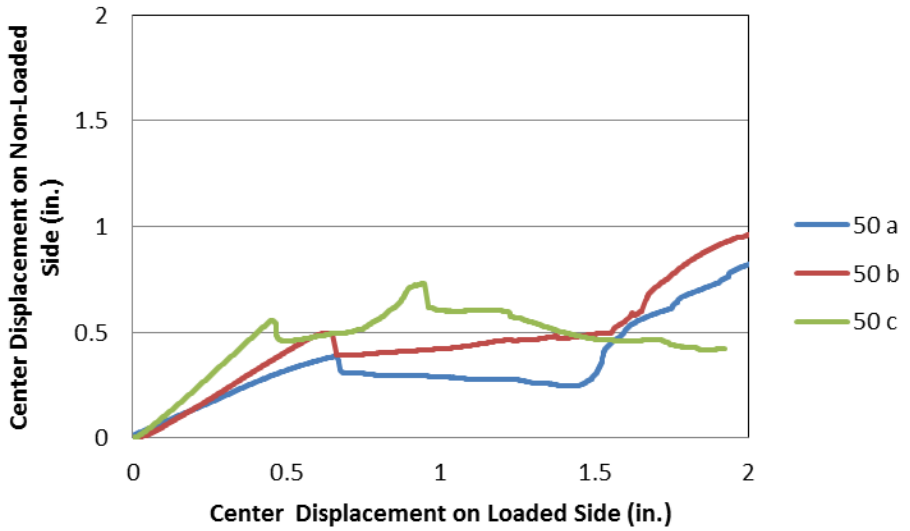

Figure 5.17: Unloaded vs. Loaded Center Panel Displacement for 35 psi Posttensioned Composite Specimens (1 in. =25.4 mm)

CHAPTER 6

FINITE ELEMENT MODELING OF TRANSVERSE BRIDGE DECK JOINTS UNDER CONCENTRATED LOADS

6.1 Abstract

The majority of research on the capacity of the grouted transverse joints between precast bridge deck panels is based on the capacity of the joint for shear and flexural strength per linear foot and does not consider the capacity of the joint as it relates to concentrated loads. The majority of loads on the transverse joint are concentrated loads from truck tires. The focus of this paper is to use finite element models to demonstrate the behavior of the unreinforced grouted transverse joint under concentrated loads.

For the purpose of this research, two different Finite Element Method (FEM) models are used to determine the load transfer and behavior of the transverse joint. The first is a localized small scale finite element model to compare local behavior of the transverse joint under posttensioned and non-posttensioned stress with those witnessed in laboratory tests. CFRP posttensioning rods were modeled in the localized small scale finite element model. The second is a global large scale finite element model with no posttensioning, used to compare global loading distribution at the transverse joint under different panel configurations for the AASHTO design truck tire load.

6.2 Introduction

Many states are implementing Accelerated Bridge Construction (ABC) methods to reduce the time that traffic is affected by bridge construction and improve the safety of the workers at the site. One of these methods is the use of precast full-depth concrete bridge deck panels. The panels are built and cured off-site and then brought on-site and placed on new or existing bridge girders. The benefit of this method of construction is the reduction of time affecting traffic and road closures for bridge.

Utah DOT is implementing a proposed design life for bridges of 75 years. The life of a bridge is dependent upon the life of its weakest component, which in most cases is the deck (Tadros et al., 1998). For precast full-depth panels the joint between precast deck panels is the most vulnerable element of the system. Bridge deck panel performance is largely dependent on and manifested in the behavior of the joint (Issa et al., 1995). The majority of the loading of the deck are concentrated loads from truck tires. In order to improve the longevity of bridge decks, it is imperative to improve the integrity of the joint and determine its capacity under concentrated loads, so that design engineers can design the jointed connections for actual loading conditions. The focus of this paper is on finite element models to demonstrate the behavior of the unreinforced grouted transverse joint under concentrated loads.

Precast bridge decks behave monolithically under design truck loads. Finite element models are beneficial for engineers because they can provide information regarding predictable behavior, loading distribution relationships of monolithic decks and reduce the requirement for further laboratory testing. For the purpose of this research, two different analysis techniques are used to determine the load transfer and behavior at

the transverse joint. The first is a small scale localized model using ANSYS (2012) to compare local behavior of the transverse joint with those witnessed in laboratory tests, including both posttensioned and non-posttensioned specimens. The second is a large scale global model using RAM CONCEPT (2013) to compare loading distribution at the transverse joint under different panel configurations for the AASHTO design truck tire load.

6.3 Literature Review

Several researchers have used the finite element method to model the transverse joint between precast concrete bridge deck panels. Issa et al. (1998) performed laboratory tests and finite element simulations to determine the amount of posttensioning required to keep the joint in compression. Based on HS20-44 truck loading it was recommended that a minimum posttensioning stress of 200 psi (1379 kPa) should be used for simply supported conditions and positive moment sections at the midspan of continuous bridge decks. It was also recommended that a posttensioning stress of 450 psi (3103 kPa) be used at the interior support of continuous decks where negative moment occurs.

Shim et al. (2001) performed finite element simulations to analyze the transverse joint and to determine how to attain no tensile stresses in the joint. The deck and girders were modeled as plate elements and remained in the linear elastic range.

Badwan (2007) used finite element modeling to analyze the behavior of precast posttensioned concrete multibeam decks under different variables and compare to experimental results. A difference of 10% was considered acceptable between

experimental and analytical results. The model used had differences between 18% and 30%; however, the model had similar trends in behavior to those found in the tests.

Research has been performed on several joint configurations in both the laboratory and with finite element models (Julander, 2009; Porter, 2009; James, 2012; Wells, 2012). These included shear and flexural tests on posttensioned transverse concave to concave joints, commonly referred to as female to female joints, strengthened through posttensioning provided by curved bolts across the joint; and female to female transverse joints strengthened by welded studs and welded rebar. It was found that the posttensioned panels had higher ultimate and initial cracking moment and shear capacity. The error regarding the cracking load predicted by the finite element method and the experimental results ranged between 2% and 32%. The error regarding the ultimate load capacity predicted by the finite element method and the experimental results ranged between 4% and 8%. The initial cracking strength and ultimate strength for the posttensioned joint depends on the bond strength between the concrete and grout.

6.4 Test Setup

Nine grouted female to female jointed precast concrete composite specimens, as shown in Figures 4.4 through 4.6, were tested monotonically to failure. The capacity and behavior of the joint was measured using strain measurements, the applied load, and displacements. Linear Variable Differential Transformers (LVDTs) were placed on the underside of the specimen to measure vertical displacements along the centerline of each half panel, as shown in Figure 6.1.

Each composite specimen was precracked by cyclic loading, with a maximum

applied load of 34 kip (151 kN). After the precracking load was removed, the composite specimens were loaded monotonically to failure under a 10 in. (254 mm) by 20 in. (508 mm) concentrated load, as described in Chapter 5.

6.5 Analytical Investigation

Two different finite element models are used to determine the load transfer and behavior at the transverse joint. The first is a detailed small scale finite element model using 3-dimensional nonlinear concrete elements to compare the local behavior of the transverse joint compared with the behavior observed in laboratory tests. The second is a large scale global finite element model using linear elastic plate elements to compare the load distribution at the transverse joint under different panel configurations for the AASHTO design truck tire load.

6.5.1 Small Scale Model

A detailed small scale finite element model was built using 3-dimensional nonlinear concrete elements to determine the load transfer and behavior at the transverse joint in ANSYS 14.5 (2013). The objective of the small scale model is to compare the progressive behavior and load transfer across the joint with those found in laboratory testing. The small scale model focused on predicting the behavior of the composite specimens under the laboratory testing conditions. This included modeling the joint geometry and mechanical properties, the concrete panel geometry and mechanical properties, bonding properties between the concrete and the grout and boundary conditions similar to those applied during laboratory testing.

Three-dimensional eight node elements were used to model the same geometry of the joint and concrete panels as those used in Figures 4.4 through 4.6. The element size was limited to a maximum size of 2 in. (51 mm) to maintain a uniformity of the element size within the model near the grouted joint and the concrete panels, as seen in Figure 6.2, which provides the typical mesh of the small model. Eight node nonlinear concrete elements (SOLID65) were used to model the concrete and grout materials because this element is capable of modeling both concrete compressive crushing and tensile cracking. SOLID65 elements are 3-dimensional eight node nonlinear elements with three degrees of freedom at each node. Input values for SOLID65 elements include shear transfer coefficients for open and closed cracks, uniaxial tensile cracking stress, and uniaxial crushing stress. The shear transfer coefficients for open and closed cracks were taken as 0.15 and 0.3 for both the grout and concrete elements. Concrete compressive and tensile strength values of 16,000 psi (110 MPa) and 950 psi (6.6 MPa) were used. Grout compressive and tensile strength values of 4,500 psi (31 MPa) and 503 psi (3.5 MPa) were also used. The tensile strength used is based on the modulus of rupture of concrete of $7.5\sqrt{f'_c}$, where f'c is the measured compressive strength. This relationship was used because of the flexural loading at the joint caused by the applied eccentric loading conditions in the experiments.

The posttensioning rod and steel reinforcement in the deck were modeled with line elements (LINK8). LINK8 elements are two node line elements with one degree of freedom per node and are often used as truss elements. The deck reinforcement elements were merged with the concrete elements to create the bonded reinforcement. The posttensioning rod elements shared a single node at each end with the panel to create an

un-bonded posttensioning system. LINK8 elements input properties consist of element area and material properties such as the modulus of elasticity.

Deck reinforcement was modeled as a bilinear material having an initial modulus of elasticity of 29,000 ksi (200 GPa) and a postyield modulus of elasticity of 2,900 ksi (20 GPa). This second slope allowed for modeling of the strain hardening that occurred at the higher tested displacements. The yield strength of the reinforcement used in the model was 60 ksi (414 MPa). The steel cross sectional area was taken as 0.44 in^2 (284 mm^2). The finite element size was limited to 2 in. (51 mm) giving a total of 12,737 elements for the half-panel symmetric model shown in Figure 6.2.

During testing, failure often occurred at the grout to concrete interface. To simulate the behavior of the bond between the concrete and grout, cohesive contact and target area elements (CONTA173 and TARGE170) were used.

Symmetry was used to model half of the composite specimen in the transverse direction. To simplify the model and decrease run time, the vertical displacement of the nodes at the supported edge of the slab was restrained to be zero for the model. The tested panels showed signs of rotating off the supports after the initial significant crack at the joint; to account for this, only 28 in. (711 mm) of the supported edge of the model was restrained for vertical displacement; 11 in. (279 mm) length along each support was unrestrained for displacement. This boundary condition is different from the condition in the laboratory tests where the panels were placed on a bearing pad and allowed to lift at the edges but is believed to be a good representation of the actual condition.

Four loading conditions were applied to the finite element model to simulate testing conditions. First, the panels were posttensioned by assigning a coefficient of

thermal expansion to the rod elements and applying a temperature load to induce posttensioning strain levels. Second, a uniform pressure totaling 34 kip (151 kN) was applied to the loading plate and then released to a load of 0.72 kip (3.2 kN) for the third loading condition, to allow for precracking conditions and attain a final smooth force vs. displacement curve for the final loading conditions as demonstrated in the panels tested to failure in the experiments. The final loading was a uniform displacement applied over a 6 in. x 12 in. (152 mm x 305 mm) area on the top of a 10 in. x 20 in. x 1 in. (254 mm x 508 mm x 25.4 mm) steel loading plate to simulate the loading conditions used in the laboratory.

Three different posttensioning levels were tested, one with no posttensioning, one with a 13 kip (58 kN) posttensioning force per CFRP rod, and one with an 18 kip (80 kN) posttensioning force per CFRP rod. These relate to a joint stress of 35 psi (241 kPa) and 48.4 psi (333.6 kPa), respectively. The posttensioning rod was modeled as a linear material with a modulus of elasticity of 22,500,000 psi (155 GPa). To adequately model the posttensioning, the posttensioning rod cross sectional area was modeled as 0.11 $in.^2$ (71 mm^2) and 0.145 $in.^2$ (94 mm^2) for the 13 kip (58 kN) and 18 kip (80 kN) posttensioning force used in the experiments. The posttensioning stress was applied as a thermal strain to the rod.

6.5.2 Large Scale Model

Six large scale global finite element models were created using linear elastic plate elements, to compare the load distribution at the transverse joint under different panel configurations in the design program RAM CONCEPT V8i. The large scale model

focused on the modeling of the global effects of varying panel dimensions on the distribution of the concentrated truck tire loads across the transverse joint. These panel variations included single span, two span, and three span specimens with panel widths ranging from 18 in. (457 mm) and 72 in. (1.8 m), while maintaining a panel thickness was 8.75 in. (222 mm) in all cases.

To adequately model the global load distribution, the large scale model used linear elastic plate elements with mechanical properties similar to those used during laboratory testing. These mechanical properties include the concrete and grout compressive strength and modulus of elasticity. A concrete compressive strength of 16 ksi (110 MPa) and a modulus of elasticity equal to 6,060 ksi (42 GPa) was used. The latter is based on the ACI 363R-10 recommended high strength concrete equation for the modulus of elasticity:

$$E_c = (40000 * f'_c + 1 * 10^6)\left(\frac{w_c}{145}\right)^{1.5} \quad (1)$$

where f'_c is the concrete compressive strength and w_c is the concrete density. Steel reinforcement in the panel was modeled as Grade 60 #6 bars at 12 in. (305 mm) on center each way, located at the top and bottom. The transverse joint was modeled as an unreinforced 4 in. (102 mm) wide concrete strip of a compressive strength equal to 4.5 ksi (31 MPa) concrete with a 7.75 in. (197 mm) thickness.

The element size was limited to 6 in. by 6 in. in plan and 8.75 in. thick (152 mm by 152 mm by 222 mm) with a total of 252 plate elements for the single span 18 in. (457 mm) composite panels. Single point connectors were used to model the restraint of the

vertical and horizontal displacements in all three directions of the deck support along the girder members.

The factored AASHTO HL-93 truck tire load of 34.3 kip (153 kN) was applied on a 10 in. by 20 in. (254 mm by 508 mm) area for each model. The 34.3 kip applied load is smaller than the initial cracking load for all the tested composite specimens, and therefore is an acceptable load to apply for predicting the load distribution prior to joint cracking.

Laboratory testing indicated that the behavior of the panels and joint were similar regardless of the applied posttensioning prior to the initial significant joint crack. For this reason no posttensioning was used in the simulations utilizing the large scale model. Figure 6.3 shows the typical model layouts and loading conditions for the 18 in. (457 mm) wide panel composite specimens.

6.6 Analytical Results

The small scale model was used to compare the progressive force vs. displacement relationship of the composite specimens. Figures 6.4 through 6.6 show the force vs. displacement diagram for the non-posttensioned, 35 psi (241 kPa) and 48 psi (331 kPa) posttensioned models, respectively. The initial force vs. center displacement prior to the initial cracking load behaved similar to the specimens tested in the lab.

The small scale model for the non-posttensioned composite panel had an initial joint cracking load of 75.1 kip (334 kN), which is 67% higher than the average tested initial joint cracking load of 45 kip (200 kN). The modeled ultimate load is 75.7 kip (337 kN), which is 22% larger than the average tested ultimate load. The initial joint cracking

load for the models with the 35 psi (241 kPa) and 48 psi (331 kPa) posttensioned composite specimens are 72.7 kip (323 kN) and 84.5 kip (376 kN), which is 1.5% and 15.7% higher than the average tested initial joint cracking load. The modeled ultimate load for the posttensioned composite specimens are 78.9 kip (351 kN) and 83.2 kip (370 kN), which is 5.3% and 4.8% larger than the average tested ultimate load for the 35 psi (241 kPa) and 48 psi (331 kPa) posttensioned specimens.

The small scale model predicted better results for the posttensioned composite specimens compared to the non-posttensioned ones. The accuracy of the model is based on the model behavior and joint cracking loads. Prior to the initial joint cracking load, the small scale model behaved similar to the tests as demonstrated by the similar slope in the force vs. displacement curves for the tested and modeled specimens. The small scale model did not capture failure of the loaded panel as witnessed in the specimens tested in the experiments. The model was more accurate prior to the initial joint cracking load than after this event. This was due to monolithic behavior of composite specimens prior to the initial joint cracking load. No effort was made to model progressive collapse because the purpose of the modal was to predict cracking.

Figure 6.7 shows the displacement relationship between the small scale model and the measurements obtained from the LVDTs during testing of the three different composite specimens (non-posttensioning, 35 psi (241 kPa) and 48 psi (331 kPa) posttensioning) at a load of 34.3 kip (153 kN). The average center displacement for the loaded side of the non-posttensioned small scale model was 0.26 in. (6.6 mm), which is 3% less than the average recorded displacement of the tested specimens of 0.27 in. (6.9 mm). The center displacement on the nonloaded side of the non-posttensioned small

scale model was 0.07 in. (1.8 mm), which is 61% less than the recorded displacement for the same location of 0.20 in. (5.1 mm). The large discrepancy between the modeled and tested displacements for the nonloaded side is likely due to the difference of boundary conditions as described earlier; thus, the panels in the test moved vertically at the supports but were restrained from doing so in the model.

The large scale model was used to evaluate the behavior of the composite specimen under the factored AASHTO design truck tire load. Figure 6.8 shows the typical displacement contour for the large scale model under the applied 34.3 kip (123 kN) tire load. The center displacement was approximately 0.275 in. (7 mm) for a typical composite specimen. This is 0.3% larger than the average recorded center displacement at 34.3 kip (153 kN) for the tested composite specimens. The nonloaded side center displacement was approximately 0.248 in. (6.3 mm), which is 21% larger than the experimental displacement. The large scale model more closely predicted the displacements found in the lab than those found from the small scale model.

A comparison between composite specimens with 18 in. (457 mm) wide panels and composite specimens with 72 in. (1.8 m) panels shows that the wider panels deflected significantly less than those of the narrower panels and had a more uniform distribution of deflection in all directions. The center displacement for the loaded 72 in. (1.8 m) panel was 0.072 in. (1.8288 mm), which is 74% less than the composite specimen with the 18 in. (457 mm) panels, as shown in Figure 6.8. Figures 6.9 and 6.10 show the typical shear and moment distribution for the composite specimens with the 18 in. (457 mm) wide panels. Shear in the y axis and moment about the x axis, as referenced in Figure 6.3, behave similar to a simple span beam spanning between the supports. Shear

in the x axis and moment about the y axis refer to the shear and moment behaving perpendicular to the joint and can be used to determine the loading across the transverse joint. The maximum shear and maximum moments refer to the combined total shear and moment.

The large scale model may be used to compare the displacement, moment and shear distribution for different panel configurations. Figures 6.11 through 6.15 show a comparison between the displacement, moment and shear distributions for single span composite specimen with 18 in. (457 mm) wide panels and the typical 72 in. (1.8 m) wide panels used in bridge construction in single and multispan panel conditions. Multispan panel conditions refer to precast panels spanning over multiple girders. Figure 6.11 is the contour of vertical displacement of the single span, two span and three span large scale model for the composite specimens with the 72 in. (1.8 m) wide panels. The simple span, two span and three span panels had very similar magnitudes of displacement near the concentrated load, thus indicating that the research performed is useful for multispan and single span precast panel conditions. Figure 6.12 is the contour for the maximum shear force for the single span composite specimens with 18 in. (457 mm) and 72 in. (1.8 m) wide panels. The composite specimens with the 18 in. (457 mm) wide panels had larger maximum shear values than the composite panels with the 72 in. (1.8 m) wide panels. This is significant because the majority of precast bridge deck panels used in the field are 72 in. (1.8 m) wide or larger, and will have lower shear values than those observed in the test. Figure 6.13 is the contour of maximum shear of the single span, two span and three span large scale model for the composite specimens with the 72 in. (1.8 m) wide panels. The simple span, two span and three span panels had similar distribution

and magnitudes of maximum shear near the concentrated load ranging from 7.03 kip/ft (103 kN/m) to 7.26 kip/ft (106 kN/m). Figure 6.14 is the contour for the shear force in the x direction for the single span composite specimens with 18 in. (457 mm) and 72 in. (1.8 m) wide panels. The composite specimens had similar shear distribution in the x direction on the nonloaded side of the concentrated load where the distribution area was larger. The maximum shear in the x direction was similar for both models. The max shear in the x direction for the composite specimen was 5.71 kip/ft (83 kN/m) for the 18 in. (457 mm) wide panels and 5.35 kip/ft (78 kN/m) for the 72 in. (1.8 m) wide panels. Figure 6.15 is the contour for the moment in the y direction for the single span composite specimens with 18 in. (457 mm) and 72 in. (1.8 m) wide panels. The distribution area for the moment in the y direction for the 72 in. (1.8 m) wide panels was larger than that of the 18 in. (457 mm) panels. The maximum moment in the y direction was similar for both models. The maximum moment in the y direction for the composite specimen was 2.75 kip - ft/ft (12 kN-m/m) for the 18 in. (457 mm) wide panels and 2.35 kip -ft/ft (10.5 kN-m/m) for the 72 in. (1.8 m) wide panels. This is significant because the bending loads for precast bridge deck panels used in the field will be less than those found in this research.

Displacements and shears of the adjacent spans were not greatly affected by the loading, showing close to zero displacement and shear forces. The shear and the moment distribution for the wider panels was more uniform in all directions.

6.7 Conclusions and Recommendations

Analytical comparisons were carried out using models of an unreinforced transverse joint for precast concrete deck panels under concentrated loads. Two models were used for the analysis. The analytical results were compared to experiments carried out on such joints. Several conclusions can be made.

1) The small scale model, using nonlinear eight-node 3-dimensional elements, had a center displacement under the applied concentrated load of 0.26 in., which is 3% less than the average recorded displacement of the tested specimens of 0.27 in. The center displacement on the nonloaded side of the small scale model was 0.07 in., which is 61% less than the recorded displacement for the same location in the lab of 0.2 in.
2) The small scale model predicted the initial cracking load 66% larger than that of the tested cracking load for the non-posttensioned composite specimens and 2% to 8% for the two posttensioned models.
3) The small scale model predicted the displacement at the initial cracking load 139% larger than the tested composite specimens for the non-posttensioned specimens and 20% to 28% larger for the two posttensioned models.
4) The large scale model, using linear elastic plate elements, had a center displacement under the applied concentrated load 0.3% larger than the average recorded center displacement under the same loading for the tested composite specimens. The center displacement on the nonloaded panel was 21% larger than the average recorded displacement under the same location and loading.
5) The small scale model may be used to show the force vs. displacement behavior

of the joint under increasing load prior to initial joint failure. The large scale model may be used under a nonincremental loading condition to analyze load distribution and deflections under the monolithic behavior prior to initial joint failure.

6) The large scale model is more realistic for design professionals to demonstrate the distribution of the loads across the joint prior to initial joint cracking, because it modeled boundary conditions found in existing bridge structures and had closer center displacements to the tested specimens than the smaller model.

Additional tests should be performed with different concentrated load location and different levels of posttensioning, in order to investigate the influence of these two parameters more fully.

6.8 Reference

ACI(2010). (n.d.). Report on high strength concrete. *Report ACI 363R-10*. Farmington Hills, MI.

ANSYS. (n.d.). Academic Research Mechanical Release 14.5.

Badwan, I. Z., & Liang, R. Y. (2007). Performance Evaluation of Precast Posttensioned Concrete Multibeam Deck. *Journal of Performance of Constructed Facilities*.

Benteley. (2013). RAM CONCEPT V8i Release 5.0.2.

Hanna, K. E., Morcous, G., & Tadros, M. K. (December 2010). *Second Genration Precast Deck Panel (NUDECK) System*. University of Nebraska, Lincoln. Lincoln, Nebraska: Nebraska Department of Roads.

Issa, M. A., Idriss, A.-T., Kaspar, I. I., & Khayyat, S. Y. (1995, January-February). Full Depth Precast and Precast, Prestressed Concrete Bridge Deck Panels. *PCI Journal*, 40, 59-80.

Issa, M. A., Ribeiro do Valle, C. L., Islam, S., Abdalla, H. A., & Issa, M. A. (2003, July-August). Performance of Transverse Joint Grout Materials in Full-Depth Precast

Concrete Bridge Deck Systems. *PCI Journal*, 48, 2-13.

Issa, M. A., Yousif, A. A., Issa, M. A., Kaspar, I. I., & Khayyat, S. Y. (1995, May-June). Field Performance of Full-Depth Precast Concrete Panels in Bridge Deck Reconstruction. *PCI Journal*, 40, 82-108.

Issa, M. A., Yousif, A. A., Issa, M. A., Kaspar, I. I., & Khayyat, S. Y. (1998, January-February). Analysis of Full Depth Precast Concrete Bridge Deck Panels. *PCI Journal*, 43, 74-85.

James, P. H. (2012). Finite Element Modeling of Full Depth Precast Concrete Bridge Deck Connections in Bending and Shear. *Master's Thesis*, Utah State University, 2012.

Julander, J. (2009). Finite Element Modeling of Full Depth Concrete Transverse Bridge Deck Connections. *Master's Thesis*, Utah State University, 2009.

Porter, S. D. (2009). Laboratory Testing of Precast Bridge Deck Panel Transverse Connections for Use in Accelerated Bridge Construction. *Master's Thesis*, Utah State University, 2009.

Shim, C.-S., Choi, K.-Y., & Chang, S.-P. (2001). Design of Transverse Joints in Composite Bridges with Precast Decks. *KSCE Journal of Civil Engineering*, 17-27.

Wells, Z. B. (2012). Peformance of Post-Tensioned Curved-Strand Connections in Transverse Joints of Precast Brigde Decks. *Master's Thesis*, Utah State University, 2012.

.

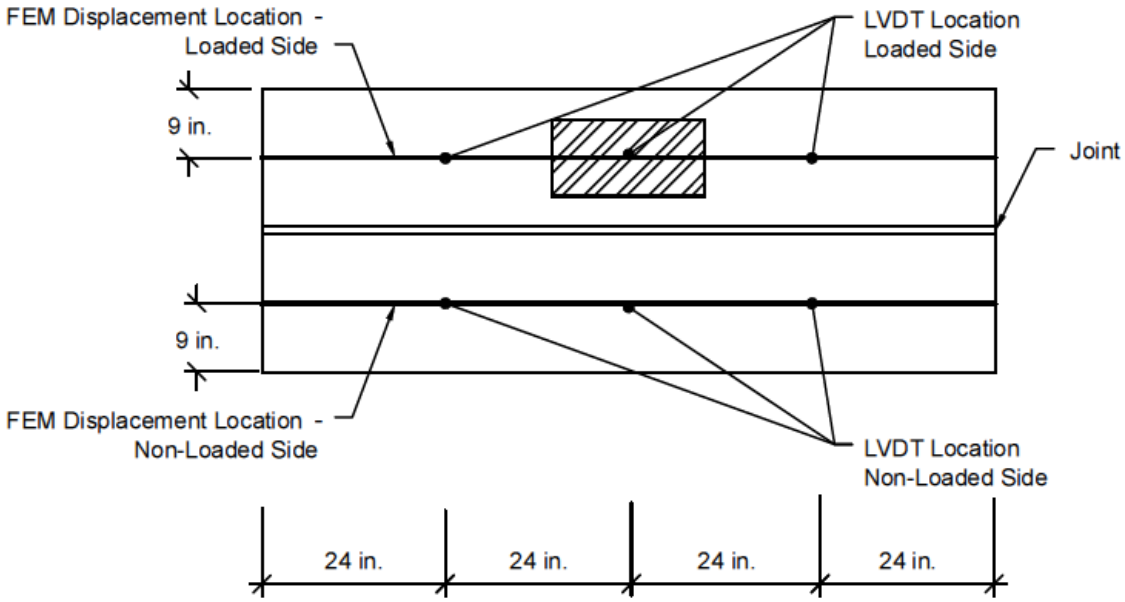

Figure 6.1: LVDT Location for Composite Specimens.

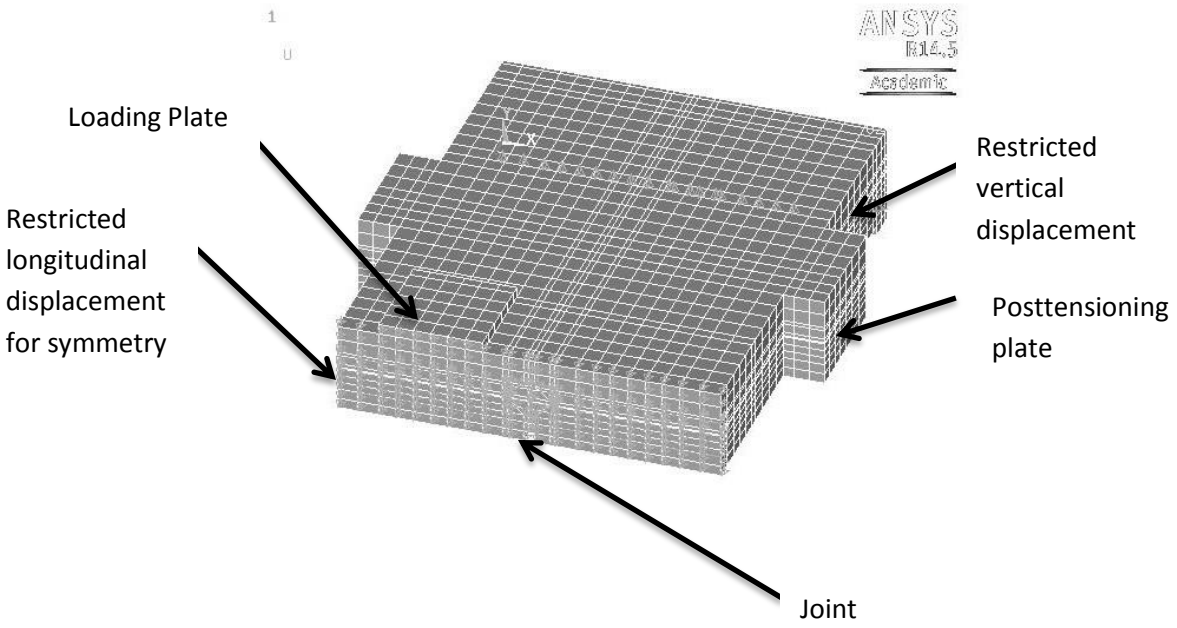

Figure 6.2: Typical Small Scale Model Mesh

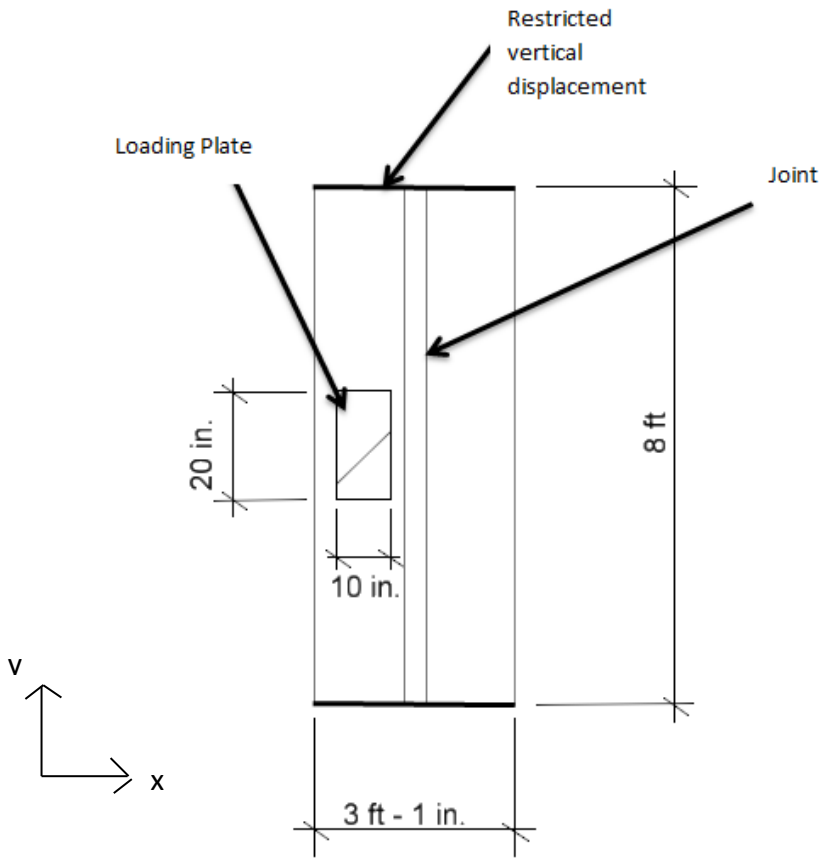

Figure 6.3: Typical Large Scale Model Layout for Single Span Condition for the 18 in. Wide Panels (1 in. = 25.4 mm, 1 kip = 4.44 kN)

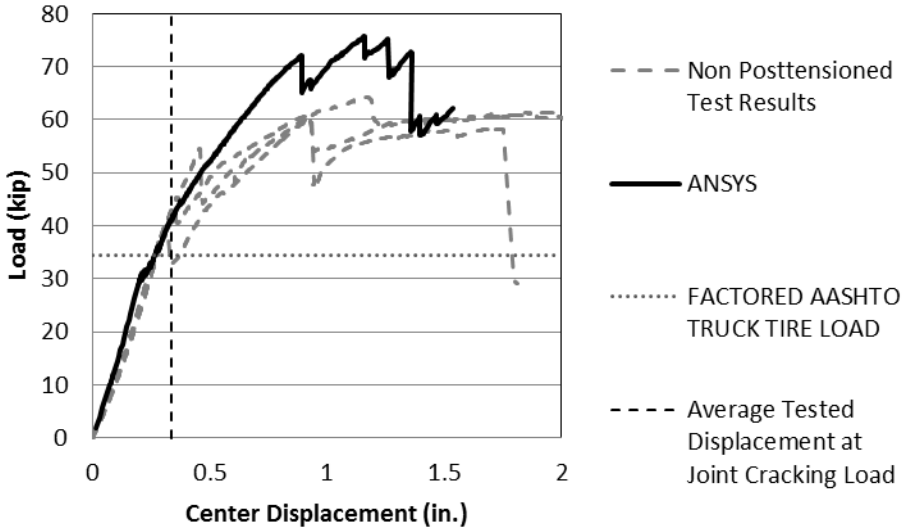

Figure 6.4: Tested and Small Scale Modeled Force vs. Displacement Graphs for Non-Posttensioned Panels (1 in. = 25.4 mm, 1 kip = 4.44 kN)

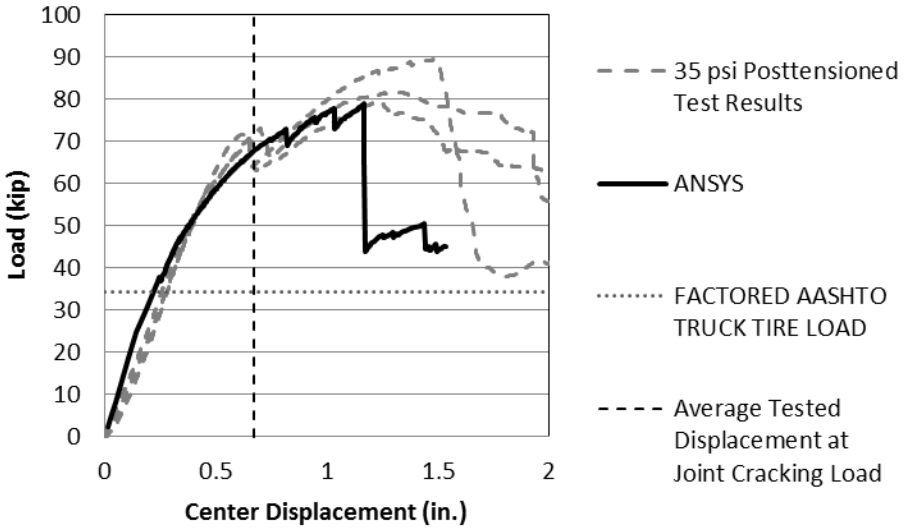

Figure 6.5: Tested and Small Scale Modeled Force vs. Displacement Graphs for 35 psi Posttensioned Panels (1 in. = 25.4 mm, 1 kip = 4.44 kN)

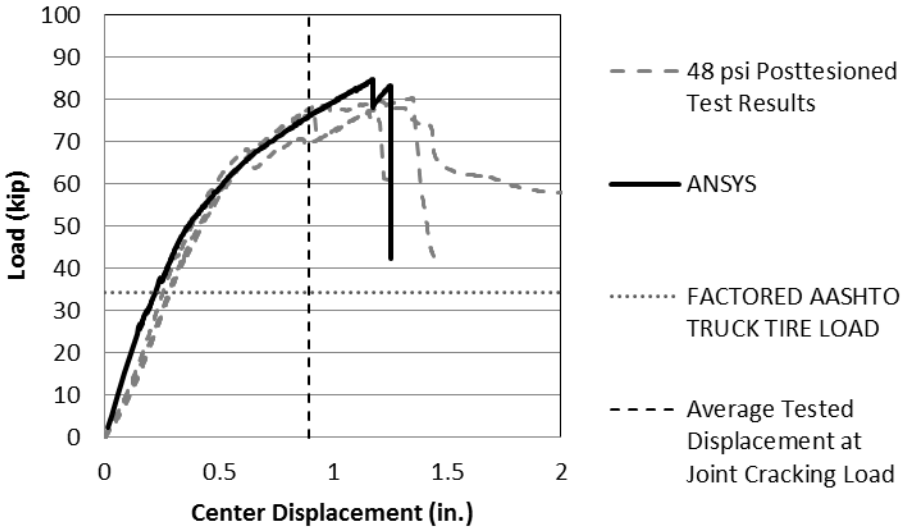

Figure 6.6: Tested and Small Scale Modeled Force vs. Displacement Graphs for 48 psi Posttensioned Panels (1 in. = 25.4 mm, 1 kip = 4.44 kN)

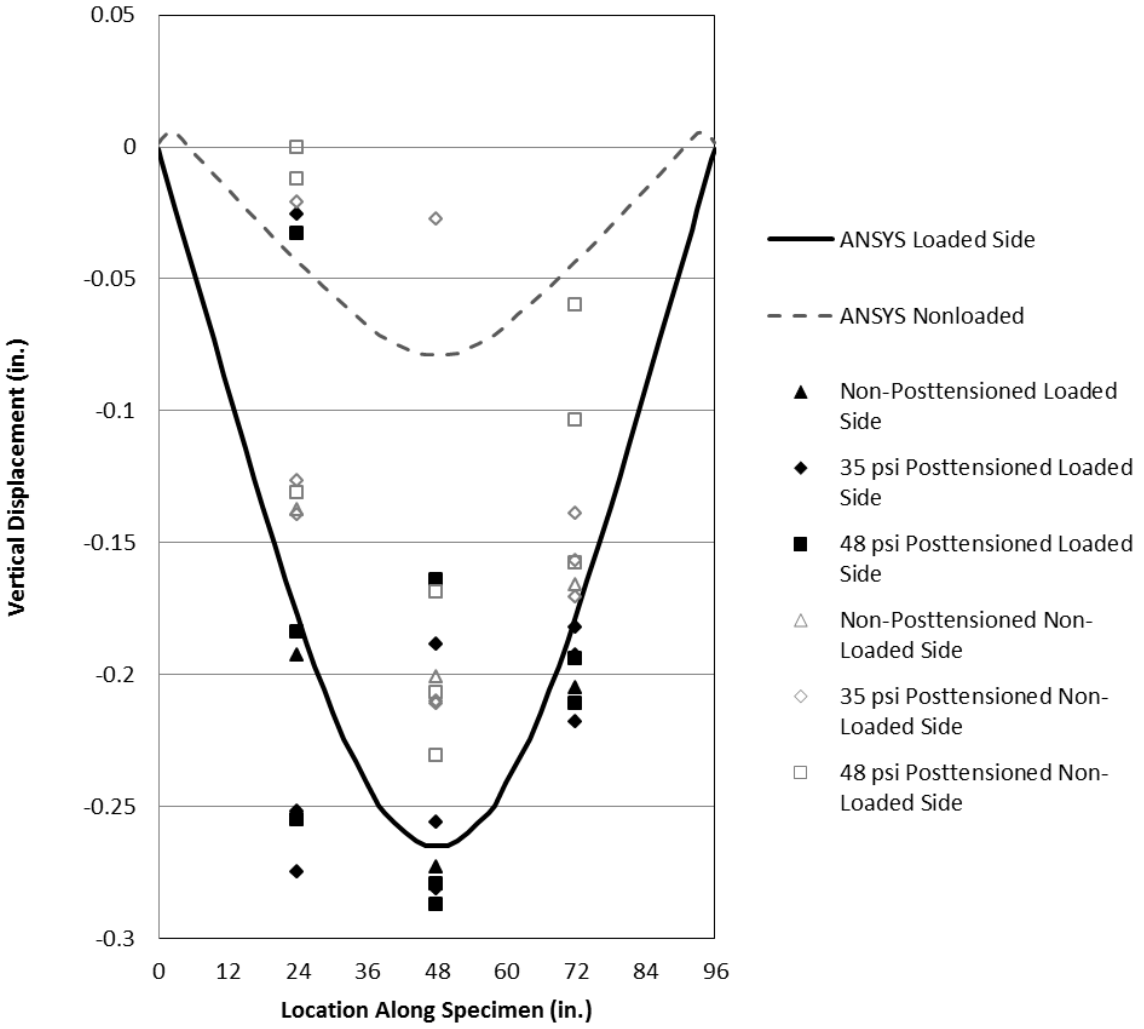

Figure 6.7: Tested and Small Scale Model Vertical Displacement Graphs at 34.3 kip Applied Load (1 in. = 25.4 mm, 1 kip = 4.44 kN)

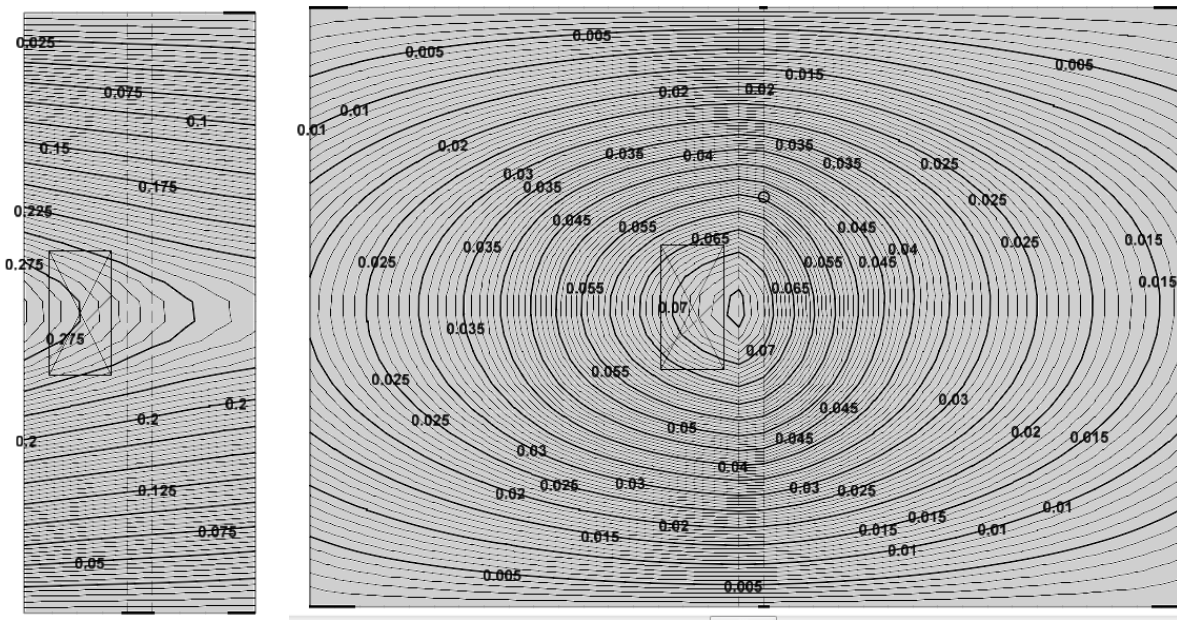

(a) (b)

Figure 6.8: Typical Vertical Displacement (in.) Distribution at 34.3 kip Applied Load for the Large Scale Model for Single Span condition: (a) 18 in. Wide Panels, (b) 72 in. Wide Panels (1 in. = 25.4 mm, 1 kip = 4.44 kN)

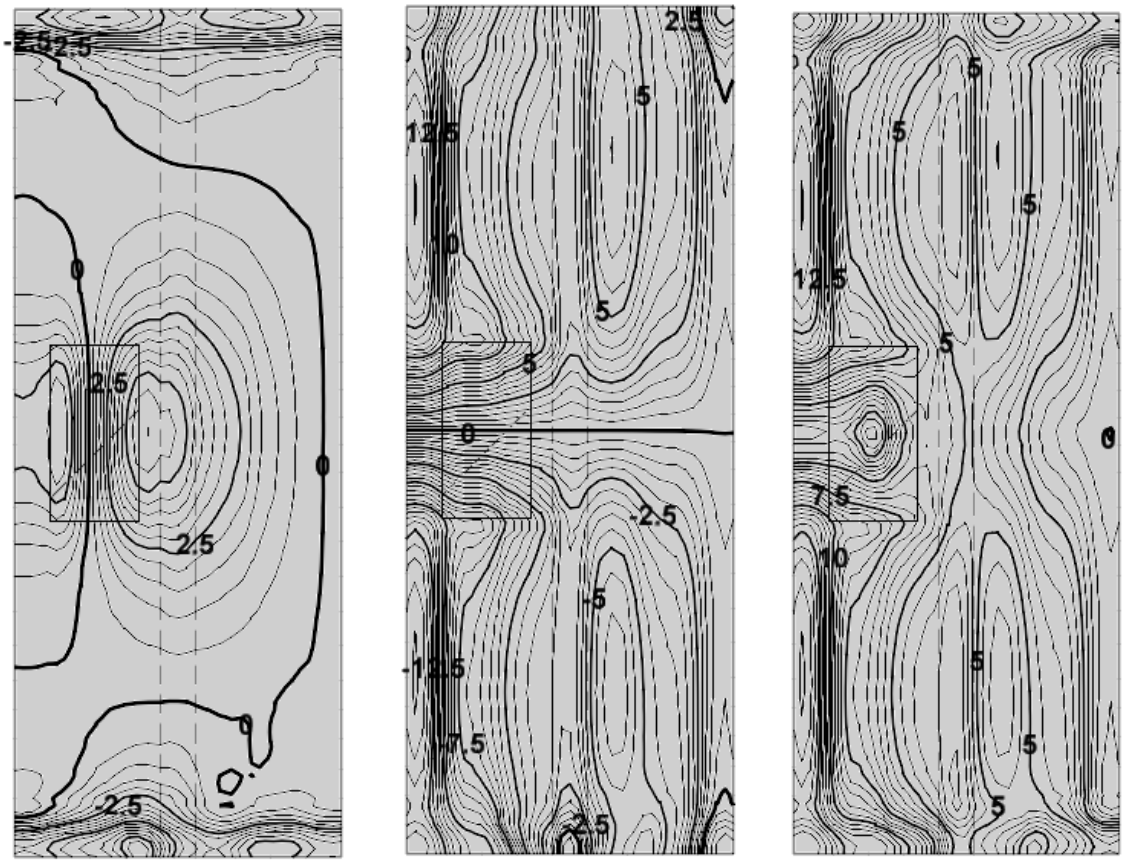

(a) (b) (c)

Figure 6.9: Typical Shear (kip/ft) Distribution at 34.3 kip Applied Load for the Large Scale Model for Single Span Condition with 18 in. Wide Panels: (a) X Axis, (b) Y Axis, (c) Maximum (1 in. = 25.4 mm, 1 kip = 4.44 kN)

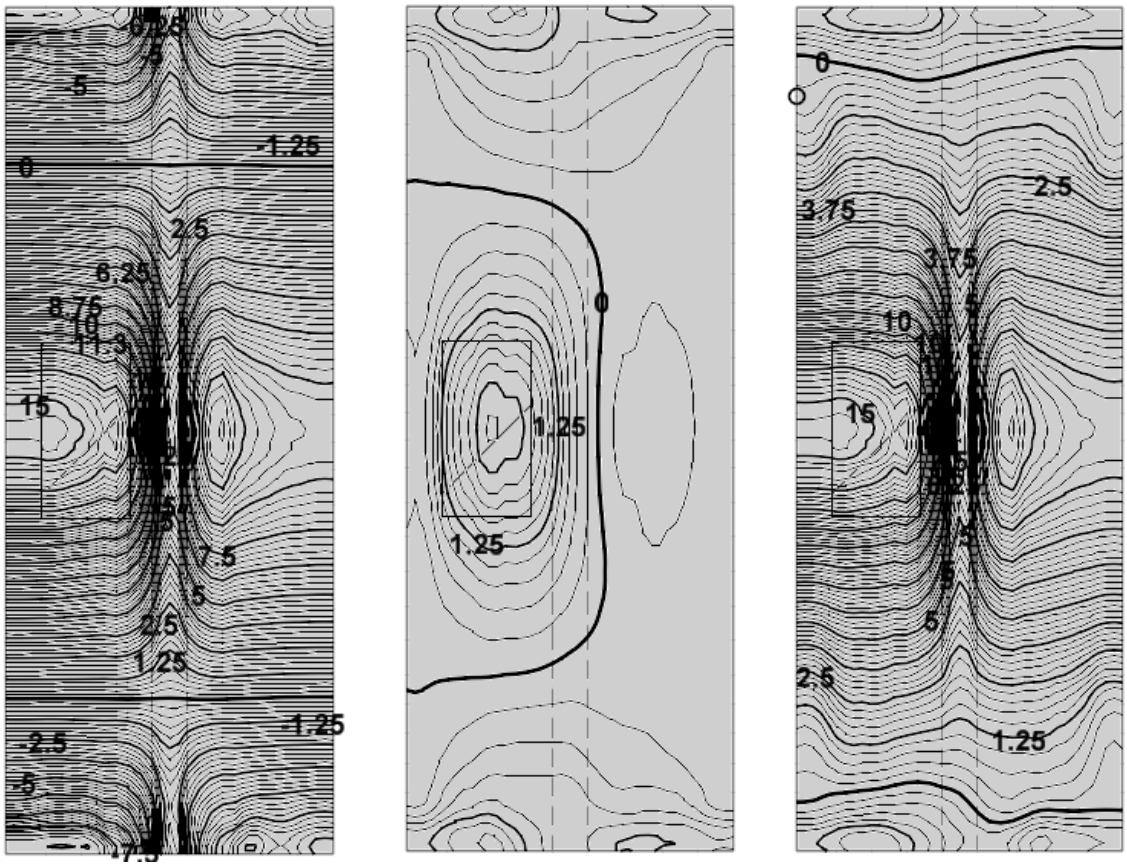

(a) (b) (c)

Figure 6.10: Typical Moment (kip-ft/ft) Distribution at 34.3 kip Applied Load for the Large Scale Model for Single Span condition with 18 in. Wide Panels: (a) X Axis, (b) Y Axis, (c) Maximum (1 in. = 25.4 mm, 1 kip = 4.44 kN)

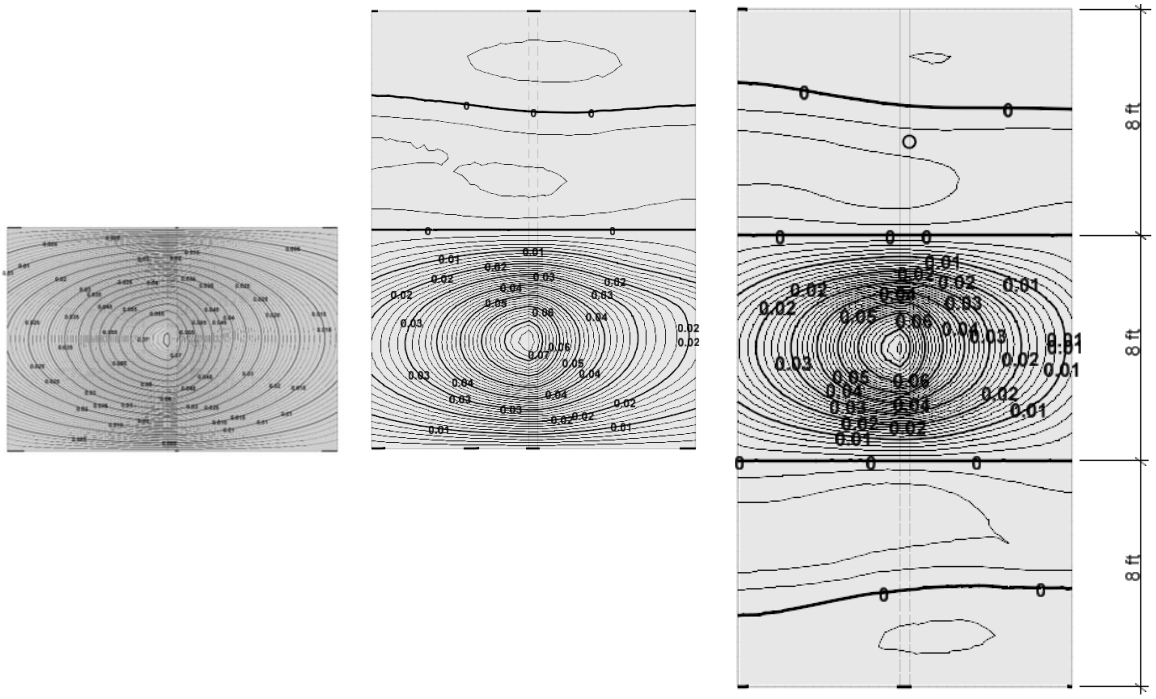

(a) (b) (c)

Figure 6.11: Typical Vertical Displacement (in.) Distribution at 34.3 kip Applied Load for the Large Scale Model for the 72 in. Wide Panels: (a) Single Span, (b) Two Span, (c) Three Span (1 in. = 25.4 mm, 1 kip = 4.44 kN)

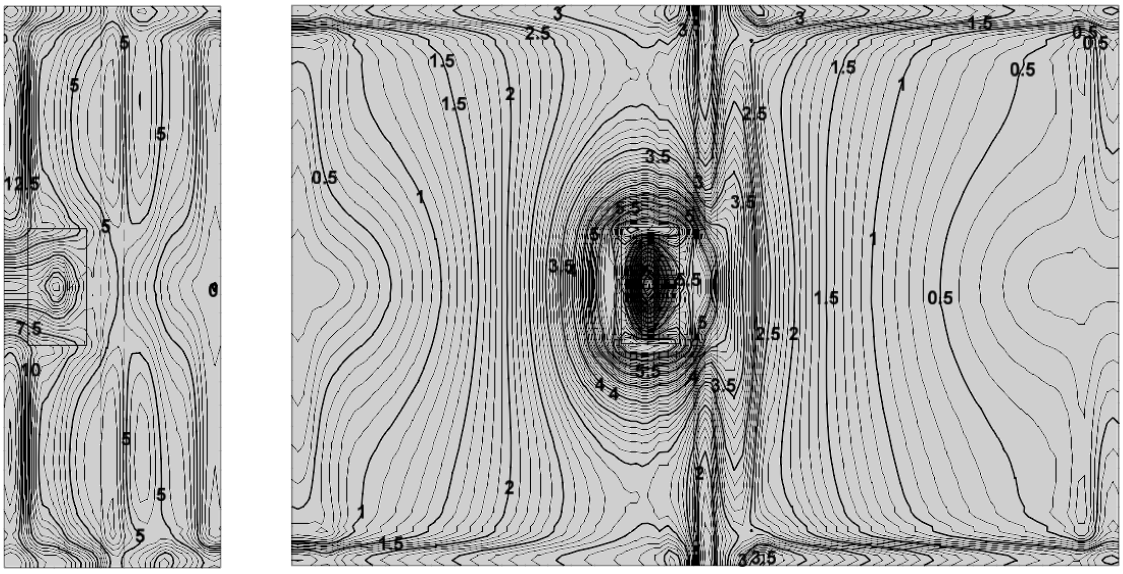

(a) (b)

Figure 6.12: Max Shear Force (kip/ft) Distribution at 34.3 kip Applied Load for the Large Scale Model for Single Span condition: (a) 18 in. Wide Panels, (b) 72 in. Wide Panels

(1 in. = 25.4 mm, 1 kip = 4.44 kN)

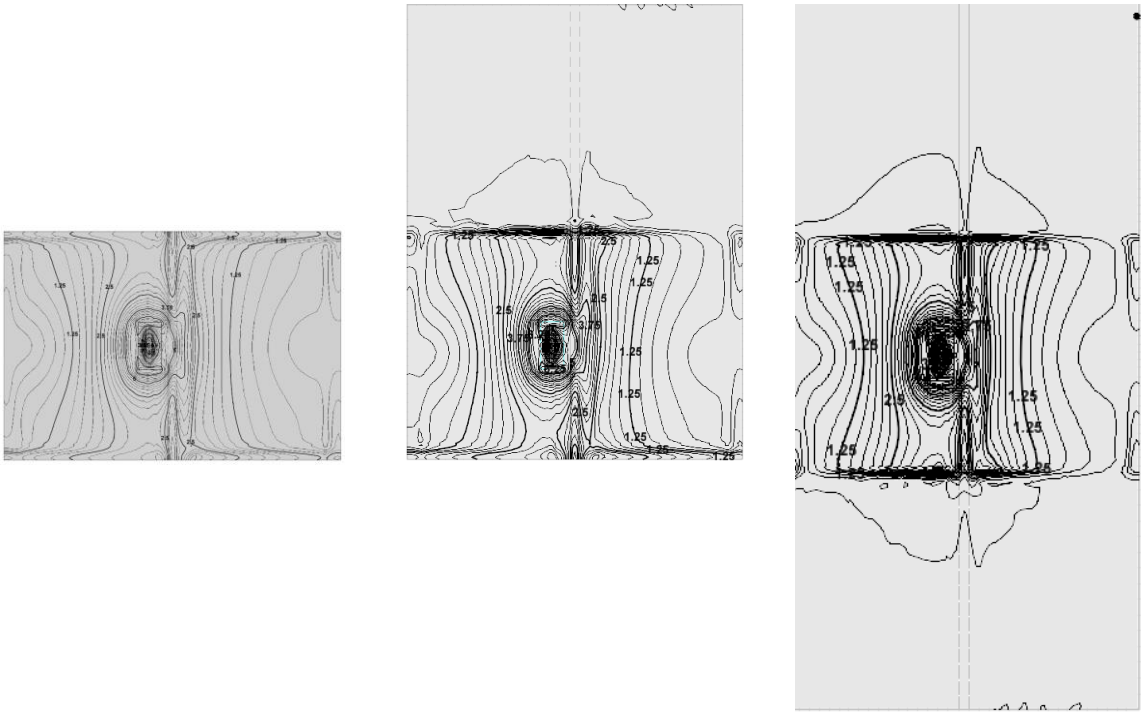

(a) (b) (c)

Figure 6.13: Max Shear Force (kip/ft) Distribution at 34.3 kip Applied Load for the Large Scale Model for the 72 in. Wide Panels: (a) Single Span, (b) Two Span, (c) Three Span

(1 in. = 25.4 mm, 1 kip = 4.44 kN)

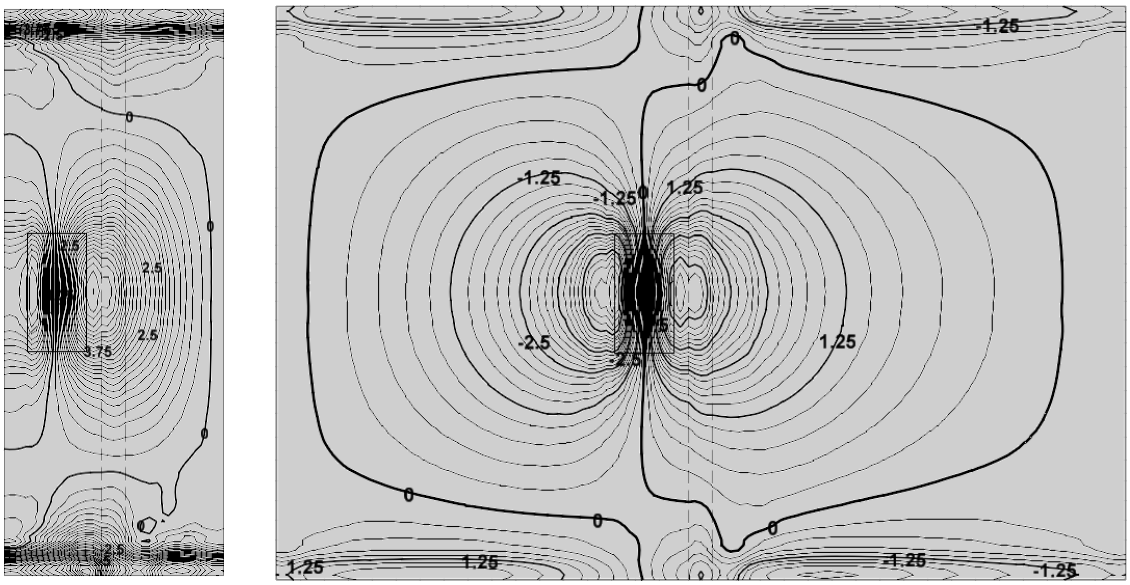

(a) (b)

Figure 6.14: Typical Shear Force (kip/ft) in the x Direction Distribution at 34.3 kip Applied Load for the Large Scale Model for Single Span condition: (a) 18 in. Wide Panels, (b) 72 in. Wide Panels (1 in. = 25.4 mm, 1 kip = 4.44 kN)

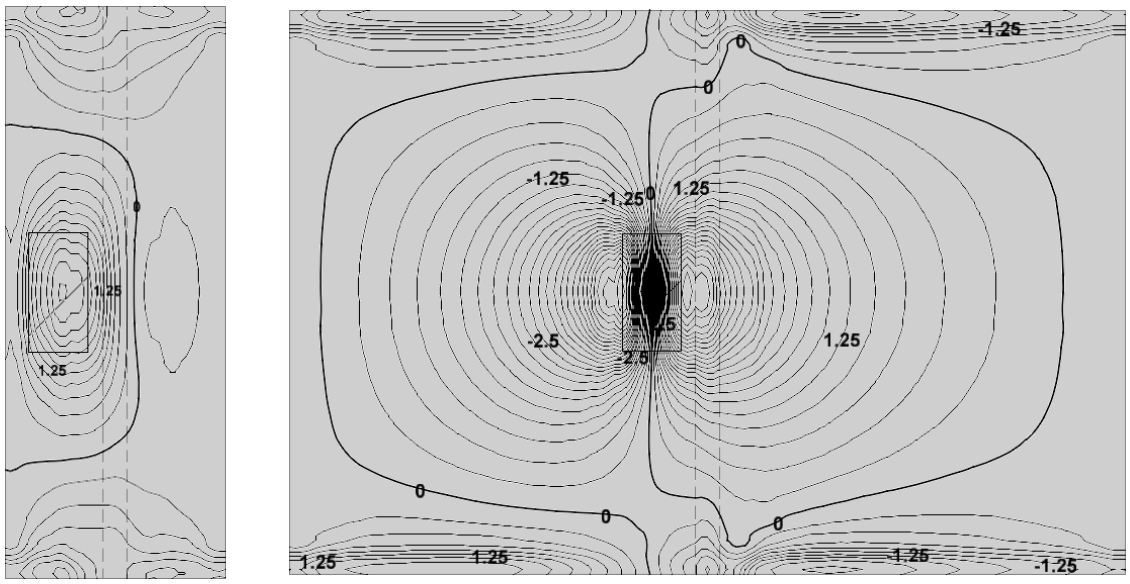

(a) (b)

Figure 6.15: Typical Moment (kip-ft/ft) in the y Direction Distribution at 34.3 kip Applied Load for the Large Scale Model for Single Span Condition: (a) 18 in. Wide Panels, (b) 72 in. Wide Panels (1 in. = 25.4 mm, 1 kip = 4.44 kN)

CHAPTER 7

CAPACITY OF TRANSVERSE BRIDGE DECK JOINTS POSTTENSIONED WITH CFRP RODS UNDER CONCENTRATED LOADS

7.1 Abstract

This research focuses on predicting the capacity of grouted transverse bridge deck joints under concentrated loads. The majority of research on the capacity of grouted transverse joints between precast bridge deck panels is based on the capacity of the joint for shear strength per linear foot and does not consider the capacity of the joint as it relates to concentrated loads. However, actual bridge loads on the transverse joint are primarily due to concentrated loads from truck tires.

For the purpose of this research a finite element model was used to determine the load and stress transfer at the joint. Two different design distribution width are compared: 28.75 in. (730 mm), based on the AASHTO code standard concentrated load distribution, and 36 in. (914 mm), based on a finite element model distribution of stress across the joint. Five analytical methods are used to calculate the capacity of the joint. These include, shear friction, cracking moment, a strut and tie model, principle tension stress, and the ACI 318 shear equations. It was found that the shear friction equation and the strut and tie model gave the most conservative capacities of the joint. In addition,

these two methods gave the most accurate capacities of the joint compared to experimental results.

7.2 Introduction

Many states are implementing accelerated bridge construction (ABC) methods to reduce the time that traffic is affected by bridge construction and improve the safety of the workers at the site. One of these methods is the use of precast full-depth concrete bridge deck panels. The panels are built and cured "off-site" and then placed on new or existing bridge girders. The benefit of this method of construction is the reduction of time affecting traffic and road closures for bridge construction.

Utah DOT is implementing a design life for bridges of 75 years. The life of a bridge is dependent upon the life of its weakest component, which in most cases is the deck (Tadros et al., 1998). For precast full-depth panels the joint between precast deck panels is the most vulnerable element of the system. Bridge deck panel performance depends on the behavior of the joint (Issa et al., 1995). Significant loads on bridge decks are primarily due to concentrated loads from truck tires. In order to improve the longevity of bridge decks, it is imperative to improve the integrity of the joint and determine the capacity of the joint under concentrated loads. The focus of this paper is to compare analytical methods to determine the capacity of unreinforced grouted transverse bridge deck joints under concentrated loads.

For the purpose of this research a finite element model using elastic plate elements was used to determine the load transfer at the joint. Two different design distribution widths are compared: 28.75 in. (730 mm), based on the AASHTO

concentrated load distribution, and 36 in. (914 mm), based on a FEM distribution of stress across the joint. The finite element model is used to compare the distribution width and the load transferred across the transverse joint based on different concentrated load locations. Five methods are used to calculate the capacity of the joint. These include, shear friction, cracking moment, strut and tie model, principle tension stress, and ACI 318 shear equations.

7.3 Literature Review

Research has been performed on the behavior of concrete bridge decks under concentrated loads as well as the capacity of the transverse joint between precast bridge deck panels. However, little research has been presented on the relationship of concentrated loads on the capacity of the transverse joint between precast bridge deck panels.

Petrou et al. (1996) performed laboratory testing of concrete decks under a concentrated load. It was found that the primary failure mode for "beam" deck strips was ductile flexural failure due to yielding of the steel reinforcement; the primary failure mode for decks was brittle failure in the form of punching shear.

Tao (2009) provided a method for determining the required transverse reinforcement for a concrete bridge deck under a concentrated load. It was observed that slabs with small width to length ratios behaved more like beams where slabs with larger width to length ratios had a biaxial bending distribution. Tao's proposed method states that the maximum moment due to uneven distribution is proportional to the average moment over the length of the panel for both directions.

The capacity of the joint prior to initial cracking for posttensioned and non-posttensioned joints has been analyzed by several researchers. Kim et al. (2003) proposed the use of principal tensile stress and the tensile strength of the grout to predict the cracking strength of grouted joints. Static shear tests were performed on three grouted joint specimens. The ratio between the calculated load at initial cracking and the tested value was ranged between 0.96 and 1.01.

Roberts (2011) compared the tested strength of posttensioned concave to concave joints, commonly referred to as female to female joints, with standard shear capacity equations found in section 11.2 of the ACI 318 Guidelines. Panels that were 10 ft x 4 ft were tested for the shear capacity across the grouted joint. The panels were posttensioned in the short direction, perpendicular to the grouted pocket. The ultimate shear strength of the posttensioned joint exceeded the calculated capacity for all three equations.

Shear friction was utilized by Saenz et al. (2004) as part of a strut and tie model for concrete in shear externally reinforced with carbon fiber-reinforced polymer (CFRP) composite laminates. Push off tests were performed and the capacity of the CFRP reinforced specimens was compared to a strut and tie model. It was found that the strut and tie model gave conservative results and was successful in representing the true behavior of the concrete.

7.4 Research Significance

The majority of research on the capacity of grouted panel to panel deck joints is based on shear capacity per linear foot along the joint and does not consider the capacity

of the joint as it relates to concentrated loads. However, actual bridge loads on transverse joints are primarily due to concentrated loads from truck tires. This research allows design engineers the ability to relate design truck tire loads with the initial cracking load capacity of the joint. The initial crack is a very important limit state in the life of the bridge deck because once it forms it establishes the conditions to initiate corrosion of the steel reinforcement of the panels and the subsequent corrosion-induced concrete deterioration as a result of application of deicing salts.

7.5 Design Methods

This research compares methods to predict the initial cracking load of a transverse deck joint due to concentrated loads. Nine composite panels were tested under concentrated loads with different posttensioning levels as discussed in Chapter 5. The results of these tests are used to compare methods for predicting the initial cracking load due to concentrated loads. The test set up and tested initial cracking load for these specimens are shown in Figure 4.8 and Table 5.2. It should be noted that the posttensioning force is provided by two CFRP composite rods that were tensioned to 50% and 70% of their design tensile capacity.

There are three steps for analyzing the capacity of the joint for concentrated loads. These include: (1) determining the portion of the concentrated load transferred across the joint as it relates to the location of the load with respect to the joint; (2) determining the appropriate design distribution width for the load; and (3) determining the capacity of the joint for concentrated loads using shear capacity equations per linear foot of the joint under the given load distribution width. This research considers the linear capacity

methods and corresponding equations of shear friction, cracking moment, strut and tie model of the joint, principle tension stress, and ACI shear strength equations.

7.5.1 Finite Element Model for Joint Loads and Design Load Distribution Width

A finite element model (FEM), as previously used and described in Chapter 6, was created using linear elastic plate elements to predict the applied shear and moment acting across the transverse joint prior to the initial cracking load. Two composite specimens were modeled using plate elements in two directions: (1) two 8.75 in x 18 in. x 8 ft (222 mm x 457 mm x 2438 mm) panels combined at the transverse joint, and (2) two 8.75 in. x 72 in. x 8 ft (0.2 m x 1.8 m x 2.4 m) panels combined at the transverse joint. For both models the factored AASHTO HL-93 truck tire load of 34.3 kip was applied as a patch load on a 10 in. x 20 in. (254 mm x 508 mm) area as shown in Figure 7.1. Each model was run 13 times with a different location of the concentrated load.

The design distribution width is the length perpendicular to the transverse joint that the design load is transferred for design purposes in determining the capacity of the joint as shown in Figure 7.1. The design distribution width may be compared to the effective flange width of a T-beam. In both cases a smaller width is used than the actual width due to the nonuniform distribution of the stress along the flange. AASHTO uses an equivalent interior transverse strip width equal to the tire width plus one half of the slab depth on either side of the concentrated load to design the bridge deck spanning between girders for concentrated loads. The AASTHO equivalent interior transverse design strip is used for the design of decks between supports and is located parallel to the joint to

design the deck. The basic design philosophy of designing a portion of the deck for the majority of the load in a given design strip is applied in this research to design the transverse joint for concentrated loads. This research considers the same AASHTO equivalent interior strip equations for a strip perpendicular to the transverse joint, referred to as the design distribution width in this research. A design load distribution width of 28.75 in. (730 mm) for the applied loads was used in this research.

Figures 7.2 and 7.3 show the typical shear and moment distributions perpendicular to the transverse joint due to the factored AASHTO HL-93 truck tire load of 34.3 kip (153 kN). Using the shear contours of Figure 7.2, linear interpolation was performed to determine the relationship between the distribution width and the portion of the shear load transferred across the joint. The distribution of shear stress due to concentrated loads is not uniform across the deck panels and the transverse joint, as shown in Figures 7.4 and 7.3. Figure 7.4 shows the shear across the joint between the zero shear contours for the 18 in. (457 mm) wide panels. Figure 7.5 shows the shear perpendicular to the joint as a function of the distribution width for the 18 in. (457 mm) panels with the 34.3 kip (153 kN) tire load located at the center of the 18 in. panel.

Linear interpolation was applied to shear contours, as shown in Figure 7.2, to determine the shear force within each distribution width. Figure 7.6 shows shear force transferred across the center of the joint for each distribution width. This relates to the shear at the 18.5 in. (470 mm) location for Figure 7.6. Figure 7.7 shows the percent of the total shear force transferred across the joint as a function of the distribution width. As shown in Figures 7.6 and 7.7, the amount of load transferred across the joint as a ratio of the distribution width has three relationships. These include the initial linear relationship

between the distribution width and the load transferred, the final plateau relationship which is flat and the third is the transitional relationship between the two. The initial linear relationship has a larger slope than the final plateau, indicating that the majority of the load is transferred closer to the load rather than uniformly across the entire joint. Design widths within the initial linear region can be conservative because only a portion of the load is actually transferred in these design widths. The final plateau indicates that the further away from the load, the less load transfer is occurring. Design widths within the final plateau region may lead to nonconservative results because the capacity of the joint is designed based on a uniform stress distribution assumptions, while in reality the stress and load distribution are not uniform for the entire length of the joint. The optimum design width would occur within the transitional region of the graph. A design width of 36 in. (914 mm) falls within the transitional region for the finite element models performed in this research where the concentrated load is located outside the transverse joint.

The 18 in. panels transferred 10.06 kip (44.7 kN) for a 28.75 in. (730 mm) width and 11.21 kip (49.9 kN) for a 36 in. (914 mm) width across the joint for the applied 34.3 kip (153 kN) load located 9.5 in. (241 mm) from the center of the joint; this is the same location used during the lab testing of the composite specimen. This corresponds to 29.3% and 32.7% of the applied load.

In the finite element simulations, the 18 in. (457 mm) wide panels had 80% and 89.2% of the total transferred load across the joint in the center 28.75 in. (730 mm) and 36 in. (914 mm). The 72 in. (1.8 m) wide panels had 77% and 86% of the total transferred load across the joint in the center 28.75 in. (730 mm) and 36 in. (914 mm)

for the applied load located 9.5 in. (241 mm) from the center of the joint.

Finite element models were created to determine the effects on the joint as the location of the load shifted horizontally from the joint. The typical vertical deflection contours for three of these conditions is provided in Figure 7.8. Figure 7.8 (a) refers to the vertical deflections for the simply supported composite specimens with 18 in. (457 mm) panels with the center of 34.3 kip (153 kN) truck tire load located 9.5 in. (241 mm) from the center of the joint. Figures 7.8(b) and 7.8(c) refer to the same panels and loading with the center of the load located 7.5 in. (191 mm) and 0.5 in. (12.5 mm) from the center of the joint. These models and provided contours, similar to those shown in Figure 7.8, were used to create influence diagrams for the loading of the joint as a function of the location of the center of the concentrated load.

This research compares the capacity of the joint using the AASHTO design distribution width and a 36 in. (914 mm) distribution width.

Figure 7.9 is the influence diagram showing the relationship of the maximum transferred shear across the joint due to a 34.3 kip (153 kN) truck tire load as a function of the distance from the centroid of the load to the center of the transverse joint for the 72 in. (1.8 m) and 18 in. (457 mm) panels. Figure 7.10 is the influence diagram showing the relationship of the shear transferred across the joint in the given AASHTO and 36 in. (914 mm) distribution width due to a 34.3 kip (153 kN) truck tire load as a function of the distance from the centroid of the load to the center of the transverse joint for the 72 in. (1.8 m) and 18 in. (457 mm) panels. Figure 7.11 is the influence diagram for the percent of the total load transferred across the joint, determined by taking the load transferred in Figure 7.9 as a percent of the load transferred. There are three separate behaviors

consistent with all three influence diagrams. There is an ascending and a descending linear relationship between the amount of shear transferred and the location of the 10 in. (254 mm) by 20 in. (508 mm) concentrated load. There is also a transitional relationship between the ascending and descending linear relationships. The ascending linear relationship which occurs as the center of the concentrated load is located between 0.5 in (12.7 mm) and 4 in. (102 mm) from the center of the joint for Figures 7.9 and 7.10. This linear relationship is caused by the fact that the concentrated load is not a point load but a uniform load applied over a 10 in. (254 mm) by 20 in. (508 mm) area. This leads to a portion of the concentrated load being applied on either side of the joint during the initial 5 in. (12.7 mm). The descending linear relationship is a typical influence diagram for a concentrated load as it is moving away from a location of interest. The transitional region is due to the distribution of shear adjacent to the concentrated load.

From the FEM simulations, the maximum total load transferred across the entire joint was 13.75 kip (61.2 kN) for the 18 in. (457 mm) wide panels and 13.84 kip (61.6 kN) for the 72 in. (1.8 m) wide panels. This is 40.1% and 40.9% of the total applied load and less than the typical 50% used for design. This is due to the concentrated load being applied as a uniformly distributed load over the 10 in. (254 mm) by 20 in. (508 mm) AASHTO tire area. The maximum percentage of transferred shear load across the joint for the 18 in. (457 mm) and 72 in. (1.8 m) wide panels was 86.9% and 85.5% for the AASHTO distribution width and 93.2% and 91.4% for the 36 in. (914 mm) distribution width.

7.5.2 Shear Friction Based Joint Capacity

The principle of shear friction has been used to determine the shear capacity of shear keys. Rizkalla et al. (1989) used the following equation for the analysis of shear key connections for precast concrete shearwalls:

$$V_u = \mu \sigma_n A_c \quad (1)$$

where V_u is the shear that can be transferred from shear friction, σ_n (psi) is the stress applied normal to the shear face, A_c (in^2) is the area of the concrete, and μ is the coefficient of friction (Rizkalla et al., 1989). For this research the predicted initial crack capacity of the joint is revised in the following equation.

$$V_u = V_o + \mu_n \sigma_n A_c \quad (2)$$

where V_o is the initial capacity of the joint. As seen in Chapter 5 the initial capacity of the joint depends on the bond between the grout and the concrete. It is assumed that the bond shear capacity is proportional to the grout shear capacity. The coefficient of friction μ_n, is the coefficient for the bond between the grout and the concrete, for this research, the value of 0.6 is used, which is the coefficient of friction for nonroughened concrete. For the purpose of this research the bond shear strength, V_o, is described in the following relationship,

$$V_o = \frac{\mu_{nr}}{\mu_m}\left(2A_c\sqrt{f_c'}\right) \quad (3)$$

where A_c (in^2) is the area of the concrete used in this research, equal to the height of the joint, 7.75 in. (197 mm) times the design load distribution width, b. The initial equation for shear strength ($2Ac\sqrt{f'_c}$) is the capacity of monolithic concrete specimens. To relate the shear strength of the monolithic concrete to the bond shear strength of the joint the ratio of two coefficients of friction are used, where μ_{nr} is taken as 0.6 and is the coefficient of friction for concrete materials not roughened, and μ_m is taken as 1.4 and is the coefficient of friction for monolithic concrete specimens.

7.5.3 Cracking Moment for Joint Capacity

The flexural capacity of an unreinforced joint may be calculated using the cracking moment stress of the unreinforced grouted section as specified in the following equation.

$$M_{cr} = \left(f_t + \sigma_{pt}\right)\frac{bh^2}{6} \quad (4)$$

The joint height, h, of 7.75 in. (197 mm) was used based on the joint geometry. The joint width, b, is the design distribution width along the joint. The grout modulus of rupture, f_t, is based on the $7.5\sqrt{f'_c}$ of the average measured grout compressive strength. The posttensioning stress, $\square_{pt}$, is based on the average posttensioning stress normal to the joint and is calculated as the applied posttensioning force divided by the vertical cross sectional area of the panel between the supports.

7.5.4 Strut and Tie Model for Joint Capacity

A strut and tie model was created for the initial cracking load capacity of the joint due to shear transfer of the grouted joint section, as shown in Figure 7.12. The strut and tie model created for this research considers only the grouted unreinforced portion of the joint, based on the grout properties and grouted joint geometry. According to ACI 318-11 Appendix A, strut and tie models may be used for D-regions of concrete structural members that are capable of transferring loads to the adjacent B-region or the supports. D-regions are discontinuity regions for which the plane sections bending remains plane after bending hypothesis does not apply. B-regions are regions where the standard beam theory applies. The shear load transferred across the joint may be considered the load for the grouted transverse joint. The grouted transverse joint may be considered an independent D region for the shear load based on the 7.75 in. (197 mm) by 4 in. (102 mm) dimensions of the joint.

The strut and tie model was created to relate the shear force across the joint to the capacity of the joint. Strut and tie models are based on the capacity of the struts, ties and nodes of the model. The strut capacity is based on the compressive strength capacity of the grout. The tie capacity is based on the tensile strength of the grout and the additional posttensioning stress across the joint when FRP rods are present. These relationships are shown in the following equations as developed by Saenz et al. (2004):

$$S = A_{sc} 0.85 \beta_s f_c' \tag{5}$$

$$T = \mu f_t A_t + \mu \sigma_{pt} A_t \tag{6}$$

where S is the strut design compressive strength and T is the tie design tensile strength. The strut area, A_{sc}, is equal to the strut thickness times the design load distribution width, b. The tie area, A_t, is equal to the tie thickness times the design load distribution width, b. The value of 1.0 for struts with a uniform cross sectional area along their length is used for factor β_s. The tie and strut width, b, is the design distribution width along the joint. The shear friction coefficient, μ, is taken as 1.4 because the strut and tie model used in this research is based on the capacity of the grout and does not cross the boundary between the grout and concrete. The grout modulus of rupture, f_t, is based on the value of $6.7\sqrt{f'_c}$ of the average measured grout compressive strength, because the tie failure is due to a tensile failure similar to those seen in split cylinder tests. The posttensioning stress, σ_{pt}, is the average posttensioning stress normal to the joint along the panel.

The nodal capacity is based on the compressive strength on the face of the node as described in the following ACI 318 equation:

$$F_{nn} = 0.85\beta_n f_c' A_{nz} \tag{7}$$

where A_{nz} is the area of the face of the node perpendicular to the load. A grout compressive strength, f'_c of 4500 psi (31 MPa) was used. The value 0.8 was used for the nodal factor β_n based on the single tie at the node.

This research focuses on the capacity of the joint; because of this, the strut, tie, and nodal thickness and areas depend on the joint geometry. The capacity of each component is considered. The strut and tie thicknesses depend on the geometry of the joint and the node. A strut thickness of 0.707 in. (18 mm) was used for this joint

configuration. The tie thickness of 1 in. (25.4 mm) was used based on the joint geometry, as shown in Figure 7.13.

The relationships between the applied shear force at the joint and the strut and tie forces can be attained by statics, and are shown in the following equations, where the ratio w/h is the slope of the strut, as shown in Figure 7.12.

$$S_1 = \frac{1}{2} V \frac{\sqrt{h_1^2 + w_1^2}}{h_1} \tag{8}$$

$$T_1 = \frac{1}{2} V \left(\frac{w_1}{h_1} + \frac{w_2}{h_2} \right) \tag{9}$$

where T_1 is the tie design tensile load and S_1 is the strut design compressive load. The strut height, h_x and width, w_x depends on the joint cross section.

7.5.5 Principle Tension Stress

Kim et al. (2003) proposed the use of principal stress within the grouted joint and the tensile strength of the grout to predict the cracking strength of grouted joints, as follows:

$$V_u = 0.67bh\sqrt{\left(f_t^2 + \sigma_{pe} f_t\right)} \tag{10}$$

V_u is the calculated applied load for initial cracking, f_t is the tensile strength (psi) of the grout, and σ_{pe} is the effective prestressing stress (psi). A joint height, h, of 3.5 in. (89

mm) is used. The joint width, b, is the design distribution width along the joint.

7.5.6 ACI 318 Shear Equations

The ACI 318 shear capacity equation for a non-prestressed members under compressive loads is as follows:

$$V_c = 2\left(1 + \frac{N_u}{2000A_g}\right)\sqrt{f'_c}bd \qquad (11)$$

where V_c is the concrete shear strength for nonseismic regions at the joint in pounds. For this research a grout depth, d, of 7.75 in (197 mm) was used. The value b is the distribution width. The ratio N_u/A_g is the posttensioning stress normal to the joint. The average grout compressive strength, f'c, of 4500 psi (31 MPa) is used for this research.

7.6 Analysis Results

For the purpose of this research a finite element model was used to determine the load transfer at the joint. Two different design distribution width values are compared, the first, 28.75 in. (730.25 mm) is based on the AASHTO concentrated load distribution, and the second is 36 in. (914.4 mm) based on the FEM distribution of stress across the joint. Five methods are used to determine the capacity of the joint. These include shear friction, cracking moment for an unreinforced section, a strut and tie model, principle stress equations and ACI 318 shear equations. Table 7.1 shows a comparison of the predicted capacities of the joint based on the strut and tie, cracking moment, ACI 318 shear and principal stress methods. Table 7.2 shows a comparison of the predicted

applied load for joint failure. The ratio, R, is used to compare the predicted capacity to the tested initial cracking load as defined in the following equation.

$$R = \frac{Predicted\ Capacity}{Tested\ Initial\ Cracking\ Load} \quad (12)$$

A value of R less than one is considered conservative for design purposes. Table 7.3 shows a comparison of the ratio between the predicted applied load and the tested applied load at failure.

The struts and nodes had a higher capacity than the tie capacity for the tested posttensioning levels, indicating that the tie dictated the capacity of the joint for shear loading for the strut and tie method. The design capacity of the joint increased as the design distribution width, b, increased.

The different capacity equations relate to different failure modes. The two major modes of failure found in the testing setup were bond failure, which relates to the shear friction capacity equations and tensile failure of the grout, which relates to the strut and tie capacity method.

The shear friction equation gave more conservative results for the non-posttensioned joints, indicating that it dictated the capacity of the non-posttensioned joint. The shear friction and strut and tie equations gave more conservative results for the posttensioned joints, indicating that they dictated the capacity of the joint. The shear friction and strut and tie model equations predicted capacities closer to the applied load than the other methods. The principal stress equation and ACI 318 shear equation gave larger predicted capacities than the other shear capacity methods. The cracking moment

capacity of the joint provided the most nonconservative results.

The shear friction capacity should dictate the capacity under the non-posttensioned conditions while the strut and tie model should dictate the capacity under the posttensioned conditions. The capacity for the shear friction equation was closest to the non-posttensioned tested results with a distribution width of 28.75 in. (730 mm). The strut and tie model gave predicted loads closer to the tested values for the 36 in. (914 mm) distribution width but conservative values for the 28.75 in. (730 mm) AASHTO distribution width. The shear friction method provided excessively conservative values for the posttensioned joint conditions, indicating that the coefficient of friction of friction of 0.6 is too low for the tested interface. A shear friction coefficient of 1.0 would provide similar capacity to those found in the test for the 28.75 in. (730 mm) AASHTO distribution width. The AASHTO distribution width is acceptable for the design capacity of the joint and is slightly conservative for the strut and tie model. A distribution width of 36 in. (914 mm) is acceptable for the capacity of posttensioned of transverse joints using the strut and tie equation. When considering the capacity of the joint for shear friction using the AASHTO distribution width, a coefficient of friction larger than 0.6 should be considered.

7.7 Design Procedure

Design engineers make several assumptions when designing. For designing grouted transverse joints these assumptions include the assumption that the entire load transferred across the joint will be transferred in the distribution width and the maximum load transferred across the joint is 50% of the total load applied load for the transverse

joint between two panels.

The factored design capacity of the joint is the calculated capacity of the joint times the AASHTO prescribed strength reduction (phi) factor. The calculated load capacity of the joint is the capacity based on the smallest of the ACI 318 shear equations, the joint strut and tie model equations, the shear friction equations and the bending moment capacity equation for the given distribution width divided by 0.5 for the assumption that a maximum of half the load will be transferred across the joint. The AASHTO □ factor used for design is 0.9. These equations may be used for grouted transverse joints regardless of posttensioning material. The posttensioning stress used in the equations is applied across the joint for unreinforced grouted joints with the posttensioning applied at the center of the joint.

The design load capacity of the joint is provided in Table 7.4 for a concentrated load located near the joint. The maximum factored design load for the joint is 23.06 kips (102.6 kN) for the non-posttensioned joint with a distribution width of 28.75 in. (730 mm) and 28.88 kips (128.5 kN) with a distribution width of 36 in. (914.4 mm). The maximum factored design load for the posttensioned joint is 31.47 kips (140 kN) with a distribution width of 28.75 in. (730 mm) and 39.41 kips (175.3 kN) with a distribution width of 36 in. (914.4 mm) for the 34.95 psi (241 kPa) posttensioned joint and 34.7 kips (154 kN) and 43.46 kips (193 kN) for the 48.39 psi (334 kPa) posttensioned joint.

7.8 Conclusions and Recommendations

Analytical comparisons were made for the capacity of unreinforced transverse joints of precast concrete deck panels under concentrated loads. Several conclusions can

be made.

1) The shear transferred across the joint is not uniformly distributed across the entire length of the joint under concentrated loading. The relationship between the amount of shear transferred and the design distribution width has three separate relationship ranges: an initial linear relationship, a transitional relationship, and a final linear relationship. Narrower design distribution widths occurring in the initial linear relationship are considered conservative. Larger distribution widths occurring in the final linear relationship can be considered nonconservative. The optimum design distribution width occurs in the transitional region of this relationship.
2) The maximum load transferred across the joint for concentrated truck tire loads is less than the 50% of the total applied load used by design engineers. The maximum total load transferred across the entire joint was 40.1% of the total applied load for the 18 in. (457 mm) wide panels and 40.9% of the total applied load for the 72 in. (1.8 m) wide panels. This is due to the concentrated load being applied as a uniformly distributed load over the 10 in. (254 mm) by 20 in. (508 mm) AASHTO tire area.
3) When designing for the capacity of the joint for concentrated loads, the shear friction concept and the joint strut and tie models should be considered. The shear friction concept and the strut and tie model governed the capacity of the joint because they had lower predicted capacity values than the ACI shear equation, principle tension stress and cracking moment methods. Moreover, the shear friction method and the strut and tie method gave the most accurate

capacities of the joint compared to the experimental results.

4) The capacity of the tie was lower than the capacity of the strut and node for the strut and tie model used to evaluate the capacity of the transverse joint between the panels and governed the capacity of the strut and tie model. To improve the capacity of the joint, the tie capacity must be increased through the addition of posttensioning forces or a much higher grout tensile strength.
5) The use of a design distribution width of 36 in. may be considered for the design of the transverse joint under posttensioned conditions for concentrated loads. The shear friction and the strut and tie model equations predicted capacities closer to the applied load compared to the other methods. The shear friction and the strut and tie model with a distribution width of 36 in. (914 mm) had predicted load capacities closer to the tested loads for the posttensioned loading conditions. The 28.75 in. (730 mm) AASHTO distribution width had predicted load capacities closer to the tested results for the non-posttensioned panels.
6) Based on joint capacity equations, as confirmed by laboratory tests, it is beneficial to posttension the joint to increase the capacity of the precast bridge deck system.

7.9 References

American Concrete Institute, (2011). ACI 318-11 *Building Code Requirements for Structural Concrete*. Farmington Hills, MI.

Hanna, K. E., Morcous, G., & Tadros, M. K. (December 2010). *Second Genration Precast Deck Panel (NUDECK) System.* University of Nebraska, Lincoln. Lincoln, Nebraska: Nebraska Department of Roads.

Issa, M. A., Idriss, A.-T., Kaspar, I. I., & Khayyat, S. Y. (1995, January-February). Full

Depth Precast and Precast, Prestressed Concrete Bridge Deck Panels. *PCI Journal*, 40, 59-80.

Issa, M. A., Ribeiro do Valle, C. L., Islam, S., Abdalla, H. A., & Issa, M. A. (2003, July-August). Performance of Transverse Joint Grout Materials in Full-Depth Precast Concrete Bridge Deck Systems. *PCI Journal*, 48, 2-13.

Issa, M. A., Yousif, A. A., Issa, M. A., Kaspar, I. I., & Khayyat, S. Y. (1995, May-June). Field Performance of Full-Depth Precast Concrete Panels in Bridge Deck Reconstruction. *PCI Journal*, 40, 82-108.

Issa, M. A., Yousif, A. A., Issa, M. A., Kaspar, I. I., & Khayyat, S. Y. (1998, January-February). Analysis of Full Depth Precast Concrete Bridge Deck Panels. *PCI Journal*, 43, 74-85.

Kim, Y.-C., Shin, S., & Park, J.-J. i. (2003). Shear and Fatigue Strength of Grout-Type Transverse Joints. *Canadian Journal of Civil Engineering*, 607-614.

Petrou, M. F., Perdikaris, P. C., & Duan, M. (1996). Static Behavior of Noncomposite Concrete Bridge Decks Under Concentrated Loads. *Journal of Bridge Engineering*, 143-154.

Rizkalla, S. H., Serrette, R. L., Heuvel, J. S., & Attiogbe, E. K. (1989, March-April). Multiple Shear Key Connections for Precast Shear Wall Panels. *PCI Journal*, 104-120.

Roberts, K. S. (2011). Performance of Transverse Post-Tensioned Joints Subjected to Negative Bending and Shear Stresses of Full Scale, Full Depth, Precast Concrete Bridge Deck Systems. *Master's Thesis,* Utah State University, 2011

.

Saenz, N., Pantelides, C. P., & Reaveley, L. D. (2004). Strut-and-Tie Model for Shear Friction of Concrete with Fiber-Reinforced Polymer Composites. *ACI Structural Journal*, 863-871.

Tao, Z. (2009). Biaxial Bending Analysis of the Slabs Under Concentrated Loads. 2009 *International Conference on Engineering Computation*, (pp. 213-216).

Table 7.1: Predicted Capacities for Joint Failure

(1 in. = 25.4 mm, 1 kip = 4.44 kN)

PT STRESS (psi)	b = 28.75 in.							b = 36 in.						
			STRUT AND TIE MODEL							STRUT AND TIE MODEL				
	Joint Shear Capacity Per Shear Friction (kip)	Mcr Capacity (kip-in)	Joint Shear Capacity Per Strut Capacity (kip)	Joint Shear Capacity Per Tie Capacity (kip)	Joint Shear Capacity Per Node Capacity (kip)	ACI Concrete Shear Capacity (kip)	Principal Stress Shear Capacity (kip)	Joint Shear Capacity Per Shear Friction (kip)	Mcr Capacity (kip-in)	Joint Shear Capacity Per Strut Capacity (kip)	Joint Shear Capacity Per Tie Capacity (kip)	Joint Shear Capacity Per Node Capacity (kip)	ACI Concrete Shear Capacity (kip)	Principal Stress Shear Capacity (kip)
0.00	12.81	144.80	109.97	18.09	62.21	29.89	30.30	16.04	181.31	137.70	22.65	77.89	37.43	37.94
34.95	17.48	158.75	109.97	19.50	62.21	30.42	31.46	21.89	198.78	137.70	24.41	77.89	38.09	39.39
48.39	19.28	164.11	109.97	20.04	62.21	30.62	31.89	24.14	205.50	137.70	25.09	77.89	38.34	39.93

Table 7.2: Predicted Applied Load for Joint Failure

(1 in. = 25.4 mm, 1 kip = 4.44 kN)

PT STRESS (psi)	Tested Applied Load (kip)	b = 28.75 in.					b = 36 in.				
		Shear Friction Capacity	Mcr Capacity	Strut and Tie Model Capacity	Principal Stress Capacity	ACI Concrete Shear Capacity	Shear Friction Capacity	Mcr Capacity	Strut and Tie Model Capacity	Principal Stress Capacity	ACI Concrete Shear Capacity
0.00	45.17	43.73	275.28	61.74	103.42	102.03	49.06	299.69	69.27	116.03	114.47
34.95	71.60	59.67	301.80	66.54	107.36	103.81	66.95	328.56	74.66	120.46	116.47
48.39	74.83	65.80	312.00	68.39	108.84	104.49	73.83	339.67	76.73	122.12	117.24

Table 7.3: Ratio Between the Predicted Applied Load and the Tested Applied Load at Joint Failure (1 in. = 25.4 mm, 1 kip = 4.44 kN)

PT STRESS (psi)	Tested Applied Force (kip)	b = 28.75 in.					b = 36 in.				
		Shear Friction Capacity	Mcr Capacity	Strut and Tie Model Capacity	Principal Stress Capacity	ACI Concrete Shear Capacity	Shear Friction Capacity	Mcr Capacity	Strut and Tie Model Capacity	Principal Stress Capacity	ACI Concrete Shear Capacity
0.00	45.17	0.97	6.09	1.37	2.29	2.26	1.09	6.64	2.57	2.88	2.53
34.95	71.60	0.83	4.22	0.93	1.50	1.45	0.94	4.59	1.68	1.88	1.63
48.39	74.83	0.88	4.17	0.91	1.45	1.40	0.99	4.54	1.63	1.82	1.57

Table 7.4: Design Applied Load for Joint Failure

(1 in. = 25.4 mm, 1 kip = 4.44 kN)

PT STRESS (psi)	b = 28.75 in.					b = 36 in.				
	Shear Friction Capacity (kip)	Mcr Capacity (kip)	Strut and Tie Model Capacity (kip)	Principal Stress Capacity (kip)	ACI Concrete Shear Capacity (kip)	Shear Friction Capacity (kip)	Mcr Capacity (kip)	Strut and Tie Model Capacity (kip)	Principal Stress Capacity (kip)	ACI Concrete Shear Capacity (kip)
0.00	23.06	260.63	32.56	54.54	53.81	28.88	326.36	40.77	68.30	67.38
34.95	31.47	285.74	35.09	56.62	54.75	39.41	357.80	43.94	70.90	68.55
48.39	34.70	295.40	36.07	57.40	55.11	43.46	369.90	45.16	71.88	69.01

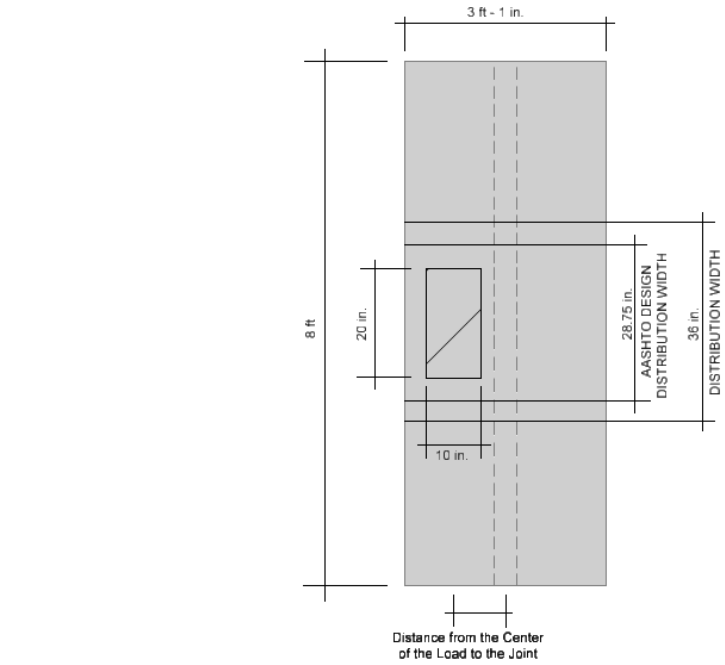

(a)

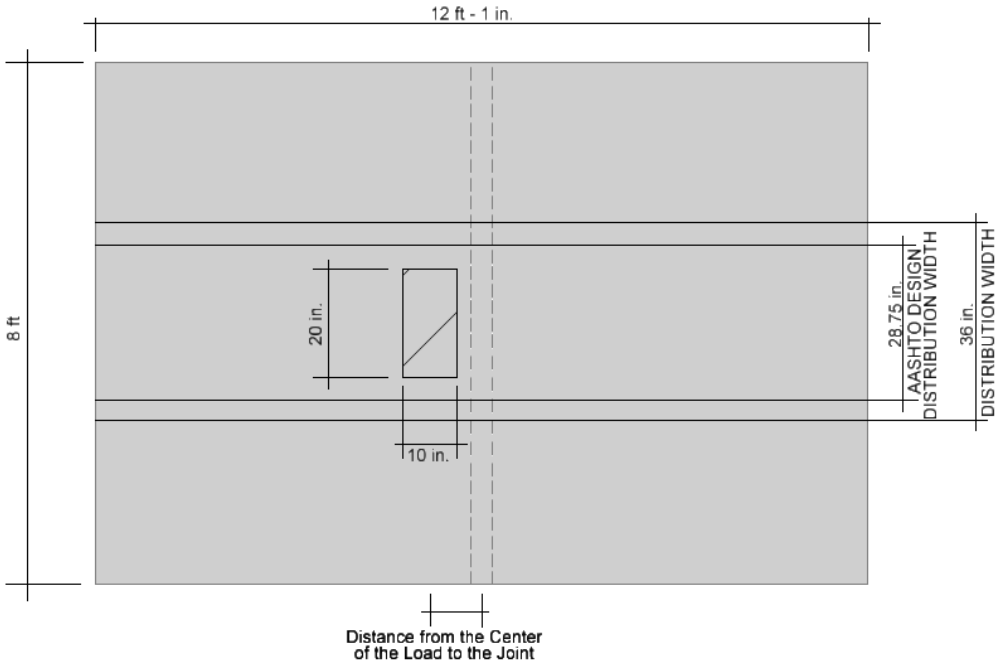

(b)

Figure 7.1: Typical Model Comparison Measurements: (a) 18 in. Wide Panels, (b) 72 in. Wide Panels (1 in. = 25.4 mm, 1 kip = 4.44 kN)

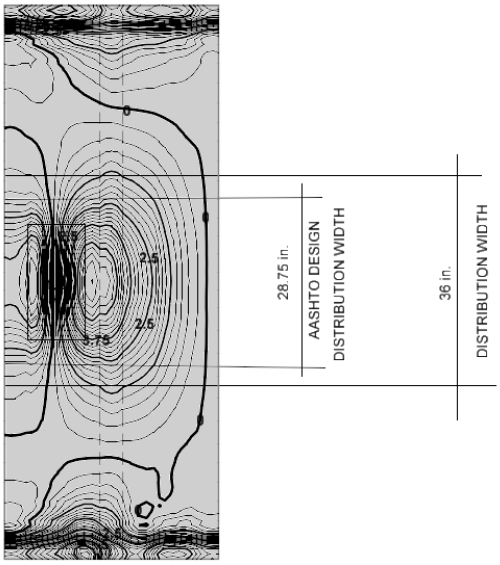

(a)

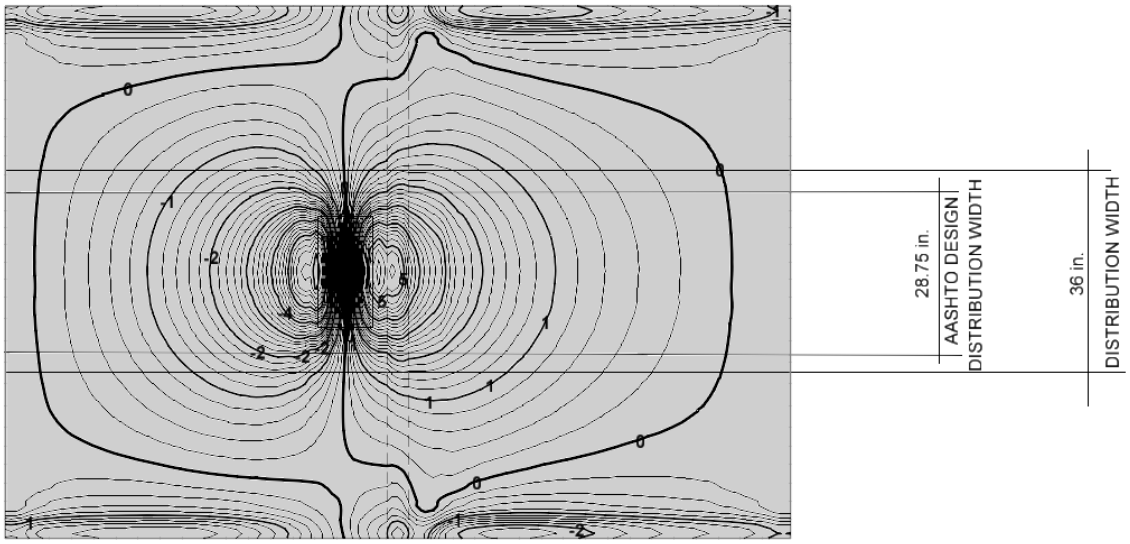

(b)

Figure 7.2: Typical Shear Force (k/ft) Distribution Perpendicular to the Transverse Joint for Composite Specimens at 34.3 k Load: (a) 18 in. Wide Panels, (b) 72 in. Wide Panels

(1 in. = 25.4 mm, 1 kip = 4.44 kN)

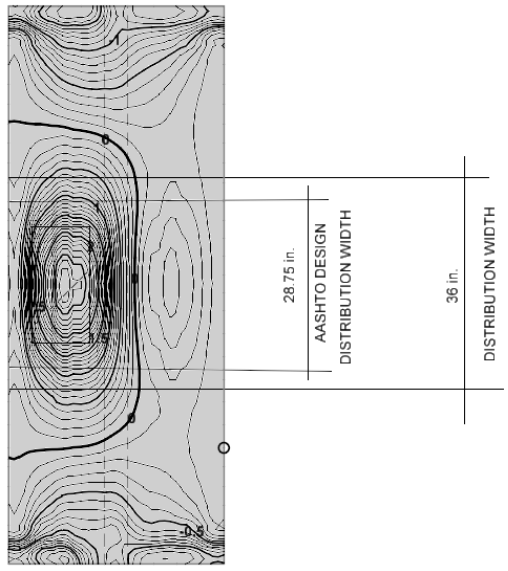

(a)

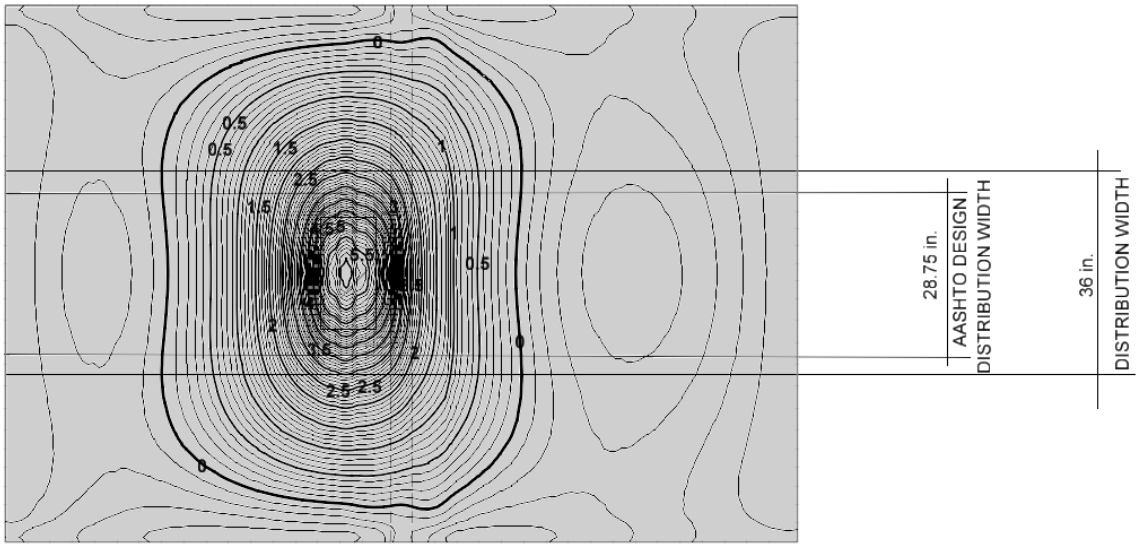

(b)

Figure 7.3: Typical Moment (k-ft/ft) Distribution Perpendicular to the Transverse Joint for Composite Specimens at 34.3 k Load: (a) 18 in. Wide Panels, (b) 72 in. Wide Panels (1 in. = 25.4 mm, 1 kip = 4.44 kN)

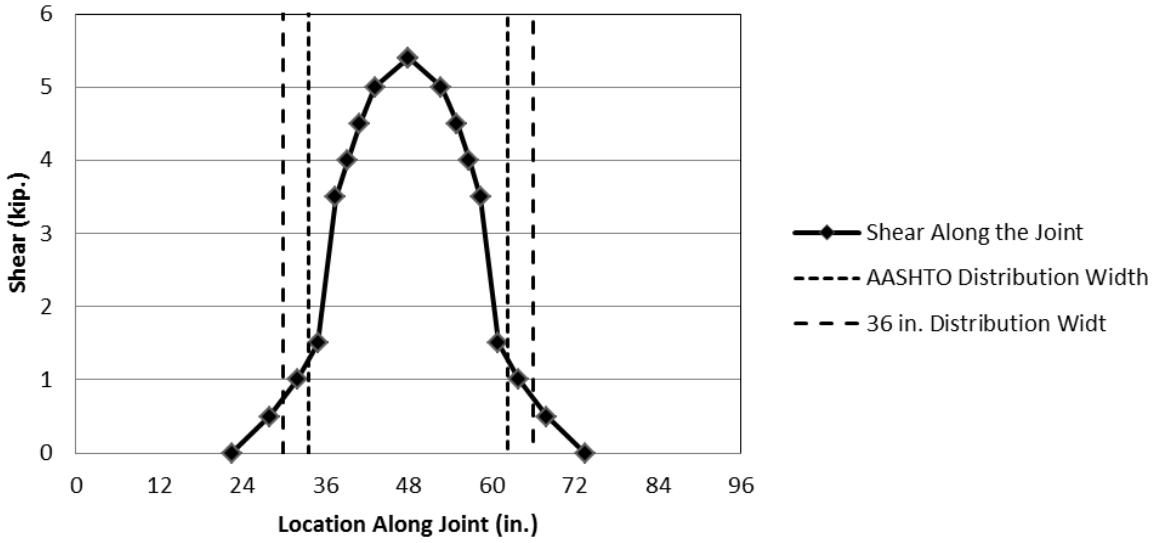

Figure 7.4: Shear Force Distribution Along the Transverse Joint for Composite Specimens at 34.3 k Load for the 18 in. Wide Panels (1 in. = 25.4 mm, 1 kip = 4.44 kN)

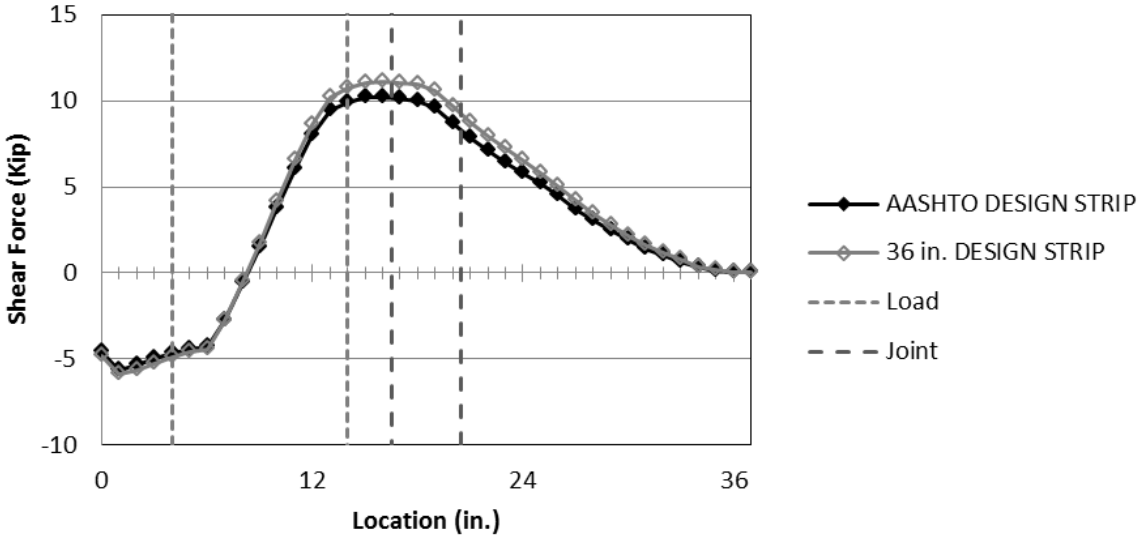

Figure 7.5: Shear Force (kip) Distribution Perpendicular to the Transverse Joint for Composite Specimens at 34.3 k Load for the 18 in. Wide Panels as a Function of the Distribution Width (1 in. = 25.4 mm, 1 kip = 4.44 kN)

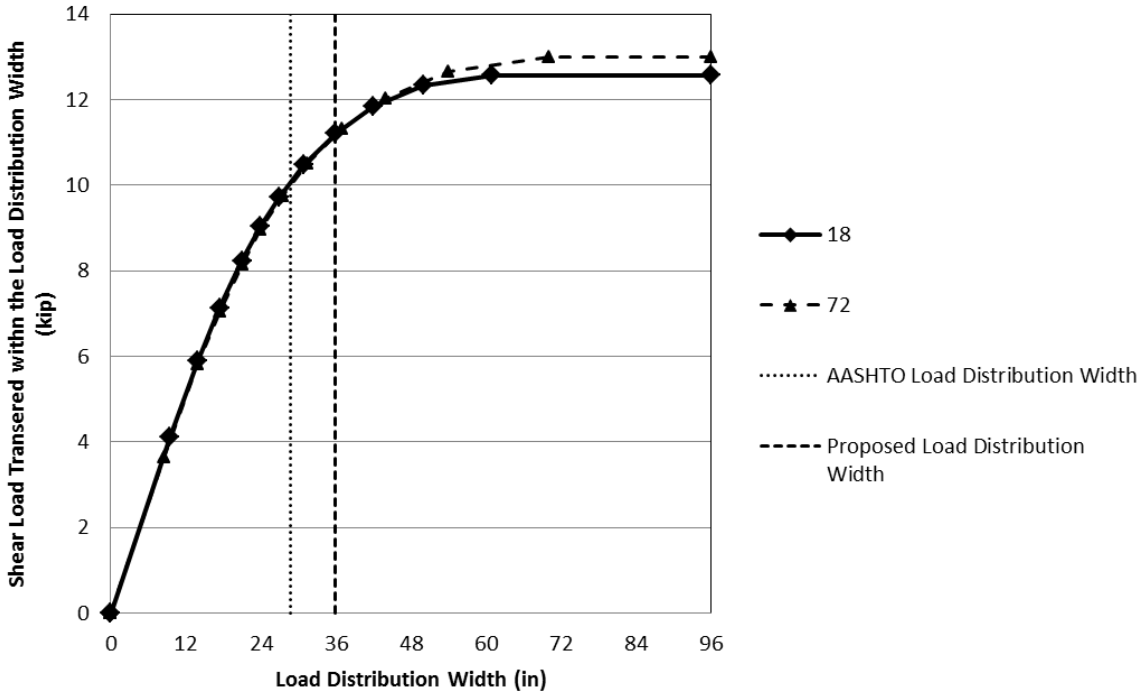

Figure 7.6: Transferred Shear for 34.4 Kip Tire Load vs. Load Distribution Width Diagram

(1 in. = 25.4 mm, 1 kip = 4.44 kN)

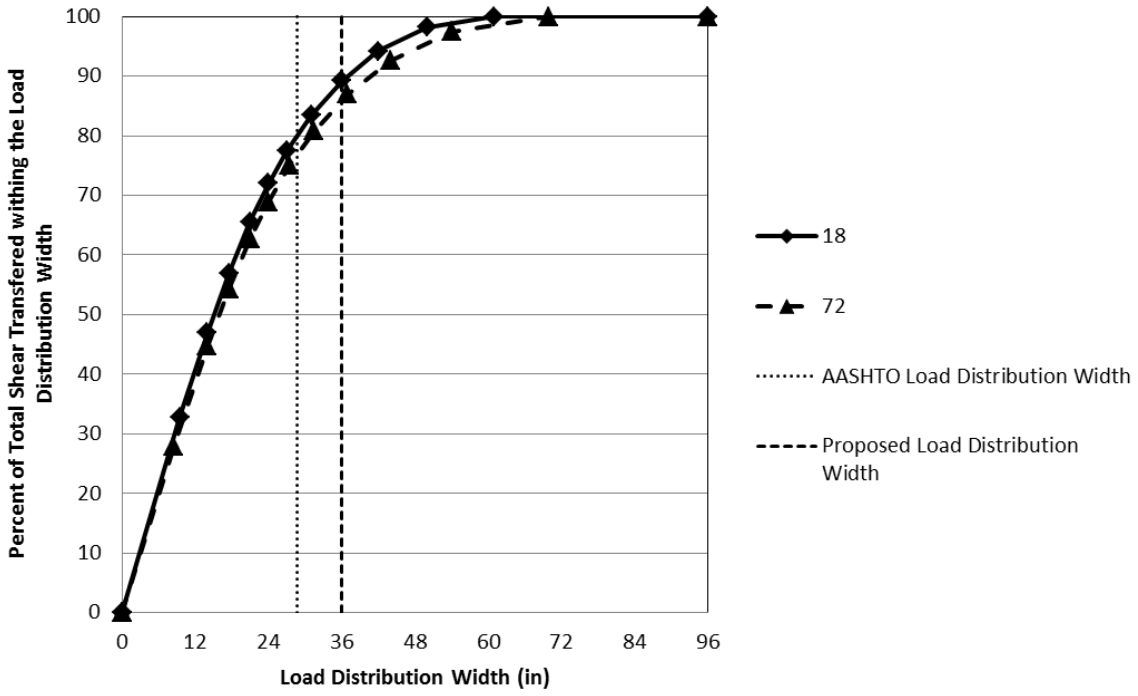

Figure 7.7: Percent of Maximum Transferred Shear vs. Load Distribution Width Diagram

(1 in. = 25.4 mm, 1 kip = 4.44 kN)

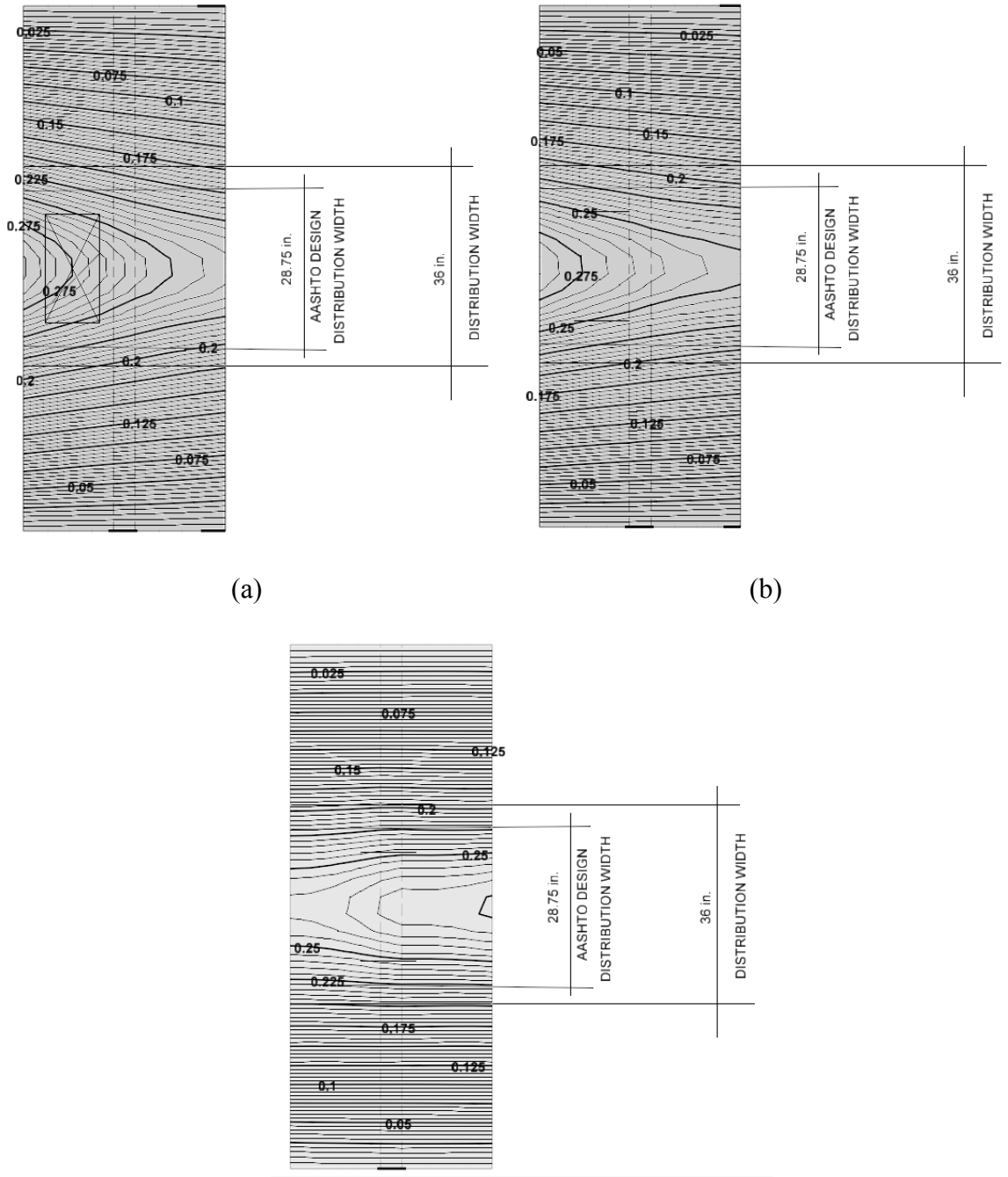

Figure 7.8: Typical Vertical Displacements (in) for Composite Specimens with 18 in. Wide Panels at 34.3 k Load at Varying Load Locations: (a) Center of Load Located 9.5 in. from Center of Joint, (b) Center of Load Located 7 in. from Center of Joint, (c) Center of Load Located 0.5 in. from Center of Joint (1 in. = 25.4 mm, 1 kip = 4.44 kN)

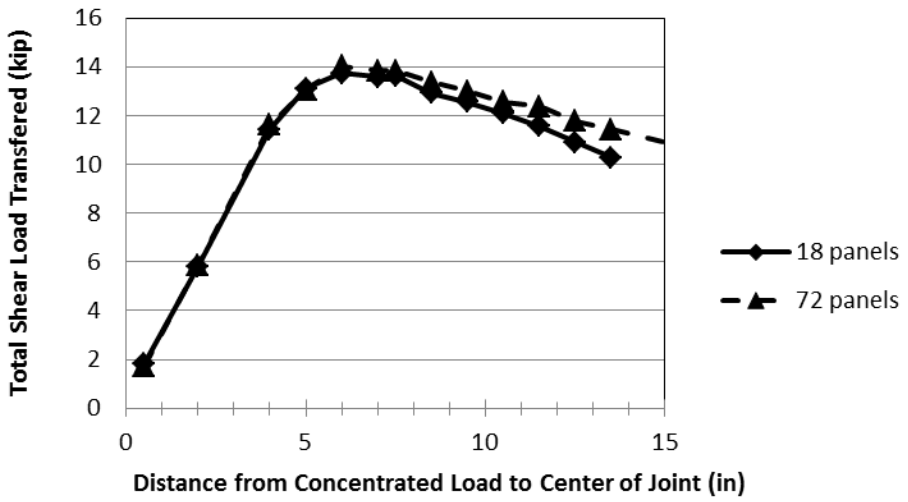

Figure 7.9: Relationship of the Maximum Transferred Shear Across the Joint Due to a 34.3 kip Truck Tire Load for 18 in. and 72 in Wide Panels as a Function of the Distance from the Centroid of the Load to the Center of the Transverse Joint for the 18 in. and 72 in. Wide Panels (1 in. = 25.4 mm, 1 kip = 4.44 kN)

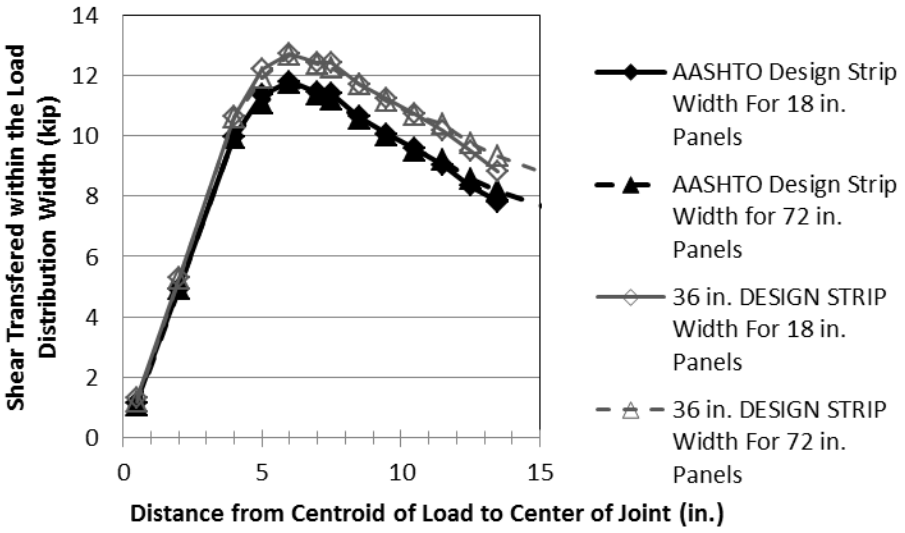

Figure 7.10: Relationship of the Shear Transferred Across the Joint in the AASHTO and 36 in. Distribution Width Due to a 34.3 kip Truck Tire Load as a Function of the Distance from the Centroid of the Load to the Center of the Transverse Joint for 18 in. and 72 in. Panels (1 in. = 25.4 mm, 1 kip = 4.44 kN)

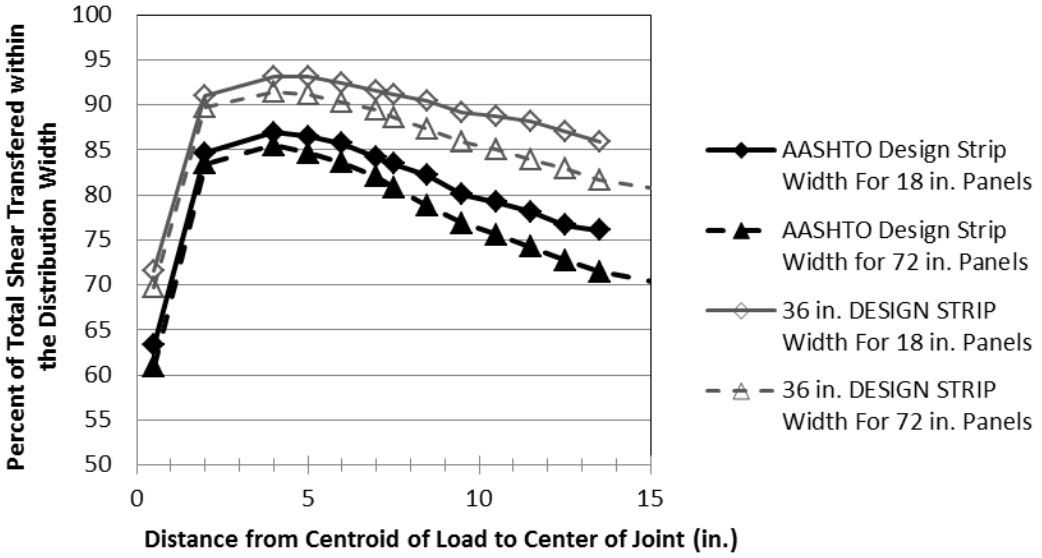

Figure 7.11: Influence Diagram for Percent of Maximum Transferred Shear vs. Load Distribution Width Diagram (1 in. = 25.4 mm, 1 kip = 4.44 kN)

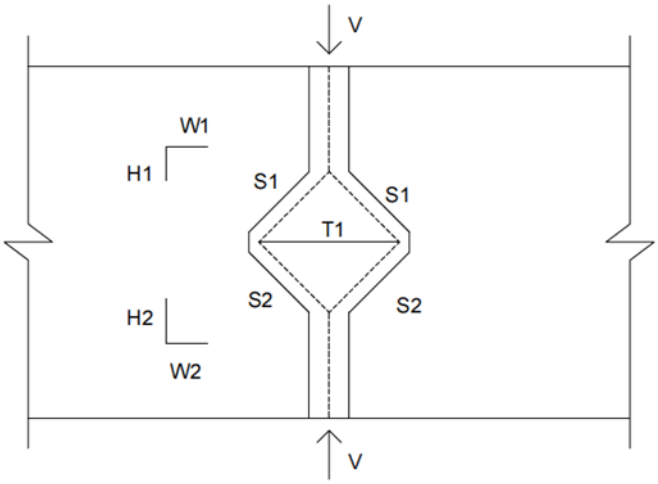

Figure 7.12: Strut and Tie Model Set up

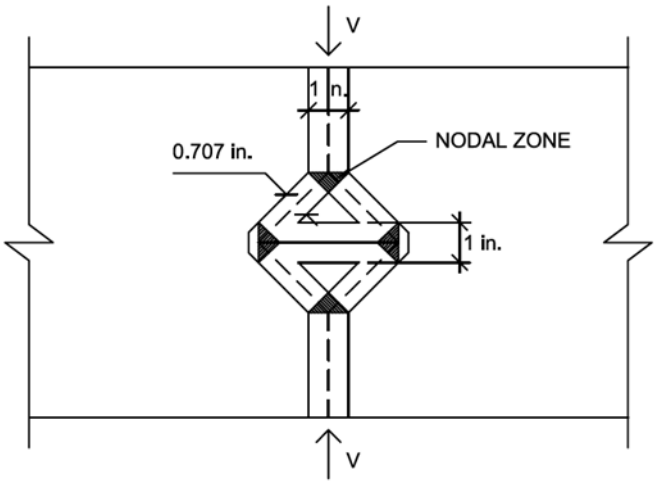

Figure 7.13: Strut and Tie Model Dimensions

(1 in. = 25.4 mm, 1 kip = 4.44 kN)

CHAPTER 8

SUMMARY AND CONCLUSIONS

The focus of this research was to compare different methods to protect, strengthen and analyze the capacity of the grouted transverse joint between precast concrete bridge deck panels. This was done by focusing on: (a) protection of the joint using different overlay systems, (b) capacity and behavior of the transverse joint using fiber reinforced polymers (FRP) composite rods at different posttensioning levels, (c) finite element modeling of the transverse joint under concentrated truck tire loads, and (d) an analytical approach to compare the applied concentrated truck tire load with the initial cracking load capacity of the joint.

Chapter 4 focused on the protection of the joint through the application of different overlays. Laboratory and field experimental studies were performed on the bond strength and the chloride intrusion after cyclic loading of different overlay systems adjacent to the grouted transverse bridge deck joint.

Two methods of application of different overlay systems applied to precast concrete panels were investigated: (a) application of the overlay applied after placement of the precast bridge deck panels and (b) application of the overlay prior to placement of the precast concrete bridge deck panels. Two properties were tested and compared to determine the performance of different overlay systems. Pull-off tests were used to

compare the mechanical characteristics of the overlay system, specifically the bond between the overlay and the concrete bridge deck panel. Ponding tests were also carried out to compare the ability of the overlay system to resist chloride intrusion from deicing salts. The following conclusions were drawn:

1) Results for all overlay systems showed no measurable chlorides. However, base specimens with no overlays had an average chloride content of 2.96 lbs/yd^3 (1.76 Kg/m^3) for the first 1/8 in. (3 mm) below the concrete surface and 2.51 lbs/yd^3 (1.49 Kg/m^3) for a depth between 1/8 in. (3 mm) to 1/4 in. (6 mm). This indicates that all overlay systems were sufficient to prevent chloride intrusion under the accelerated 90 day testing procedures.
2) The average pull strength of thin polymer overlay systems was 41% larger than the methacrylate based overlay. The polyester polymer concrete overlay system pull strength was 39% larger than the methacrylate system.
3) The majority of failures in the pull off tests for thin polymer overlays occurred in the concrete, which is the desired failure plane. This proves that the tensile strength of the thin polymer overlay and bond strength between the thin polymer and the concrete deck were stronger than the tensile strength of the concrete and met Utah DOT specification.

The joint did not crack during overlay test loading. Overlay systems are effective when the joint integrity is not compromised. To get a greater understanding of the behavior and failure modes of the transverse joint with no and low posttensioning under concentrated loads, testing was performed on precast composite panels posttensioned with carbon fiber rods, as discussed in Chapter 5. Laboratory tests were carried out on

nine precast concrete composite specimens to determine the effects of posttensioning on the grouted transverse joint. Several conclusions are drawn from this study.

1) Carbon fiber rods are effective to posttension across the transverse joint to strengthen the joint for concentrated truck tire loads. They are especially attractive because of their corrosion resistance.
2) The use of posttensioning increased the initial cracking load by an average of 58% to 65% and the ultimate capacity by an average of 28% to 34% of the joint with no posttensioning.
3) The two significant failures of the tested grouted transverse joint were bond failure and tensile failure of the grout. The initial mode of failure for the non-posttensioned panels was the bond failure between the grout and concrete deck. The use of posttensioning was sufficient to overcome bond failure, but not sufficient to overcome shear or tensile failure of the grout.
4) The composite panels behave monolithically under typical design truck loads. All specimens tested had an initial cracking capacity larger than the required AASHTO capacity for the HL-93 truck tire. The initial cracking load of the non-posttensioned panels was 10% to 59% larger than the factored AASHTO design HL-93 truck tire load, of 34.3 kips. This ranged from 103% to 113% for the 35A, 35B, and 35C posttensioned panels and 98% to 129% for the 48A, 48B, and 48C posttensioned panels.

Chapter 6 focused on the analytical modeling of the grouted transverse joint for determining the behavior of the grouted transverse joint under concentrated loads. Analytical comparisons were made on the modeling of the unreinforced transverse joint

for precast concrete deck panels under concentrated loads using ANSYS and RAM CONCPET finite element modeling programs. Several conclusions are drawn from this research.

1) Due to the nonlinear modeling properties of the concrete elements, the small scale model can be appropriately used to show the force vs. displacement behavior of the joint under increasing load prior to initial joint failure. Due to the linear elastic plate element assumptions used in the large model, the large model can be appropriately used under a nonincremental loading condition to analyze load distribution and deflections under the monolithic behavior prior to initial joint failure.
2) The large model used similar boundary conditions to those found in real concrete bridge deck construction and had more accurate displacement results than the small model with the laboratory tested specimens. The large model had a center displacement under the applied concentrated load 0.3% larger than the average recorded center displacement under the same loading for the tested composite specimens. The center displacement on the nonloaded panel of the composite specimens was 24% larger than the average recorded displacement under the same location and loading.

Chapter 7 focused on empirical methods to predict an acceptable design capacity of the grouted transverse joint under concentrated loads. Load distribution results from finite element modeling were used to develop an effective distribution width on the capacity of the precast bridge deck transverse joint under concentrated loads. Different empirical methods were compared with laboratory results to validate the use of these

methods. Several conclusions were drawn from this research.

1) The shear transferred across the joint is not uniformly distributed across the entire length of the joint under concentrated loading. The relationship between the amount of shear transferred and the design distribution width has three separate relationship ranges: an initial linear relationship, a transitional relationship, and a final linear relationship. Narrower design distribution widths occurring in the initial linear relationship are considered conservative. Larger distribution widths occurring in the final linear relationship can be considered nonconservative. The optimum design distribution width occurs in the transitional region of this relationship.
2) The use of a design distribution width of 36 in. can acceptably be considered for the design of the transverse joint under posttensioned conditions for concentrated loads. The 28.75 in. AASHTO distribution width had predicted load capacities closer to the tested results for the non-posttensioned panels.
3) When designing for the capacity of the joint for concentrated loads, the shear friction concept and the joint strut and tie models should be considered. The shear friction concept and the strut and tie model governed the capacity of the joint because they predicted capacities closer to the applied load and had lower predicted capacity values than the ACI 318 shear equation, principle tension stress and cracking moment methods. These ranged from a design capacity of 17% less to 9% larger than the results for the tested composite specimens for the shear frictions equations and 9% less and 4% larger than the results for the tested posttensioned composite specimens for the strut and tie model. All other

methods had a calculated capacity ranging from 57% to 564% larger than the results for tested composite specimens. The shear friction and the strut and tie model with a distribution width of 36 in. had predicted load capacities closer to the tested loads for the posttensioned loading conditions.

4) Based on joint capacity equations it is beneficial to posttension the joint to increase the capacity of the precast bridge deck system.

CHAPTER 9

FUTURE CONSIDERATIONS

Additional research on grouted transverse joints should be performed. It is recommended that this research include overlay research on non-posttensioned grouted joints, testing with higher levels of posttensioning, and concentrated load tests with varying locations of the concentrated load with respect to the joint. Research should also be performed comparing the capacity of the joint under concentrated loads for bridge deck panels with varying material strengths, including different grout strength and concrete strength. The capacity of the joint under concentrated loads should be tested for panels with larger widths. Consideration should also be made on long term creep effects of posttensioning CFRP rods.